



The Journal of The Royal Astronomical Society of Canada
Journal
Le Journal de la Société royale d'astronomie du Canada

PROMOTING
ASTRONOMY
IN CANADA

August/août 2017
Volume/volume 111
Number/numéro 4 [785]

Inside this issue:
Diamond Ring and
Black-Drop Effects
Maps of Light Pollution
Exoplanet τ Boötis b

Blossoming Rosette

The Best of Monochrome.

Drawings, images in black and white, or narrow-band photography.



Lynn Hilborn imaged the Cave Nebula, also known as Sh2-155 or Caldwell 9, from his WhistleStop Observatory in Grafton, Ontario. He used TEC 140 scope at f5.6 and FLI ML8300 camera with Baader filters on a Takahashi NJP Temma2 mount to image this diffuse nebula located in Cepheus, at a distance of 2900 light-years.

contents / table des matières

Research Articles / Articles de recherche

149 Diamond Ring and Black-Drop Effects during Eclipses of the Sun—Mechanisms of Formation

by Michel Duval and Laurent Lamarre

156 Detection of Exoplanet τ Boötis b at the Simon Fraser University Trottier Teaching and Outreach Observatory

by Howard Trottier

Feature Articles / Articles de fond

154 Maps of Light Pollution

by Peter D. Hiscocks and Christopher C.M. Kyba

Columns / Rubriques

164 Pen and Pixel:

The Crab Nebula / M71 / Prominence / Milky Way

by Brian McGaffney / Ron Brecher / Gary Palmer / Michael Watson

172 Skyward: Of Observatories and Eclipses

by David Levy

174 Imager's Corner: Masks Basic 2

by Blair MacDonald

176 Second Light: An Exoplanet Around a B0-A9.5 Star

by Leslie J. Sage

178 Dish on the Cosmos: The Shadows of Galaxy Clusters

by Erik Rosolowsky

180 Binary Universe: Solar Eclipse Timings

by Blake Nancarrow

183 CFHT Chronicles: Wannabe Stars and CFHT in Canada

by Mary Beth Laychak

186 John Percy's Universe: Science "Culture" in Canada

by John R. Percy FRASC

Departments / Départements

188 Astrocryptic and June Answers

by Curt Nason

188 It's Not All Sirius

by Ted Dunphy

143 News Notes / En manchettes

Compiled by Jay Anderson

142 President's Corner

by Craig Levine

iii Great Images

by Bill Longo

Dan Meek photographed open cluster NGC 2244 with the Rosette Nebula from his Stardust Observatory in Calgary using his Tele Vue NP127is telescope and a QSI583wsg CCD camera. The six-hour image was processed in the Hubble palette.



Journal

The *Journal* is a bi-monthly publication of The Royal Astronomical Society of Canada and is devoted to the advancement of astronomy and allied sciences.

It contains articles on Canadian astronomers and current activities of the RASC and its Centres, research and review papers by professional and amateur astronomers, and articles of a historical, biographical, or educational nature of general interest to the astronomical community. All contributions are welcome, but the editors reserve the right to edit material prior to publication. Research papers are reviewed prior to publication, and professional astronomers with institutional affiliations are asked to pay publication charges of \$100 per page. Such charges are waived for RASC members who do not have access to professional funds as well as for solicited articles. Manuscripts and other submitted material may be in English or French, and should be sent to the Editor-in-Chief.

Editor-in-Chief

Nicole Mortillaro
Email: editor@rasc.ca
Web site: www.rasc.ca
Telephone: 416-924-7973
Fax: 416-924-2911

Associate Editor, Research

Douglas Hube
Email: dhube@ualberta.ca

Associate Editor, General

Michael Attas
Email: attasm1@mymts.net

Assistant Editors

Michael Allen
Martin Beech
Dave Chapman
Ralph Chou
Ralph Croning
Dave Garner
Patrick Kelly

Editorial Assistant

Michele Arenburg
Email: mcarenburg@gmail.com

Production Manager

James Edgar
Email: james@jamesedgar.ca

Contributing Editors

Jay Anderson (News Notes)
Ted Dunphy (It's Not All Sirius)
Mary Beth Laychak (CFHT Chronicles)
David Levy (Skyward)
Blair MacDonald (Imager's Corner)
Blake Nancarrow (Binary Universe)
Curt Nason (Astrocryptic)
John R. Percy (John Percy's Universe)
Randall Rosenfeld (Art & Artifact)
Eric Rosolowsky (Dish on the Cosmos)
Leslie J. Sage (Second Light)
Rick Saunders (Maker's Minute)
David Turner (Reviews)

Proofreaders

Michele Arenburg
Ossama El Badawy
Margaret Brons
Angelika Hackett
Kim Leitch

Design/Production

Michael Gatto, Grant Tomchuk
Email: gattotomatto@eastlink.ca,
granttomchuk@eastlink.ca

Advertising

Julia Neeser
Email: mempub@rasc.ca

Printing

Cansel
www.cansel.ca

His Excellency the Right Honourable **David Johnston**, C.C., C.M.M., C.O.M., C.D., Governor General of Canada, is the Viceregal Patron of the RASC.

The *Journal* of The Royal Astronomical Society of Canada is published at an annual subscription rate of \$93.45 (including tax) by The Royal Astronomical Society of Canada. Membership, which includes the publications (for personal use), is open to anyone interested in astronomy. Applications for subscriptions to the *Journal* or membership in the RASC and information on how to acquire back issues of the *Journal* can be obtained from:

The Royal Astronomical Society of Canada
203 – 4920 Dundas St W
Toronto ON M9A 1B7, Canada
Email: nationaloffice@rasc.ca
Web site: www.rasc.ca
Telephone: 416-924-7973
Fax: 416-924-2911



Canadian Publications Mail Registration No. 09818
Canada Post: Send address changes to 203 – 4920 Dundas St W, Toronto ON M9A 1B7

Canada Post Publication Agreement No. 40069313
We acknowledge the financial support of the Government of Canada through the Canada Periodical Fund (CPF) for our publishing activities.

© 2017 The Royal Astronomical Society of Canada.
All rights reserved. ISSN 0035-872X

Canada



President's Corner



by Craig Levine, London Centre
(craiglevine@gmail.com)

This will be my last column as President of the RASC. Whenever I read columns in other media with a similar portentous (or pretentious?) beginning, I brace myself for either a maudlin litany of regret, or a somewhat stale recounting of timeline highlights covering the tenure of the author in whatever role they are vacating. My intentional avoidance of these clichés and related metaphorical tropes has less to do with any dislike of them per se, and nearly everything to do with a genuine excitement for the future of the RASC.

First, having been a member of both the former RASC governing body, the RASC Council, and then the current Board/Executive Director structure, the current model has the advantage. It affords an agility that allows for greater flexibility and creativity in the face of rapid changes in the environment that we operate in, and the division of labour is much more effective in practical ways. Having an Executive Director allows for an office that is tightly focused on execution of strategy and managing the operations of the organization: membership services; Centre services; publications; relations with the corporate, scientific, and greater community; fundraising, and so on. With some overlap with the Executive Director's office, this allows the Board to focus on the whole playing field in the realms of vision, strategy, policy, governance, and oversight.

Second, with the new strategic plan, crafted with input from those we serve, we have a roadmap of things that must be done to enhance the value of membership, serve the needs of our Centres to enhance their ability to bring value to their members and the wider communities that they are part of, and to broaden our reach into Canadian society. We have an abundance of opportunities to welcome younger Canadians, women, and the many diverse communities that make up the social fabric of our country into the RASC tent. I'm excited to be a part of that effort and to watch it unfold over the next several years.

Last (and only last because of space constraints), I remain enthusiastic about the RASC, perhaps even more so than ever before. Our many volunteers, publications editors, staff, and members are truly remarkable people. I honestly feel that I've gained so much more from the RASC than I've given, hence my passion for volunteering and serving it however I can. In the past 20 or so years, I've gained confidence as a public speaker, gained confidence in myself, became a better visual observer of the deep sky, made cherished lifelong friend-

ships, visited parts of the country I'd not seen before, pushed myself well outside of my comfort zone, and had myself knocked down a peg or two and became a better person for it.

To all my fellow RASCals, thank you for allowing me to serve. I'm looking forward to our next meeting under dark skies, at your Centre meetings, and at the next General Assembly in Calgary for our 150th! ✨

News Notes / En Manchette

Compiled by Jay Anderson FRASC

The ESO's Extremely Large Telescope breaks new ground

On May 26, ground-breaking ceremonies celebrating the beginning of construction of the European Southern Observatory's Extremely Large Telescope (ESO ELT) were held in northern Chile at the Paranal Observatory site. The event was attended by the President of the Republic of Chile, Michelle Bachelet Jeria, who was welcomed by Tim de Zeeuw, Director General of ESO, Roberto Tamai, the ELT Program Manager, and Andreas Kaufer, the Director of the La Silla Paranal Observatory. The ceremony was attended by many distinguished international and Chilean guests from government and industry, along with ESO scientists and engineers, and local and international media representatives.

In her address to the assembly, President Jeria emphasized: *"With the symbolic start of this construction work, we are building more than a telescope here: it is one of the greatest expressions of scientific and technological*

capabilities and of the extraordinary potential of international cooperation."

With a main mirror 39 metres in diameter, the ELT will be the largest optical/infrared telescope in the world. It will be housed in an enormous rotating dome 85 metres in diameter—comparable in area to a football pitch (a soccer field). The ELT will be the biggest "eye" ever pointed toward the sky and will tackle a wide range of scientific challenges: probing Earth-like exoplanets for signs of life; studying the nature of dark energy and dark matter; and observing the Universe's early stages to explore our origins. It will also raise new questions we cannot conceive of today and introduce new technology and engineering breakthroughs.

In related news, the secondary mirror for the ELT, 4.2 metres in diameter and weighing 3.5 tonnes, was successfully cast by SCHOTT at Mainz, Germany. It is the largest secondary mirror ever employed on an optical telescope, larger even than some research telescopes in use today. The mirror blank was cast in Zerodur® glass-ceramic, which will now be ground and polished to produce the finished mirror. The blank now has to go through a slow cool-down, machining, and



Figure 1 — This artist's rendering shows the Extremely Large Telescope in operation on Cerro Armazones in northern Chile. The telescope is shown using lasers to create artificial stars high in the atmosphere. Image: ESO/L. Calçada.

Cassini completes sixth pass through Saturn's rings

Cassini made its sixth high-speed pass through the space between Saturn's rings and the planet on May 28, an orbit that came close enough to the innermost D ring that its instruments could directly sample the ring particles. The May 28 flyby was the closest Cassini will come to Saturn's D ring, though it is the first of four to pass through the region. As in the earlier passages, the High Gain Antenna (HGA) was pointed in the direction of travel in order to intercept any particles that might be big enough to affect the spacecraft's instruments and engineering systems. During the six-minute ring crossing, the Radio and Plasma Wave Science (RPWS) instrument recorded impacts of ring particles on the spacecraft, which are detectable to RPWS by the plasma clouds they generate when they hit. Just before speeding southbound past Saturn's equator and prior to the HGA shielding turn, Cassini's Radar instrument carried out a first-ever observation of rings using the Synthetic-Aperture Radar imaging technique. Scanning from the outer edge of the A ring inward through the C ring, the resulting imaging resolutions are expected to range from 4 kilometres down to 100 metres. They are sensitive to centimetre-scale ring particles and larger, and so the results will allow ring scientists to study a different portion of the ring particles' size distribution.

Also around the ring-plane crossing, other optical remote-sensing instruments were active, making the best use of the opportunity to observe Saturn's rings at close range, including the sunlit side and the unlit side. In all, these instruments collected data for 14.6 hours, including some of the highest-resolution ring images ever obtained. After the ring crossing came an 8.5-hour Radio Science ring occultation experiment, involving four Deep Space Network and two ESA ground stations,



Figure 2 — Opening of the ELT secondary mirror blank mould, containing the still very hot ZERODUR® glass at first annealing. The blank was transferred from the SCHOTT melting facility to the SCHOTT 4-metre blank annealing facility in Mainz, Germany, in May. The casting of this mirror is a major step toward building the world's biggest eye on the sky, one of ESO's greatest feats. Image: SCHOTT/ESO

heat treatment sequence over the next year, when it will then be ready to be ground to precisely the right shape and polished. The blank will be shaped and polished to a precision of 15 nanometres across the entire optical surface.

When completed and installed, the M2 mirror will hang upside down above the telescope's huge primary mirror and form the second element of the ELT's novel five-mirror optical system. The mirror is strongly curved and aspheric and is a major challenge to make and test.

Compiled with material provided by the ESO

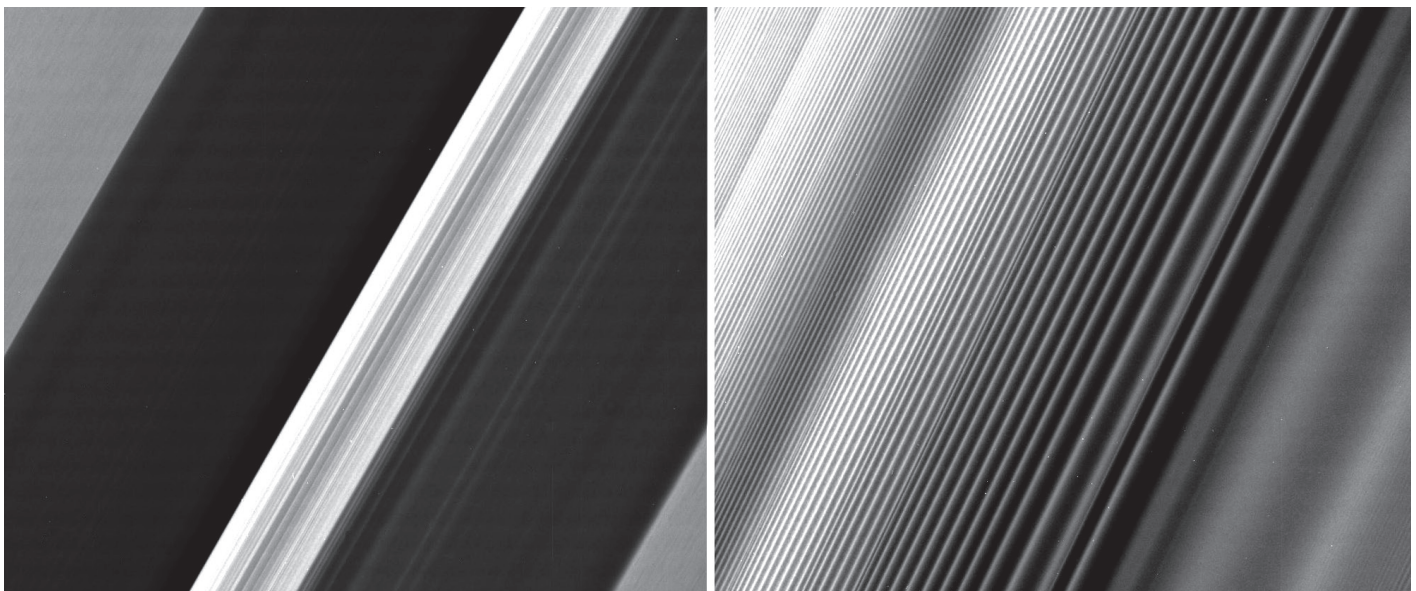


Figure 3 — Oblique views of Saturn's rings acquired during the sixth pass through the planet's ring system. Images: NASA.

There are a million reasons to stay home.
And billions more not to.
SubaruDarkSky.ca



OUTBACK



spanning three continents, to record Cassini's radio transmitters as the spacecraft passed behind the rings.

On May 29, Cassini made a 7.1-hour observation of the icy plume that is constantly coming from Saturn's small active moon Enceladus, and on May 30, turned its attention to the two-tone moon Iapetus. That day was capped by a 17-hour observation of Saturn's small, irregular moon Bebhionn, one of the few objects orbiting Saturn that might have a binary or contact-binary nature.

Cassini has 16 more Grand Finale Proximal orbits, which have a period of 6.4 days in a plane inclined 62.4 degrees from the planet's equatorial plane. Each orbit stretches out to an apoapsis altitude of about 1,272,000 km from Saturn, where the spacecraft's planet-relative speed is around 6,000 km/hr. At periapsis, the distance shrinks to about 2,500 km above Saturn's visible atmosphere, reaching an orbital speed of around 123,000 km/hr.

Compiled in part with material provided by NASA

Another moon for the Solar System

The combined power of three space observatories, including NASA's *Hubble Space Telescope*, has helped astronomers uncover a moon orbiting the third largest dwarf planet, catalogued as 2007 OR₁₀. The pair resides

in the frigid outskirts of the Kuiper Belt, a realm of icy debris left over from our Solar System's formation 4.6 billion years ago. With this discovery, most of the known dwarf planets in the Kuiper Belt larger than 600 miles across have companions. These bodies provide insight into how moons formed in the young Solar System. "The discovery of satellites around all of the known large dwarf planets—except for Sedna—means that at the time these bodies formed billions of years ago, collisions must have been more frequent, and that's a constraint on the formation models," said Csaba Kiss of the Konkoly Observatory in Budapest, Hungary. He is the lead author of the science paper announcing the moon's discovery. "If there were frequent collisions, then it was quite easy to form these satellites."

The objects most likely slammed into each other more often because they inhabited a crowded region. "There must have been a fairly high density of objects, and some of them were massive bodies that were perturbing the orbits of smaller bodies," said team member John Stansberry of the Space Telescope Science Institute in Baltimore, Maryland. "This gravitational stirring may have nudged the bodies out of their orbits and increased their relative velocities, which may have resulted in collisions."

But the speed of the colliding objects could not have been too fast or too slow, according to the astronomers. If the impact velocity was too fast, the smash-up would

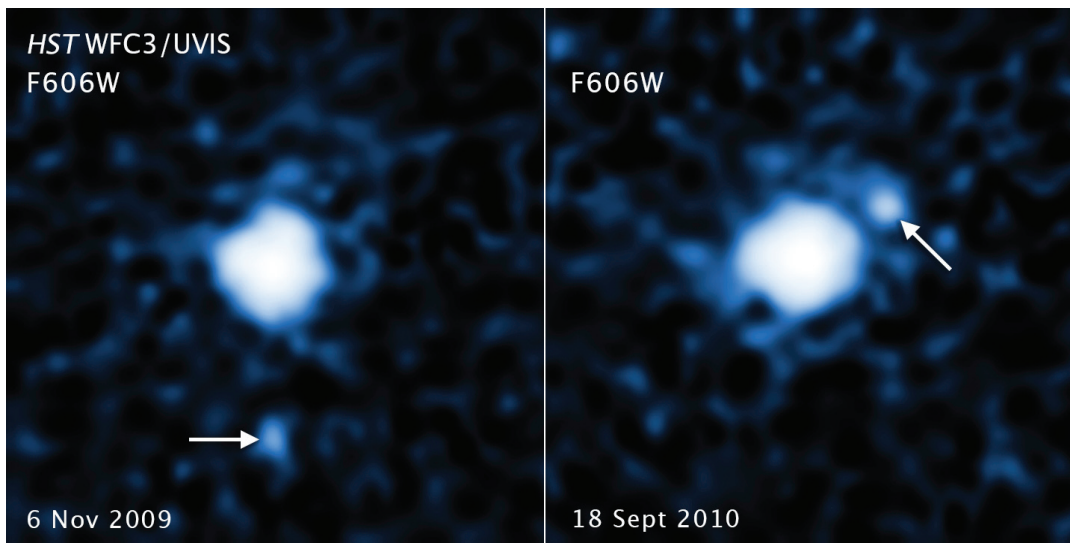


Figure 4 — Legacy Hubble Space Telescope images of 2007 OR₁₀ and its newly identified moon. Image: NASA, ESA, and C. Kiss (Konkoly Observatory), and J. Stansberry (STScI).

have created lots of debris that could have escaped from the system; too slow and the collision would have produced only an impact crater.

Collisions in the asteroid belt, for example, are destructive because objects are travelling fast when they smash together. The asteroid belt is a region of rocky debris between the orbits of Mars and the gas giant Jupiter. Jupiter’s powerful gravity speeds up the orbits of asteroids, generating violent impacts.

The team uncovered the moon in archival images of 2007 OR₁₀ taken by *Hubble’s* Wide Field Camera 3. Observations taken of the dwarf planet by NASA’s *Kepler Space Telescope* first tipped off the astronomers of the possibility of a moon circling it. *Kepler* revealed that 2007 OR₁₀ has a slow rotation period of 45 hours. “Typical rotation periods for Kuiper Belt Objects are under 24 hours,” Kiss said. “We looked in the *Hubble* archive because the slower rotation period could have been caused by the gravitational tug of a moon. The initial investigator missed the moon in the *Hubble* images because it is very faint.”

The astronomers spotted the moon in two separate *Hubble* observations spaced a year apart. The images show that the moon is gravitationally bound to 2007 OR₁₀ because it moves with the dwarf planet, as seen against a background of stars. However, the two observations did not provide enough information for the astronomers to determine an orbit. “Ironically, because we don’t know the orbit, the link between the satellite and the slow rotation rate is unclear,” Stansberry said.

The astronomers calculated the diameters of both objects based on observations in far-infrared light by the *Herschel Space Observatory*, which measured the thermal emission of the distant worlds. The dwarf planet is about 950 miles across, and the moon is estimated to be 150 miles to 250 miles in diameter. 2007 OR₁₀, like Pluto, follows an eccentric orbit, but it is currently three times farther than Pluto is from the Sun. 2007 OR₁₀ is a member of

an exclusive club of nine dwarf planets. Of those bodies, only Pluto and Eris are larger than 2007 OR₁₀.

Prepared using material supplied by NASA.

The Boomerang returns

An ancient, red-giant star in the throes of a frigid death has produced the coldest known object in the cosmos—the Boomerang Nebula. How this star was able to create an environment strikingly colder than the natural background temperature of deep space has been a compelling mystery for more than two decades.

The answer, according to astronomers using the Atacama Large Millimetre/submillimetre Array (ALMA), may be that a small companion star has plunged into the heart of the red giant, ejecting most of the matter of the larger star as an ultra-cold outflow of gas and dust. This outflow is expanding so rapidly—about 10 times faster than a single star could produce on its own—that its temperature has fallen to less than half a degree Kelvin (−272 °C). The cooling process is analogous to the cool flow of air when a tire valve is released, allowing the contents to expand adiabatically into the surrounding air. The ALMA observations enabled the researchers to unravel this mystery by providing the first precise calculations of the nebula’s extent, age, mass, and kinetic energy.

“These new data show us that most of the stellar envelope from the massive red-giant star has been blasted out into space at speeds far beyond the capabilities of a single, red-giant star,” said Raghvendra Sahai, an astronomer at NASA’s Jet Propulsion Laboratory in Pasadena, California, and lead author on a paper appearing in the *Astrophysical Journal*. “The only way to eject so much mass and at such extreme speeds is from the gravitational energy of two interacting stars, which would explain the puzzling properties of the ultra-cold outflow.” Such close companions may be responsible

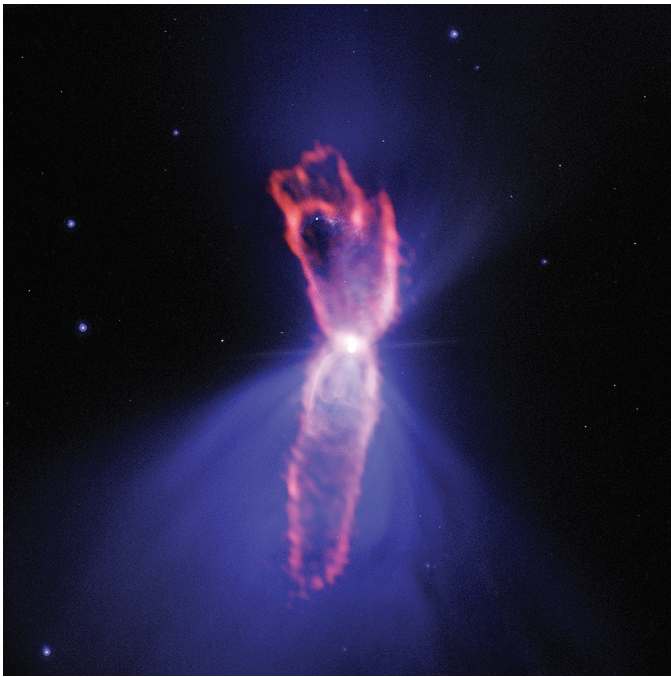


Figure 5 — A composite image of the Boomerang Nebula, a pre-planetary nebula produced by a dying star. ALMA observations (orange) show the hourglass-shaped outflow, which is embedded inside a roughly round ultra-cold outflow. The ALMA data are shown on top of an image from the Hubble Space Telescope. Image: ALMA (ESO/NAOJ/NRAO); NASA/ESA Hubble; NRAO/AUI/NSF

for the early and violent demise of most stars in the Universe, Sahai noted.

The Boomerang Nebula is located about 5000 light-years from Earth in the constellation Centaurus. The red-giant star at its centre is expected to shrink and get hotter, ultimately ionizing the gas around it to produce

a planetary nebula—a nebula created when stars like our Sun (or a few times bigger) shed their outer layers as an expanding shell near the end of their nuclear-fusion-powered life. The Boomerang Nebula represents the very early stages of this process, a so-called pre-planetary nebula. It's a short-lived transition phase, lasting only about 1000 years, and so our view of the Boomerang comes at a unique time in its life.

When the Boomerang Nebula was first observed in 1995, astronomers noted that it was absorbing the light of the Cosmic Microwave Background, which is the leftover radiation from the Big Bang. This radiation provides the natural background temperature of space—only 2.725 degrees above absolute zero. For the Boomerang Nebula to absorb that radiation, it had to be even colder than this lingering, dim energy that has been continually cooling for more than 13 billion years.

The new ALMA observations also produced an evocative image of this pre-planetary nebula, showing

Coaching can transition you to a more senior position, make you a better executive and develop a stellar strategic plan for your company.

- Achieve better results
- Build trust with employees
- Become more productive, decisive and effective



Call Dr. Wilma Slenders for a no-obligation consultation today



TRANSCEND
MANAGEMENT ADVISORS INC

1 403 547 7900 | www.transcendmgt.com | wilma@transcendmgt.com | [in](#) [tw](#)

an hourglass-shaped outflow inside a roughly round, ultra-cold outflow. The hourglass outflow stretches more than a third of a light-year, the result of a jet that is being fired by the central star, sweeping up the inner regions of the ultra-cold outflow like a snowplow. The ultra-cold outflow is more than 10 times bigger, about 3 light-years in extent. Travelling more than 150 kilometres per second, it took material at its outer edges approximately 3500 years to reach these extreme distances after it was first ejected from the dying star. These conditions, however, will not last long. Even now, the Boomerang Nebula is slowly warming.

“We see this remarkable object at a very special, very short-lived period of its life,” noted Lars-Åke Nyman, an astronomer at the Joint ALMA Observatory in Santiago, Chile, and co-author on the paper. “It’s possible these super cosmic freezers are quite common in the Universe, but they can only maintain such extreme temperatures for a relatively short time.”

Compiled using material provided by the National Radio Astronomy Observatory

Who needs *New Horizons* anyway?

On June 3, July 7, and July 17, MU69 will occult three separate stars. Why do we care?

Well, 2014 MU69 is the Kuiper Belt object to which the *New Horizons* spacecraft is headed after its successful flypast of Pluto. And, if the observations are successful, they won’t detract from the up-close-and-personal view that the enormously successful spacecraft has planned for 2019 January 1. NASA teams are pulling out all the stops to observe the occultations, and, as of this writing, have successfully captured the first of the eclipses.

To observe the June 3 “stellar occultation,” more than 50 team members and collaborators were deploying along projected viewing paths in Argentina and South Africa. They were fitted with camera-equipped portable telescopes to focus on the occultation star and watch for changes in its brightness that can tell them much about MU69 itself. Clear skies on the critical night allowed each team to collect around 5400 half-second images of the field around MU69, though the good weather also left them facing an extended period of data analysis before results are available.

“Our primary objective is to determine if there are hazards near MU69—rings, dust, or even satellites—that could affect our flight planning,” said *New Horizons* Principal Investigator Alan Stern, of Southwest Research Institute (SwRI) in Boulder, Colorado. “But we also expect to learn more about its orbit and possibly determine its size and shape. All of that will help feed our flyby planning effort.”

Marc Buie, the *New Horizons* co-investigator from SwRI who is leading the occultation observations, said that because MU69 is so small—thought to be about 40 kilometres across—the occultations should only last about two seconds. But scientists can learn a lot from even that, and observations from several telescopes that see different parts of the shadow can reveal information about an object’s shape as well as its brightness.

The mission team had 22 new, portable, 40-centimetre telescopes (some are Dobsonians!) at the ready, along with three other portables and over two-dozen fixed-base telescopes that are located along the occultation path through Argentina and South Africa. But deciding exactly where to place them was a challenge.

This particular Kuiper Belt object was discovered just three years ago, so its orbit is still largely unknown. The team used star-position data from the extensive catalogue of the European Space Agency’s *Gaia* mission and *Hubble Space Telescope* position measurements of MU69 to predict the narrow occultation path. But without a precise fix on the object’s position—or on the exact path its narrow shadow might take across Earth—the team spaced the telescope teams along “picket fence lines,” one every 10 or 25 kilometres, to increase the odds that at least one or more of the portable telescopes will catch the centre of the event and help determine the size of MU69.

For the July 10 occultation, the team gets help from above in the form of a powerful 2.5-metre telescope on NASA’s airborne Stratospheric Observatory for Infrared Astronomy (SOFIA). Enlisting SOFIA, with its vantage point above the clouds, takes the bad weather factor out of the picture. The plane also should be able to improve its measurements by maneuvering into the very centre of the occultation shadow. This continues a history of coordination between SOFIA and *New Horizons* missions. Researchers used SOFIA to make similar observations of Pluto as it passed in front of a background star, just before *New Horizons* flew past Pluto in 2015. ★

Compiled in part from material supplied by NASA

Is your address correct? Are you moving?

If you are planning to move, or your address is incorrect on the label of your Journal, please contact the office immediately.

By changing your address in advance, you will continue to receive all issues of SkyNews and the Observer’s Handbook.

(416) 924-7973 www.rasc.ca/contact

Diamond Ring and Black-Drop Effects during Eclipses of the Sun—Mechanisms of Formation

By Duval, Michel* and Lamarre, Laurent

*Member of RASC and Amateur astronomy clubs of Montreal (SAM) and Dorval (CADFS) (duvalm@ireq.ca)

Abstract

The mechanism of formation of diamond rings and limb-darkening/black-drop effects during eclipses of the Sun is shown to be due to the halos of diffraction around the Moon and the Sun and to the imperfect optical resolution of the instruments used. It is similar to the mechanism of formation of black-drop effects during the Transits of Venus and Mercury against the Sun. The differences between the black drops of Mercury, Venus, and the Moon are due to their differences in diameter.

Résumé

Le mécanisme de formation des bagues de diamant et des effets de noircissement de bord et de goutte noire pendant les éclipses du Soleil est dû aux halos de diffraction autour de la Lune et du Soleil, en raison de la résolution optique imparfaite des instruments utilisés. Ce mécanisme est semblable à celui de la goutte noire pendant les Transits de Vénus et Mercure devant le Soleil. Les différences entre les gouttes noires de Mercure, Vénus, et la Lune sont attribuables à leurs différences de diamètre.

1. Light and Darkness

Cycles of the Sun (day and night, light and darkness, summer and winter) have been associated with cycles of life and death and resurrection in all cultures and religions. The animal and vegetal worlds are also sensitive to these cycles, although in more subtle ways, using chemical messages that we do not fully understand yet.

During eclipses of the Sun, these cycles of light and darkness and light again occur in just a few minutes rather than days or months, dramatically reminding observers of the glory of light and life, the terror of darkness and death, the shortness of life and its miraculous resurrection through new generations, explaining why eclipses are so emotionally charged.

2. Diamond Ring Effects during Total Eclipses of the Sun

Total eclipses of the Sun occur during transits of the Moon against the Sun, when the disk of the Moon is equal to or slightly larger than the disk of the Sun, and their centres both located on the trajectory of the Moon in the sky.

Among the remarkable phenomena occurring during total eclipses of the Sun, attracting thousands or millions of observers, are the gradual disappearance of the Sun, the sudden passage of light to darkness and the sudden drop in air temperature on the ground.

Even more spectacular is the formation of “diamond rings” and corona flares around the Sun, as illustrated in Figure 1 during the total eclipse of March 2016 in Libya (*SkyNews*, July/August 2016, p.12).

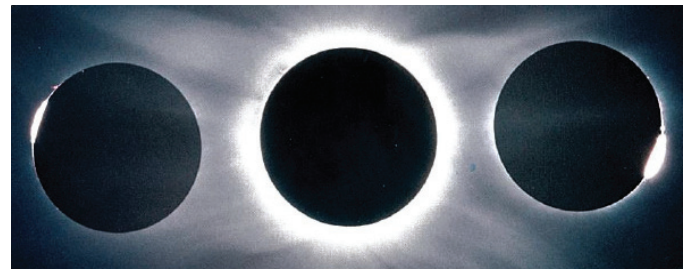


Figure 1 — Total Eclipse of the Sun of March 2016 in Libya

While the diamond ring effect has been widely observed and photographed in past decades, its mechanism of formation has not been explained in detail yet. This paper shows that it is very similar to the mechanism of formation of the black-drop effect during transits of Venus and Mercury against the Sun (Duval et al., *JRASC*, 2005, 2012, and 2017).

It is essentially due to the formation of optical halos of diffraction above dark objects (e.g., black disk of planets, dark sky) in contact with the bright disk of the Sun. These halos of diffraction are in turn due to the imperfect optical instruments used to observe them (eyes, cameras, telescopes). They are formed by the “blurring” of bright light of the Sun over and above dark objects in contact with it.

Because of these halos of diffraction, the apparent black disks of planets and Moon transiting over the Sun are smaller than their real disks, while the apparent bright disk of the Sun in contact with the dark sky is larger than its real disk. This is illustrated schematically in Figures 2a to 2d, where the Moon is moving progressively over the Sun from left to right, just after the total eclipse in Fig 2a and Fig 1 (centre).

The real and apparent disks of the Moon and the Sun have been identified as during the transits of Venus and Mercury:

-A = real (black) disk of the Moon in the photo on the left of Figure 1.

- B = real disk of the Sun, indicated in astronomical handbooks as $B = A/1.044$ on the day of the eclipse of March 2016 (RASC *Observer's Handbook*, 2016).
- H = halos around A and B appearing in Fig. 2c-2d when A does not cover B entirely any more.
- C = $A - H$ = apparent disk of the Moon in contact with B, smaller than the real disk of the Moon A
- D = $B + H$ = apparent disk of the Sun against the dark sky, larger than its real disk B
- C and D appear in Fig. 2c-2d

H has been evaluated as half the width (perpendicular to the disk of the Moon) of the diamond ring in the photo on the left of Fig 1, i.e. $\sim 100''$ (arcseconds), by comparison with the angular diameter of the Sun ($\sim 1920''$). H is related to the optical resolution of the camera used for the photos in Fig. 1. In photos of other eclipses, the size of H may be different, depending on the resolution of the instrument/ camera used and of seeing conditions.

The abbreviations used in Fig. 2a to 2d are summarized in Table 1.

A	Real Disk of the Moon (in blue)
B	Real Disk of the Sun (red)
C	Apparent Disk of the Moon (green)
D	Apparent Disk of the Sun (orange)
E, F	Points Where A and B Intersect

Table 1 – Abbreviations Used in Fig. 2a to 2d

The faint horizontal and vertical coordinates (x,y) in Fig 2a to 2d are those used in the Excel program developed to represent disks A, B, C and D, the diamond ring and the crescent of Sun. Each disk in Fig. 2a to 2d has been built from ~ 2000 individual Excel (x,y) points, in order to very precisely determine the positions of A, B, C, D, E, and F, which sometimes are extremely close to one another.

Fig. 2a (top left) corresponds to the total eclipse of the Sun in the centre of Fig. 1, when the real disk of the Moon A entirely covers the real disk of the Sun B, which is slightly smaller. There are no halos around A and B at this stage and therefore no apparent disks C and D, because not a single part of B is in contact with A or the sky.

The October *Journal* deadline for submissions is 2017 August 1.
See the published schedule at
www.rasc.ca/sites/default/files/jrascschedule2017.pdf

In Fig. 2b (top right), A has moved slightly from left to right, becoming just tangent to B, but still totally covering B.

In Fig. 2c (bottom left), A has moved further to the right, intersecting B at points E and F, with a small arc of B now not covered any more by A between these two points. The very bright light of the Sun in this small arc of B immediately creates a halo H above and inside A and therefore a smaller apparent disk of the Moon C. It also creates a halo above the sky in contact with B, and therefore a larger apparent disk of the Sun D.

The width of these halos H (perpendicular to the Moon and Sun) gradually decreases when they approach points E and F, where B is still totally covered by A and cannot produce any halo, creating the diamond-ring shape observed in Fig.2c and Fig. 1.

The width of the small arc of B between E and F has been measured as $1.6''$, which is very small. By comparison, the diameter of Mercury in the sky is $\sim 8''$.

In Fig. 2d (bottom right), A has moved still further to the right, transforming the diamond ring into a crescent of bright Sun. Further displacements of A to the right, into the formation of a partial eclipse, are available upon demand from the authors.

Prior to the total eclipse in Fig. 2a, a symmetrical diamond effect had formed in the photo on the right of Fig. 1, following a mechanism of formation similar to the one in Fig. 2c but in the opposite part of A.

3. Black-Drop and Other Effects during Annular Eclipses

Annular eclipses of the Sun occur during transits of the Moon against the Sun, when the disk of the Moon is smaller than the disk of the Sun, and their centres are both located on the trajectory of A in the sky, as in the case of total eclipses.

Spectacular “rings of fire” are formed during these annular eclipses (Fig. 3a). Also, limb-darkening or “black-drop” effects similar to those observed during transits of Venus and Mercury against the Sun (Fig. 3b and 3c). These limb-blackening/black-drop effects, however, are rarely reported because they are less spectacular than the rings of fire.

In rare cases, combinations of a limb-darkening effect and small diamond ring (“Baily’s bead”) can also be observed (Fig. 3c).

Photos in Fig. 3a, 3b, and 3c were taken during the annular eclipses of May 2012 in the US, 2016 September 1 in the island of La Réunion, and 2017 February 26 in Chubut, Argentina, respectively.

The mechanism of formation of limb-darkening/black-drop effects during the transits of the Moon against the Sun is the

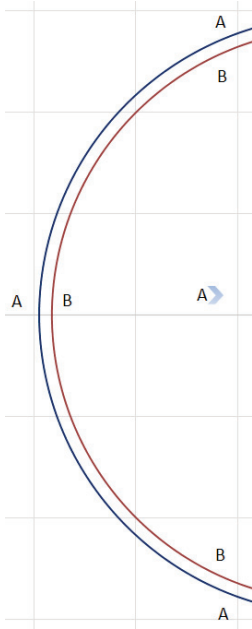


Fig 2a: Total Eclipse of the Sun (Real Disk of Moon A is larger than Real Disk of Sun B) (Fig 1, centre)

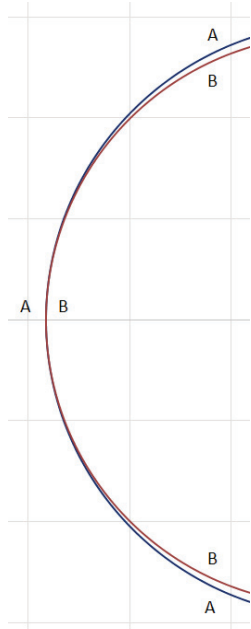


Fig 2b: A has moved to the right, but A and B are still tangent

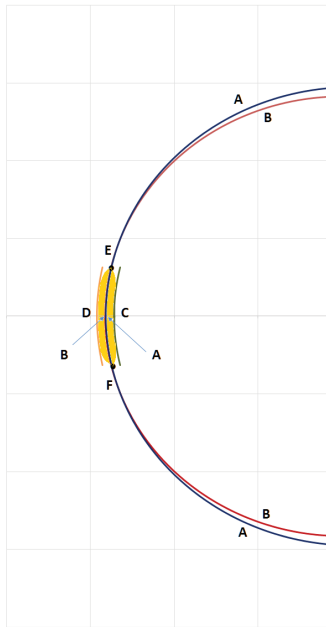


Fig 2c: A and B intersect in E and F. Apparent Disks of Moon C and Sun D and a "Diamond Ring" are formed between E and F (Fig 1, left)

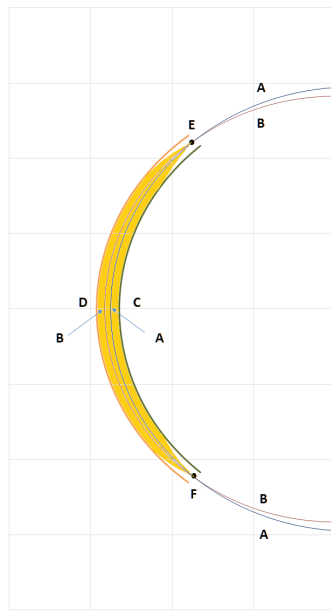


Fig 2d: Moments later, a crescent of Sun is formed

Figures 2a (top left) to 2d (bottom right) — Mechanism of Formation of Diamond Ring and Apparent Disks of the Moon C and Sun D, just after the Total Eclipse of Fig. 2a and Fig. 1 (centre). Moon A is moving over Sun B from left to right in Fig. 2a to 2d. A and B intersect at points E and F.



Fig 3a: Ring of fire

Fig 3b: Limb-darkening/Black-Drop Effect

Fig 3c: Bailey's bead

Figures 3a to 3c — Annular Eclipses of May 2012, April 2014, and February 2017, respectively

same as during transits of Venus and Mercury (Duval et al., *JRASC*, 2005, 2012, and 2017), i.e. they are due to the formation of optical halos around the real disks of the Moon and the Sun, and of apparent disks of the Moon and the Sun that are different from their real disks.

This is illustrated schematically in Fig. 4a to 4d, starting in Fig. 4a (top left) from the photo in Fig. 3a. The Moon is moving over the Sun from right to left in these Figures.

The apparent and real disks of the Moon and the Sun have been identified in the photo of Fig. 3a as during the transits of Venus and Mercury against the Sun:

- C = apparent black disk of the Moon against the Sun
- D = apparent bright disk of the Sun against the sky.
- H = red halo, apparently around C but actually inside and above A.
- H = red halo, apparently inside D but actually above the sky.
- A = C + H = real disk of the Moon, larger than its apparent disk C.
- B = D - H = real disk of the Sun, smaller than its apparent disk D.

The abbreviations used in Fig. 4a to 4d are the same as in Fig. 2a to 2d and are indicated in Table 1.

The width of the red halos H (perpendicular to the Moon and Sun) has been evaluated as $\sim 90''$, by comparison with the angular diameter of the Sun ($\sim 1920''$), and is related to the optical resolution of the camera used for the photo in Fig. 3a.

The horizontal and vertical coordinates (x,y) in Fig. 4a to 4d are those used in the Excel program developed to precisely

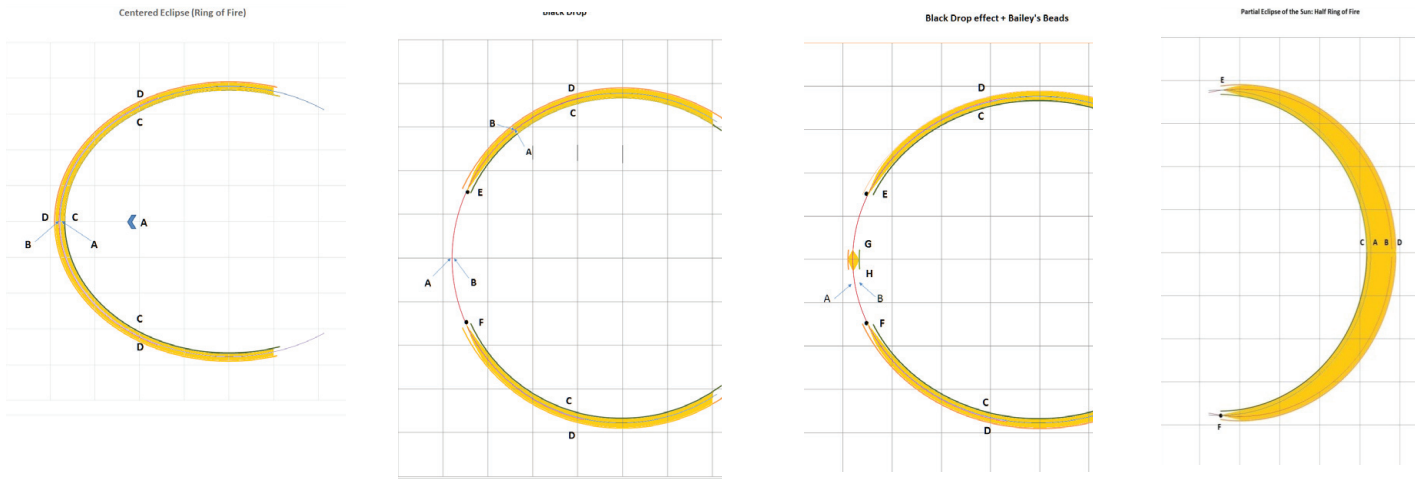


Fig. 4a (top left) schematically shows the annular eclipse of Fig. 3a at its peak, appearing as a “ring of fire” between the apparent disks of the Moon C and Sun D.

In Fig. 4b (middle left), A has moved slightly to the left, totally covering B between points E and F, where the halos and the apparent disks C and D totally disappear, creating a limb-darkening effect as in Fig. 3b.

Fig. 4c (middle right) shows how small diamond rings can be formed in rare cases at this stage, when a very small area of the real disk of the Sun B appears in a small notch between plateaux or mountains at the surface of the real disk of the Moon A. The halos immediately reappear in this small area, forming a small diamond ring or “Bailey’s bead”. A large limb-darkening/black-drop effect is also apparent in Fig. 4c and 3c

In Fig. 4d (top right), as A moves further to the left the ring of fire becomes a crescent of Sun on the opposite side of the Sun.

Figures 4a (top left) to 4d (top right) – Mechanism of Formation of Ring of Fire, Limb-Darkening/Black-Drop and Bailey’s Bead Effects during the Annular Eclipses of Fig. 3a to 3c. The Moon is moving over the Sun from right to left of Fig. 4a to 4d.

represent disks A, B, C, and D, the limb-darkening/black-drop effect, Bailey’s bead and crescent of Sun.

The length L of the limb-darkening/black-drop effect (tangent to disks A and B) is visually longer during transits of the Moon than during transits of Venus and Mercury, and its width W (perpendicular to disks A and B) is narrower. Also, the L/W ratios for the Moon, Venus, and Mercury (60, 12 and 1, respectively) are linearly correlated with their diameters in arcseconds (1920”, 50”, and 8”, respectively), as predicted during the investigation on the black-drop effect of Mercury (Duval et al., JRASC 2017).

4. Predictions of Eclipse Effects

The Excel program developed for this paper allows predicting eclipse effects that have not been photographed or reported yet.

For instance, Fig. 5a shows a predicted, smaller black-drop effect that could be observed during annular eclipses, looking more like the black-drop effects observed during the transits of Venus and Mercury.

Fig. 5b shows what should be observed during total eclipses slightly outside of the path of totality (or on the edges of it, where the totality is shorter). The path of totality typically is ~100 km wide.

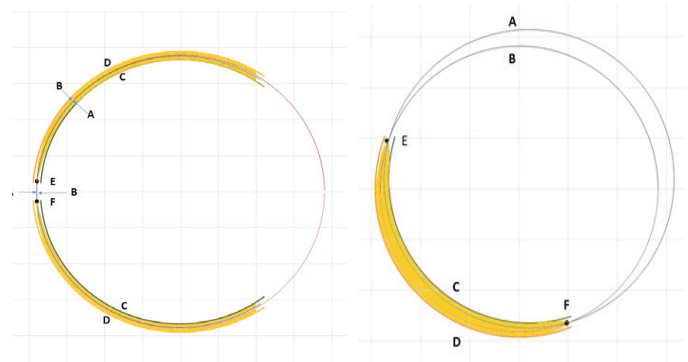


Fig 5a: Predicted Black-Drop Effect During Annular Eclipses

Fig 5b: Predicted Eclipse Slightly Outside of Path of Totality during Total Eclipses

Figure 5 – Predictions of Eclipse Effects with the Excel Program

The Excel program also allows simulating the eclipse effects observed with instruments of different optical resolution (eyes, low resolution cameras, high resolution telescopes), at different ground locations around the eclipse and at different stages of it. Readers interested to receive such a simulation corresponding to their specific situations can contact the authors.

5. Conclusions

The formation of diamond rings, limb-darkening and black-drop effects and Baily's beads during total and annular eclipses of the Sun is due to the formation of optical halos of diffraction of the bright light of the Sun around the Moon and the sky, and to the formation of apparent disks of the Moon and the Sun, which are different from their real disks, as during the transits of Venus and Mercury against the Sun.

These halos of diffraction are related to the imperfect optical resolution of the instruments used to observe the eclipses (eyes, cameras, telescopes). The lower the resolution, the larger the halos.

The size of the limb-darkening/black-drop effects during the transits of Venus, Mercury and the Moon against the Sun is related to their diameters, becoming wider, narrower, and more flattened as these diameters increase.

Observers of the August 2017 total eclipse in the US and of future annular eclipses are invited to take time-lapse photos of the diamond ring and black-drop effects, in order to confirm the mechanisms of formation described in this paper. A webcam camera able to record 10 frames per second as

during the transits of Venus (Duval et al., *JRASC*, 2005) would be suitable for that purpose. ★

References

- Duval, M., Gendron, A., St-Onge, G., and Guignier, G. (2005), The Black-Drop Effect during the Transit of Venus on June 8, 2004, *JRASC*, 99 (55), 170-176.
- Duval, M., Brault, M., Gendron, A., Gohier, J.M., Guignier, G., St-Onge, G., Sauv , R., Savoie, M., Stefanescu, A., Tomaras, F., and Tremblay Y. (2012), Size of the Black-Drop Effect versus Telescope Resolution, *JRASC*, 106 (6), 227-229.
- Duval, M., Sauv , R., and St-Onge, G., (2017), A Comparison of the Black-Drop Effects during the Transits of Mercury in 2016 and Venus in 2004-2012, *JRASC*, 111 (1), 7-9.
- Anderson, J., (2016), Waiting for the Big One, *SkyNews*, July/Aug., 10-14.
- Observer's Handbook*, Toronto, Canada, RASC, 2016.
- Associated Press, (2012), And it Burns, Burns, Burns –the Ring of Fire! Solar eclipse Dazzles in the Sky above Western U.S. and Asia, *MailOnline*, May 21.
- Mc Carty, C., Matthiew, B., and Johnson, M., (2014), Southern Annular Eclipse, *NASA Astronomy Picture of the Day*, April 26.
- Bedingfield, S. (2017), A Solar Eclipse with a Beaded Ring of Fire, *NASA Astronomy Picture of the Day*, March 1.

All-Star Telescope
www.All-StarTelescope.com

FREE SHIPPING
on most items*
*see website for details

NOW AVAILABLE—ONLY FROM ALL-STAR!

"I've just sat through the first lesson, and I ABSOLUTELY LOVE what you've done. The information is clear, practical and very well thought out. Your presentation style is warm and inviting, and the production quality is superb! This is, without question, one of the absolute best (if not *the* best) photo tutorials I've ever seen."
Angelo Ioanides, *ExtraOrdinary Vision* magazine

Canada's recipient of Celestron's Perspectives on Imaging award
1-866-310-8844
Didsbury, Alberta

Celestron's New CGX Mount

Nightscapes and Time-Lapses
A video tutorial by Alan Dyer
A VIDEO TUTORIAL BY ALAN DYER
Nightscapes and Time-Lapses
FROM FIELD TO PHOTOSHOP

Background photo: Flame Nebula by Ken From of All-Star Telescope

Featured Articles / Articles de fond

Maps of Light Pollution

by Peter D. Hiscocks (phiscock@ee.ryerson.ca) and Christopher C.M. Kyba, *Deutsches GeoForschungsZentrum GFZ, Potsdam, Germany, Leibniz-Institute of Freshwater Ecology and Inland Fisheries, Berlin, Germany.* (kyba@gfz-potsdam.de)

Introduction

Would you like to know the about the amount of artificial light at some location on the planet? There are two excellent online world maps that contain this information.

The first is the *Atlas of Light Pollution*¹. Figure 1 shows a screenshot.

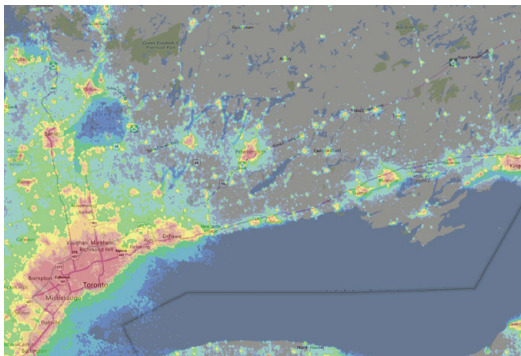


Figure 1 — *Atlas of Light Pollution* showing upward emissions of light in the areas north of Lake Ontario.

This is a world map containing measurements of upward emitted radiance from the satellite data *Visible Infrared Imaging Radiometer Suite (VIIRS) Day/Night Band (DNB)* instrument on the *Suomi NPP* satellite. The spacial resolution of this map is excellent. You can type in a location and the map will move to and identify that location. As an overview of the location of areas with little installed lighting—for an amateur astronomer who is searching for a stargazing site for example—it's very useful.

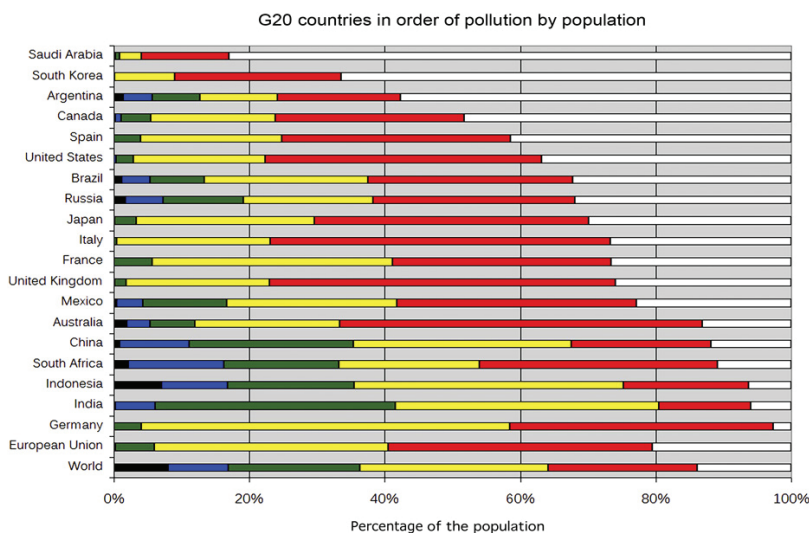


Figure 2 — Percentage of population living under different levels of artificial sky brightness (in mcd/m). Figure from [8] reproduced with permission.

A distance-measuring tool is available on the menus. For example, exploration with this tool shows that light from the Greater Toronto Area affects an area 80 to 100 kilometres in radius.

The light levels on this map are the radiance in $nanowatts/cm\text{-steradian}$. This is a measure of the total power received by the satellite from some location on earth, integrated over the measurement bandwidth from approximately 500-900 nm².

For those who wish to work with the original data, it is available on the web³.

Generally, astronomers quantify the sky brightness in units of *magnitudes per square arcsecond* ($mag/arcsec^2$).

A strongly light-polluted sky is about 18 $mag/arcsec^2$ (27 times brighter than a natural sky). Good observing sites generally have sky brightness above 21 $mag/arcsec^2$ (less than twice as bright as natural), which is the threshold for a “silver” designation by the International Dark-Sky Association.

Magnitudes per square arcsecond is a measure of luminance that can be measured by a Sky Quality Meter from Unihedron⁴, or it can be determined from the image of a calibrated digital camera^{5,6,7}.

To estimate the sky brightness from satellite observations, it is necessary to perform a radiative transfer simulation. Such a simulation takes into account the emission angles of the light, atmospheric scattering processes, and the sensitivity of the human eye. This was done by Fabio Falchi et al, who have produced another global map of light pollution.

The academic paper, *The New World Atlas of Artificial Night Sky Brightness*⁸ describes this process and discusses some of the results. For example, Figure 2 shows the ranking of G20 countries by percentage of population exposed to different levels of sky brightness. Canada ranks number 4, not something to be particularly proud of. Our country thankfully includes large areas with dark skies, but most Canadians live in an urban centre that is light polluted.

This second map, which contains luminance data that can be converted to SQM readings, is *The New World Atlas of Artificial Sky Brightness — CIRES*⁹. Figure 3 shows the map rendition of the area around Toronto.

Click on View Map Legend to see the range of luminances for each map colour. These values of luminance (not radiance) correspond to the brightness of the sky as seen by a human observer from a ground location. The values of luminance can be converted into SQM units using the formula:

$$\text{SQM}_{\text{pred}} = -2.5 \log_{10} \left(\frac{A + N}{10.8 \times 10^7} \right)$$

where

A is the artificial surface brightness in milli-candela per square metre from the map.

N is the natural sky brightness, approximately 0.236 milli-candela per square metre

SQM_{pred} is the predicted value of sky brightness in mag/arcsec².

For example, in the Toronto area, the second map shows a luminance of about 7.3 mcd/m². Substitute 7.3 for A in the formula yields an SQM value of 17.9. Typical measurements of SQM over Toronto using a Unihedron Sky Quality Meter are in the order of 18.2, so the prediction is very close to the measured value. The difference between map predictions and the SQM observations used in calibrating the map typically had a standard deviation of about 0.25 mag/arcsec².¹

The spacial resolution and location labelling of the first map is somewhat better than the second map, so it can be useful to identify an unlit location in the first map and then use the second map to determine the luminance and SQM value at that location.

In addition to the CIRES browser, you can access a KMZ layer with the World Atlas map for viewing in Google Earth¹⁰.

While satellite images are useful for looking at light pollution on a global scale, local observations are still extremely important. Local areas have different lighting technology compared to those assumed by the analysis, and local orthography and typical atmospheric clarity can also affect the results¹¹. If you have an SQM, it's now extremely easy to share your data with researchers around the world. The "Loss of the Night" app for iOS and Android devices allows you to upload handheld SQM observations with your position and time recorded automatically. For those who prefer submitting data via the web, Globe at Night allows users to submit SQM data via their webapp www.globeatnight.org/webapp. By submitting your data through these projects, it is automatically made available for everyone worldwide, and saved for posterity.

If you don't have an SQM, you can still contribute to monitoring changes in sky brightness by using your own eyes. Both Globe at Night and the Loss of the Night app are mainly designed for this purpose. While visual observations are less precise, they have the great advantage of being based on a well understood and slowly changing spectral response function. Data submitted to these projects can be viewed online at the My Sky at Night website^{12, 13}.

Congratulations and thanks to the scientist authors for these excellent tools and the supporting documentation. ★

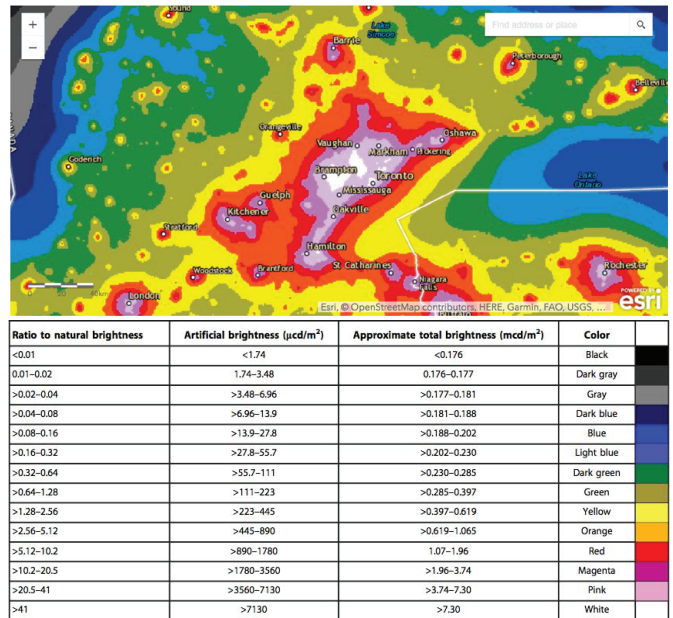


Figure 3 – The New World Atlas of Artificial Sky Brightness – CIRES

References

- 1 *Atlas of Light Pollution* www.lightpollutionmap.info
- 2 Illuminating the Capabilities of the Suomi National Polar-Orbiting Partnership (NPP) Visible Infrared Imaging Radiometer Suite (VIIRS) Day/Night Band, Miller et al., 2013 *Remote Sensing, Volume 5, Issue 12* www.mdpi.com/2072-4292/5/12/6717
- 3 DMSP & VIIRS Data Download <https://ngdc.noaa.gov/eog/download.html>
- 4 Unihedron <http://unihedron.com/projects/darksky/magconv.php>
- 5 *Measuring Luminance with a Digital Camera* Peter D. Hiscocks, 2014 www.ee.ryerson.ca/~phiscock
- 6 *LUMA: Luminance Analysis Software* Peter D. Hiscocks, 2016 www.ee.ryerson.ca/~phiscock
- 7 *Imaging and mapping the impact of clouds on skyglow with all-sky photometry*, Jechow, Kolláth, Ribas, Spoelstra, Hölker, Kyba, 2017 <https://arxiv.org/abs/1705.04968>
- 8 The new world atlas of artificial night sky brightness Falchi, Cinzano, Duriscoe, Kyba, Elvidge, Baugh, Portnov, Rybnikova and Furgoni *Science Advances, Vol 2, No. 6*, 2016 June 3 <http://advances.sciencemag.org/content/2/6/e1600377.full>
- 9 *The New World Atlas of Artificial Sky Brightness — CIRES* <http://cires.colorado.edu/Artificial-light>
- 10 *KMZ Data* http://pmd.gfz-potsdam.de/contact/NewWorldAtlas_ArtificialSkyBrightness.kmz
- 11 *Light pollution offshore: zenithal sky glow measurements in the Mediterranean coastal waters* Ges, Bará, García-Gil, Zamorano, Masana, 2017 <https://arxiv.org/abs/1705.02508>
- 12 *My Sky at Night* www.myskyatnight.com
- 13 Citizen Science Provides Valuable Data for Monitoring Global Night Sky Luminance Kyba, Christopher C.M., et al. *Scientific Reports 3* (2013)

Detection of Exoplanet τ Boötis b at the Simon Fraser University Trottier Teaching and Outreach Observatory

by Howard Trottier (trottier@sfu.ca)

Abstract

This is a report on the first detection of an exoplanet at Simon Fraser University's Trottier Observatory, based on radial-velocity (RV) measurements of the host star. The observatory is a teaching and public outreach facility with a 0.7-m aperture telescope under suburban skies. Measurements were done using a commercially manufactured, off-the-shelf, echelle spectrograph that is comparable in cost to high-end imaging systems, and that can be used to study a remarkable variety of astrophysical objects. The detected exoplanet is τ Boötis b, one of the first to be discovered by professionals, and is a "hot Jupiter." The exoplanet host star, τ Boötis A, is of magnitude 4.5, and spectral class F7V, and has one of the largest orbital RVs of any known host. Nevertheless, the Doppler shifts are tiny, and careful control of systematic uncertainties and sophisticated data-analysis methods are necessary for a successful detection. The RV was measured on ten nights, between mid-March 2016 and the end of June. The results cover most of the orbital cycle, and are in excellent agreement with the RV determined by professionals. This study provides one example of the many types of advanced spectroscopy projects that can be undertaken by undergraduate students at university teaching observatories, and by amateur astronomers, with increasingly affordable and easy-to-use equipment.

Introduction

Astronomical spectroscopy has long been a part of amateur astronomy, though until recently it has been practised by relatively few enthusiasts, generally using homemade equipment with limited capabilities. However, we may now be at the threshold of a new era of amateur spectroscopy, thanks to commercially available equipment of varying degrees of cost and sophistication. These include systems that can produce results of professional quality, and that are available at costs comparable to high-end astronomical imaging systems.

This situation seems reminiscent of the revolution in amateur astrophotography that began about 20 years ago, when CCD cameras first became widely available to hobbyists, opening up vast new realms of imaging possibilities. Amateur spectro-



Figure 1 — Nighttime view of the Trottier Observatory and Science Courtyard at Simon Fraser University. Image courtesy of PWL Landscape Architects, Inc.

pists can now make measurements of astonishing variety and precision, and in addition to investigations done for personal education and reward, can participate in research collaborations with professionals (for a recent introduction to amateur spectroscopy, see Ref. [1]).

This also seems like an opportune time for universities with small teaching observatories to reconsider the educational opportunities associated with astronomical spectroscopy. Students from both the arts and sciences can engage in sophisticated scientific observations, with only a modest background in the relevant astrophysics, and after relatively straightforward equipment training. A remarkable variety of fascinating astrophysical systems can be studied, many of which possess distinctive spectral signatures that can yield very interesting quantitative results, after straightforward data analysis and interpretation (a largely qualitative introduction to astronomical spectra can be found in Ref. [2]). Such activities can provide educational experiences that closely emulate the practice and excitement of cutting-edge science.

Curriculum of the aforementioned nature is being developed at the Simon Fraser University (SFU) Trottier Observatory. The observatory, which opened in April 2015, is the anchor of a high-profile public space devoted to science, situated near the centre of the Burnaby campus (see Figure 1). The observatory houses a PlaneWave Instruments CDK700 alt-az telescope system, with a 0.7-m aperture operating at $f/6.5$, under a 20' Ash dome. The observatory is used for public outreach, student education, and as a resource for local amateur astronomers, especially members of the RASC Vancouver Centre.

A central component of the earliest plans for development of the observatory was to equip it with a large-format astronomical imaging camera system, and a high-resolution spectrograph. We settled on a Finger Lakes Instruments PL16803

16-Megapixel imaging camera, and a high-resolution “echelle” spectrograph made by a small French company, Shelyak Instruments. The spectrograph is marketed as the *eSbel*, at a cost that is comparable to our imaging system, and is intended for use primarily by advanced amateurs.

The camera was up and running before the observatory was officially opened, and some of our first images have been published [3], [4]. The spectrograph was installed in early summer of 2015, and an extensive set of initial studies was completed by the end of that year; an informal report on some of that work can be found on the observatory website [5].

The *eSbel* is mainly intended for high-resolution spectroscopy of brighter stars, owing to a trade-off between resolution and sensitivity that is characteristic of all spectrometers, although many diffuse objects are bright enough to be studied. High-quality data for naked-eye stars can be collected in minutes, and in less than an hour for stars down to about 8th magnitude, even with modest apertures under suburban skies. An impressive set of measurements made with a wide range of amateur spectrographs, including the *eSbel*, has been compiled by a leading French astronomer, Christian Buil, and is available on his website [6].

Measurements that have been done at SFU so far include: radial velocities of stars in double-lined spectroscopic binaries,

including Mizar A; properties of circumstellar disks (radial velocities and radii of the inner and outer rims), including that of the companion to the giant star VV Cephei A [7],¹ and of stars in the Pleiades; stellar-wind speeds, including those of Wolf-Rayet 140 (one of the brightest stars of that class), and P Cygni (the prototype of an entire class of stars with “optically thick” winds); rotational speeds of many stars, including Vega, and the extremely fast rotator ζ Aquilae (which has an equatorial radial velocity about of 0.1% of the speed of light!); Jupiter’s rotational speed; and the emission spectrum of the Ring Nebula.

Even one night of data taking was enough to yield high signal-to-noise spectra in the cases listed above, with quantitative results that were generally within about 10% of known values, and several interesting systems could often be measured in one night.

This situation is very different from acquiring a high-quality astronomical image, which requires many nights of telescope time. And, unlike astronomical image processing, which demands many hours of effort, with lots of trial-and-error, to obtain the best possible final image, the processing of spectroscopic data requires relatively little time and intervention by the user, once the initial setup for a particular spectrometer/telescope system has been made.

This report details the most ambitious spectroscopic study that has been done at SFU to date: the detection of the exoplanet τ Boötis b, from measurements of the radial velocity (RV) of its host star, τ Boötis A. This star has one of the largest known orbital RVs of any host, but even so, this measurement is near the limits of spectrographs that are likely to be available at university campus teaching observatories and to amateur astronomers, including the *eSbel* (an exhaustive on-line compilation of known exoplanets can be found in Ref. [8]).

To set the scale for this measurement, the orbital RV of τ Boötis A generates fractional wavelength shifts of less than 1 part in 600,000. The detection of τ Boötis b requires careful control of systematic uncertainties in the data-acquisition process, and a sophisticated approach to the data analysis; moreover, measurements must be done over many nights, in order to map out a decent portion of the host star’s orbital cycle.

τ Boötis b was one of the first exoplanets to be discovered, in 1997 [9], and was the first to be detected by amateur astronomers from RV measurements, in 2004 [10] (the detection has since been repeated by a handful of other amateurs, see, for example, Ref. [6]). It is a so-called “hot” Jupiter, with a mass about 6 times Jupiter’s mass, an orbital semi-major axis of only 0.046 AU (compared with 0.39 AU for Mercury), and an orbital period of just over 3 days (compared with 88 days for Mercury). The host star is a 4.5-magnitude main-sequence star of spectral type F7, and it has a maximum orbital radial velocity of 470 ± 15 m/sec. Interestingly, spectral lines in the



SERVING AMATEUR ASTRONOMERS FOR OVER 29 YEARS

toll-free 1-800-580-7160
info@khanscope.com
www.khanscope.com

ALL MAJOR BRANDS, INCLUDING:
AstroTrac • Meade • Celestron • Tele Vue • Kowa • Coronado • Levenhuk • ADM
Sky-Watcher • Nikon • Kendrick • William Optics • Antares • Hotech • Farpoint
Baader • iOptron • QSI • Telrad • TeleGizmos • Orion • Vixen • MoonLite • Lunt
Explore Scientific • MallinCam • Rigel • Starlight Instruments • Vernonscope

SERVING BEGINNERS AND ADVANCED AMATEURS

**WE SHIP CANADA WIDE | WE ACCEPT TRADE-INS
WIDE SELECTION OF NEW AND USED EQUIPMENT**

We service and repair most brands of telescopes and binoculars

TO ORDER TOLL-FREE, CALL **1-800-580-7160**
OR LOCAL 416-783-4140
OR ORDER ONLINE VIA OUR SECURE WEB SERVER AT **www.khanscope.com**

KHAN SCOPE CENTRE
3243 Dufferin Street, Toronto, ON M6A 2T2
in Toronto: 416 783 4140
facebook.com/khanscope

**VISIT OUR SHOWROOM!
OVER 70 SCOPES
ON DISPLAY**

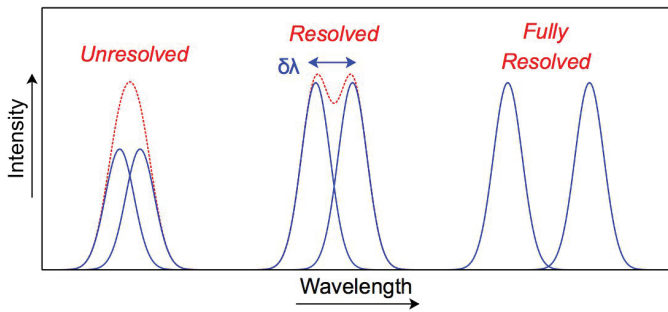


Figure 2 — Three sets of emission lines separated in wavelength by different amounts. The dotted curves plot the total intensity of overlapping lines.

infrared radiation from the planet itself have recently been detected, which show that water exists in its atmosphere [11].

The rest of the report is organized as follows. Section II provides an overview of the spectrograph, including its configuration at SFU, and an example of a stellar spectrum acquired with it. Section III briefly surveys the two techniques that amateurs have used to detect exoplanets, namely photometric detection of transiting exoplanets and RV measurements, and quantifies the challenges in obtaining sufficiently precise results in the latter case. Section IV outlines the strategy used for the data acquisition and analysis, and Section V presents a detailed analysis of the data, including estimates of the systematic and statistical uncertainties. Section VI presents a fit to the results for the orbital motion of the host star, compares the results with professional measurements, and extracts the mass of the exoplanet. The report concludes in Section VII, which includes a brief outlook for future work. An Appendix provides a qualitative introduction to the basic principles of echelle spectrometers for interested readers (a fuller introduction to spectrographs can be found in Ref. [1], while Ref. [12] provides a treatise for advanced undergraduates and graduate students).

Note: This report contains equations that are included for readers with sufficient mathematical background. However, the text is written for a non-mathematical readership, and the equations can be skimmed, or skipped entirely, without loss of continuity.

The spectrograph

Echelle spectrometers, such as the Shelyak Instruments *eShel*, are advantageous compared to other designs because of their inherently superior resolution. Spectral resolution is characterized by the smallest possible wavelength interval between two neighbouring spectral features that can be individually identified, as illustrated in Figure 2. Resolution is usually specified in terms of a fractional measure R that is defined by

$$R \equiv \frac{\lambda}{\delta\lambda} \quad (1)$$

The *eShel* has a resolution R of about 10,000, meaning that it can distinguish between visible-light spectral features separated by about 0.5 \AA . Many professional echelles by comparison have resolutions above 100,000.

The *eShel* layout, when in use at the SFU observatory, is shown in Figure 3. The spectrograph is remarkably compact, and sits on top of a small dolly that is wheeled into the dome area to collect data. A light-weight acquisition/guiding unit is attached to one of the telescope's two ports². The acquisition unit houses a small plane mirror with a hole: the mirror deflects almost all the incoming starlight to a guide camera mounted on the side of the unit, while a fibre-optic cable mounted behind the hole in the mirror feeds light to the spectrometer. The spectrometer's diffraction grating disperses the light, and a CCD camera (the *Atik 460ex*, in our case) that is mounted on the spectrometer images the resulting spectrum. USB cables connect the equipment to the control-room computer.

The spectrograph has calibration sources, and the light that they produce when activated is fed to the acquisition unit at the telescope through a separate fibre-optic cable; a flip mirror in the acquisition unit redirects the calibration light to the pickup fibre, and back to the spectrograph, so that the calibration is done along the same optical path that is followed by incident starlight.

The fibre-optic cable that transmits the incoming starlight is only 50 microns in diameter! The small size of the fibre is necessary for the high resolution of the spectrometer, but also necessarily limits its sensitivity. The images of the Ring Nebula and Vega in Figure 3 (the latter is highly over-exposed!) were taken through the guide camera, and show the tiny region occupied by the hole in the mirror. This illustrates why this unit is suited to stellar spectroscopy, and not so

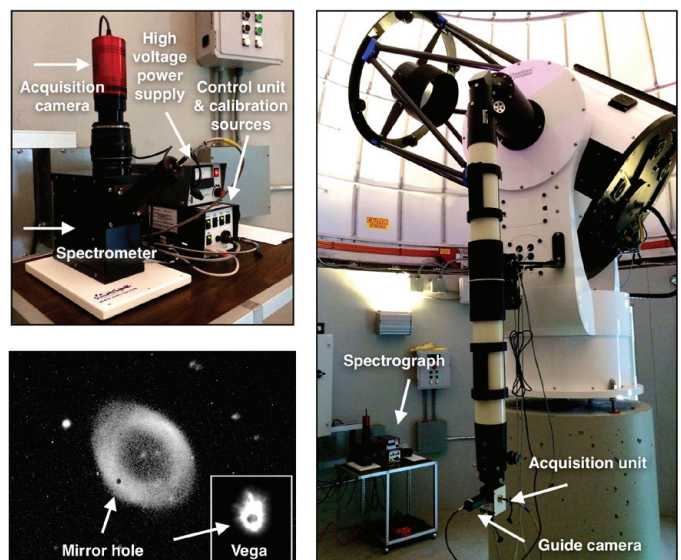


Figure 3 — Spectrograph layout at the SFU observatory.

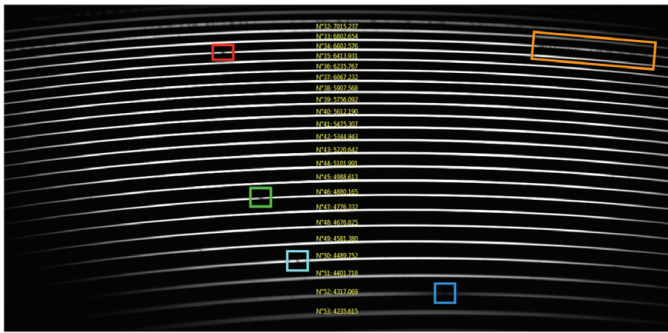


Figure 4 — *eShel* acquisition image for Vega. The yellow text identifies the central wavelength in each of the displayed orders. The coloured boxes identify some significant spectral features, as detailed in the text.

much to extended sources, though brighter nebulae can be measured. These images also demonstrate the importance of auto-guiding, to keep the target starlight on the hole!

An acquisition image of the spectrum of Vega obtained with our *eShel* is shown in Figure 4; Vega is so bright that this spectrum required less than three minutes of total exposure. As is evident from this image, echelle spectra take the form of a set of narrow bands stacked one on top of the other. Each band corresponds to the output from one order of the diffraction grating (the bands have no colour here because we use a monochrome acquisition camera). This characteristic pattern gives rise to the adjective “echelle” (French for ladder).

In the case of the *eShel*, some 25 orders cover the entire optical band, from just below 4000 Å to well beyond 7000 Å. Some of the absorption lines that stand out in Figure 4 are identified with coloured boxes. On the left side of the image, running from top to bottom are: the hydrogen-alpha line at 6562 Å (red box); the hydrogen-beta line at 4861 Å (green); and a

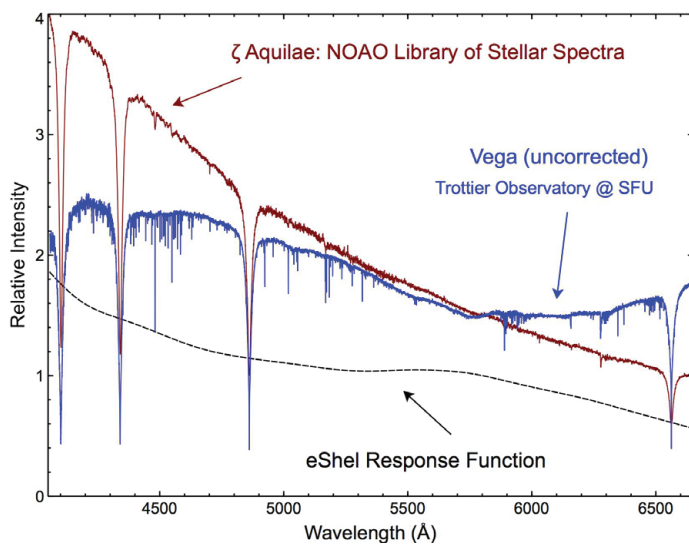


Figure 6 — Spectrum of Vega without correction for the overall response of the *eShel*/CCD chip, compared with a standardized spectrum of a star of the same spectral type. The dashed line is the computed response function of the spectrometer.



Figure 5 — Acquisition image produced by the *eShel*'s thorium-argon hollow cathode lamp.

magnesium line at 4481 Å (cyan). On the right side, again from top to bottom, there is a very dense set of absorption lines due to oxygen molecules in our own atmosphere, running from about 6850–7000 Å (orange box), and the hydrogen-gamma line at 4340 Å (blue).

Data acquisition with the *eShel* is conveniently handled using a freeware package that has specially-designed utilities for this purpose [13]. Analysis of raw acquisition images, like the one in Figure 4, is done by professionals using very powerful but arcane command-line software packages [14], [15]. A relatively user-friendly GUI freeware package better suited to non-experts has been written by Christian Buil [6], and was used to process the data in this study.

To turn an image like the one in Figure 4 into a graph of intensity versus wavelength requires calibration of the spectrometer/camera system. Calibration is needed for four reasons: to map the geometry of the echelle rungs; to correct for intrinsic variations of the echelle output within each rung; to map the pixel position at which light reaches the imaging

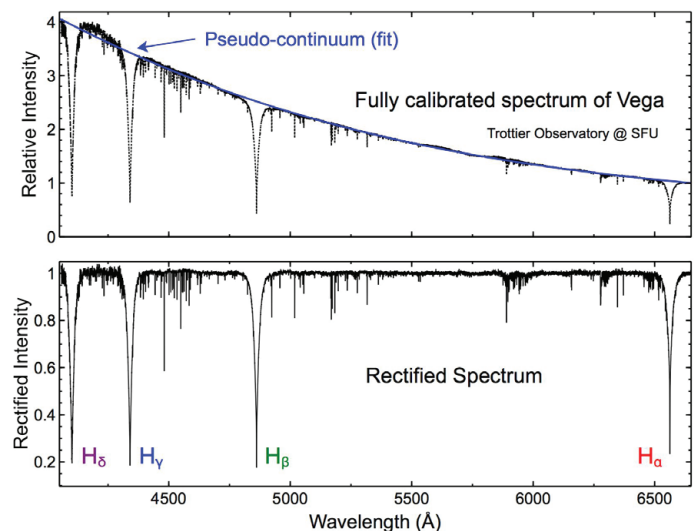


Figure 7 — Full-calibrated spectrum of Vega, and a fit to the underlying trend (upper panel); Rectified spectrum (lower panel). The four optical hydrogen Balmer lines are labelled.

CCD to the corresponding wavelength; and to correct for overall variations in the response of the spectrometer and CCD chip.

The *eSHEL* is equipped with continuous sources (a tungsten lamp and blue LEDs) that are used to characterize the echelle rungs. A hollow cathode lamp containing a mixture of thorium and argon gases is used for wavelength calibration: when a voltage is applied to the tube, atomic transitions are induced that emit light at hundreds of precisely known wavelengths. Figure 5 shows the spectrum produced by the cathode lamp.

To correct for the overall response of the spectrometer/CCD chip, one can measure the spectrum of a star and compare the result with a standard reference spectrum of the same star, or of another star of the same spectral type; the ratio between the uncorrected and reference spectra yields the response function of the spectrometer, which can then be used to produce corrected spectra of other stars. Figure 6 shows an uncorrected spectrum of Vega obtained with the *eSHEL*, and a standardized spectrum [16] for another star of the same spectral type (A0V), along with the computed response function.³

It is often more convenient to divide out the smooth underlying trend in a star's spectrum, which is produced by the continuous radiation emitted by the body of the star (and that is usually of less interest than the absorption lines produced by the star's atmosphere), to obtain a so-called "rectified" spectrum. Figure 7 shows the fully calibrated spectrum of Vega, and the result of a fit to the underlying trend (referred to as the pseudo-continuum), along with the resulting rectified spectrum. If only the rectified spectrum is required, it can be obtained without need of the spectrometer/CCD response function.

Exoplanet detection

Exoplanets have been discovered by at least five techniques (a non-specialist overview of these techniques can be found in Ref. [17], while Refs. [18] and [19] provide introductions for advanced undergraduates and graduate students). Two of these methods are accessible at small university teaching and amateur observatories: photometric measurement of an exoplanet transit across the host star; and spectroscopic measurement of a host star's motion (projected along the line of sight of the observer), due to the gravitational influence of an exoplanet.

The general principles of transit and radial-velocity measurements are illustrated in Figure 8 (other methods include gravitational micro-lensing, direct imaging, and astrometry). Transits are inferred from a drop in the apparent brightness of the host star, and can be used to determine the size of the exoplanet: the larger the exoplanet diameter, the deeper the drop. Radial velocities are measured from Doppler shifts of absorption lines in the star's spectrum, which vary in

wavelength as the star moves around the centre of mass of the system, and the results can be used to infer a lower bound on the mass of the exoplanet: the greater the planet mass, the faster the host star moves in an orbit of a given size.

Only a fraction of exoplanets transit their host star along our line of sight, and relatively few produce an RV motion in the host star that is large enough to be measured. In those rare cases where both measurements can be done, one can infer the density of the exoplanet; this is how professionals have identified exoplanets that are likely to be gaseous in composition, and those that are likely to be rocky terrestrials.

Detection of transiting exoplanets is relatively straightforward, with dozens of cases within the reach of modest telescopes and cameras (for an introduction to transit detection for amateurs, see Ref. [22]). In the most favourable cases, the drop in apparent brightness during the transit is about 0.02 magnitudes, which can be measured using routine differential photometry, not unlike variable-star measurements. Data reduction is also routine, thanks to an on-line compendium to which amateurs can upload their data [23].

Photometric detection of a transiting exoplanet was done at the SFU Observatory shortly after it opened, by one of the observatory's most proficient users, local amateur astronomer Oleg Mazurenko, who has since detected several additional systems; a report on Oleg's results is available at the observatory website [5].

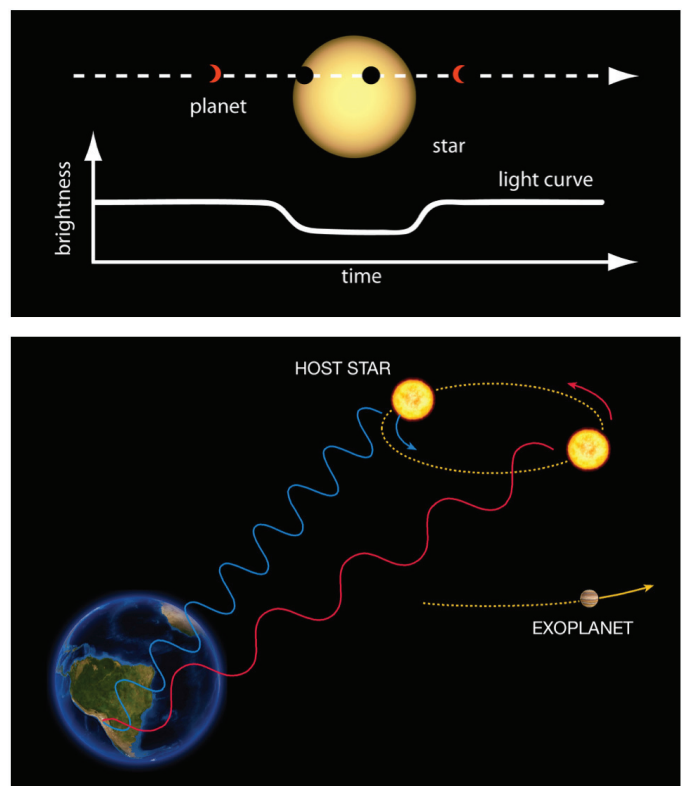


Figure 8 — Exoplanet detection by transit of the host star (upper panel, NASA image [20]), and from Doppler shift measurements of the host star's radial velocity (lower panel, ESO image [21]).

RV detection of an exoplanet on the other hand requires an exacting combination of carefully controlled measurements, and painstaking data analysis, owing to the very small orbital RVs to be measured. Even the “easiest” case is near the limits of the capabilities of spectrographs that are likely to be available at small observatories, including the *eShell*, and only a handful of exoplanets are within the reach of such instruments.

To quantify the challenge of these measurements, consider the formula for the Doppler shift⁴,

$$\Delta\lambda = \lambda \frac{v_r}{c} \quad (2)$$

where $\Delta\lambda$ is the shift in wavelength of light emitted or absorbed by a source at wavelength λ in its rest frame, v_r is the radial velocity (the component along the line of sight) of the source relative to the observer, and where $c = 300,000$ km/sec is the speed of light. τ Boötis A has one of the largest known orbital RVs due to an exoplanet, about 470 m/sec (roughly only 1.5 times the speed of sound in air), which produces a maximum fractional wavelength shift $\Delta\lambda/\lambda$ of about 1 part in 600,000. To make a convincing detection, however, will require the Doppler shift to be measured at the level of one part in a few *million*, so that statistical fluctuations in the measured RVs will be smaller than maximum RV by a reasonable margin.

For another indication of the challenge of RV exoplanet detection, let’s suppose that the uncertainty in any one measurement of the RV is required to be about 10% of its maximum value, or about 50 m/sec. Since it turns out that the *eShell*/camera pixel scale is about 0.15 Å/pixel, a velocity shift of 50 m/sec is equivalent to a shift in the position of a spectral line of only 1/200 of a pixel! By comparison, professionals measure RVs equivalent to shifts of 1/1000 of a pixel!

Since it is not possible to directly measure such tiny positional shifts, the RVs are actually inferred from changes in the

intensities of spectral lines, rather than in their wavelengths. If the intensity of a spectral line is measured with sufficient precision (i.e. with sufficient signal-to-noise), and if the intensity varies sufficiently rapidly as a function of wavelength (i.e. if the line is sufficiently deep), then a Doppler shift will result in a measurable change to the intensity of the line [24] [25], even if the pixel spacing is much larger than the wavelength shift.

Cooler host stars, which have many deep absorption lines, are favoured for exoplanet detection. Most professional studies have been done for spectral types ranging from about F5 to M5, which have up to several thousand well-separated absorption lines; hotter stars on the other hand have too few lines, while the lines in cooler stars are too overlapped. The advantages of stars of appropriate spectral types are evident from Figures 9 and 10, which compare rectified spectra taken at SFU of Vega (spectral type A0V), τ Boötis A (type F7V), and 45 Boötis (type F5V), a reference star used in this study.

A survey of results from a variety of spectrometers [19] shows that a device with a resolution comparable to the *eShell* can produce RV measurements with a precision of around 50 m/sec, if the target spectrum has a few thousand deep absorption lines, and is acquired with a signal-to-noise ratio of about 100:1 (which in our case takes less than an hour for stars down to about 8th magnitude). However, dealing adequately with potential thermal or mechanical changes to the spectrometer is essential, since even tiny uncontrolled shifts in pixel positions can be enough to swamp the effects of the small Doppler shifts to be measured.

Measurement and analysis strategies

As detailed in the previous section, detection of an exoplanet will stretch the capabilities of our spectrograph. A convincing detection will therefore require many observations, spread out

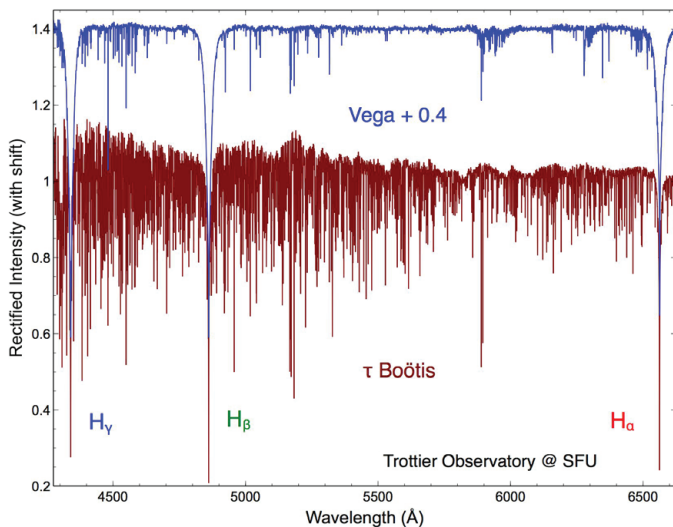


Figure 9 — Rectified spectra of Vega and τ Boötis. For clarity, the spectrum of Vega was shifted upwards by the indicated amount.

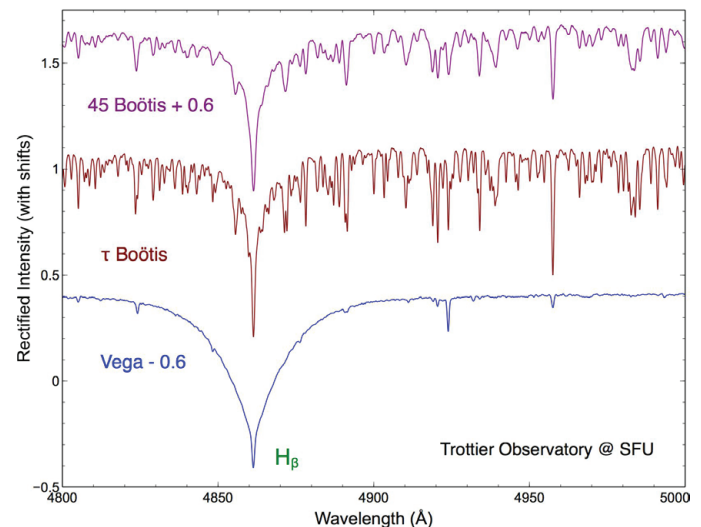


Figure 10 — Rectified spectra of 45 Boötis, τ Boötis, and Vega, near the H_β line. For clarity, two of the spectra were shifted vertically by the indicated amounts

over a good portion of the orbital cycle, owing to the relatively large uncertainties that will be present in any one measurement. In this study, data were taken on ten nights that covered most of the orbital cycle. Moreover, to reach meaningful conclusions, one must estimate the scientific uncertainties in the quantitative results. To estimate the uncertainties, between six and nine measurements were made each night, and the resulting averages and standard errors were computed. Examples of the dispersion in individual measurements will be shown below.

One of the most difficult challenges in any scientific measurement is to estimate the systematic uncertainties that are associated with any apparatus and technique. As indicated in the last section, it is critical to deal with possible systematic effects that can arise from thermal and mechanical changes in the spectrometer over the course of the night, or from one night to the next; systematic effects of this sort are often referred to as spectrometer or calibration “drift” [19].

The setup currently in use at the SFU observatory makes spectrometer drift very challenging to deal with (though only at the high level of precision required for exoplanet detection). The limited space available in the rest of the observatory requires that the spectrograph be operated in the open environment of the dome area, which can produce significant thermal drift over the course of the night; the spectrograph must be also be moved into storage when not in use for extended periods, which can cause significant mechanical and thermal changes from one night of observations to the next.

To control for spectrometer drift, a two-part strategy was used. First, calibration data were taken at regular intervals over the course of the night, generally before and after each data set was acquired (professional setups normally take object and calibration data simultaneously, by feeding object and calibration light to the spectrometer at the same time, through separate fibres). This helps to reduce the effects of thermal drift over the course of the night.

The second part of the calibration strategy was to take the spectrum of a reference star, either immediately before or immediately after each measurement of the spectrum of τ Boötis. This further reduces the effects of thermal drift, and controls for mechanical changes when the spectrograph is stored between nights.

A good choice for a reference star is one that is of similar spectral type to the target, and that is bright, and nearby on the sky. For this study, 45 Boötis was used: it has a visual magnitude of 4.9 and spectral class F5V, compared with magnitude 4.5 and class F7V for τ Boötis, and the two stars are reasonably close on the sky (separated by about 20°).

The standard approach used by professionals to estimate a radial velocity is to compute a so-called *cross-correlation*

function (to be defined precisely below), which compares the measured spectrum of the target object with a reference spectrum [18] [19]. The reference spectrum is usually an idealized “template” of the spectra of objects of similar spectral type as the target. In this study, the reference spectrum will be the measured spectrum of 45 Boötis.

A total exposure of ten minutes was used for each spectrum acquisition (five two-minute exposures were added together, to avoid saturation in the camera response), while each calibration data set took one or two minutes. It typically required about 30 minutes to complete 1 measurement cycle (consisting of data acquisition for the 2 stars, spectrometer calibration, and target slewing); measurement cycles will be labelled in the following by a sequential “bin” number.

The cross-correlation between the two measured spectra will be denoted by $C_{12}(v_r)$, and will be evaluated as a function of the relative radial velocity v_r between the two stars. The best estimate of v_r will be the value that produces the closest possible match between the two spectra. The velocities will be evaluated separately for each data bin, and an overall average value and standard error will be estimated from the ensemble of measurements taken each night.

This combination of data acquisition and analysis yields very precise results, since, in essence, one exploits the difference between two measurements, taken with the same instrument and at nearly the same time, to largely cancel out systematic uncertainties.

[Before considering the precise form of $C_{12}(v_r)$, the reader who wishes to skip the mathematical details need only be aware that the function is bounded by “1” in absolute value, and will precisely equal “1” only for a perfect match between the two spectra. If desired, the reader can now skip to the paragraph following Eq. (5).]

The cross-correlation function is defined by⁵

$$C_{12}(v_r) = \frac{\sum_{\lambda} I_1(\lambda) I_2\left(\lambda\left(1 + \frac{v_r}{c}\right)\right)}{\sqrt{\langle I_1^2 \rangle \langle I_2^2 \rangle}} \quad (3)$$

where I_1 and I_2 are the two stellar spectra, and where the wavelength in one spectrum is Doppler shifted relative to the other, here using the standard non-relativistic formula, cf. Eq. (2). The angle brackets in the denominator in the above expression are normalizing factors, defined by⁶

$$\langle I_{1,2}^2 \rangle = \sum_{\lambda} I_{1,2}^2(\lambda) \quad (4)$$

One can show that the cross-correlation satisfies the so-called Schwarz inequality

$$-1 \leq C_{12} \leq 1 \quad (5)$$

If $C_{12} = 1$ then the two spectral functions are said to be completely correlated, while if $C_{12} = -1$ they are said to be completely anti-correlated. The best-fit value for the relative velocity v_r is the one that is found to numerically maximize the cross-correlation function.

The cross-correlations were evaluated by summing over wavelengths from 4400 Å to 6400 Å. Although useful measurements can be made with the *eShel* over a slightly wider range (from about 4000 Å to well over 7000 Å), the data at shorter wavelengths is generally very noisy, and the data at longer wavelengths is strongly contaminated by absorption lines due to the Earth's atmosphere. The numerical results do not depend significantly on the precise wavelength range that is used, though more-accurate results are generally obtained by using a wider range.

Figure 11 shows the cross-correlation between the spectra of τ and 45 Boötis, using averages of the spectra extracted from the individual data bins acquired on the indicated date. The RV at which the cross-correlation is maximized is indicated on the plot (this includes barycentric corrections, which are described in the next section). The cross-correlation function typically has a Gaussian shape around its maximum, as illustrated by the solid line in Figure 11, which is the result of a fit to the data points in that region.

Evaluating uncertainties in the estimates of the radial velocities is done in the next section. Before doing so, it is very useful to first get a visual impression of the quality of the data. Figure 12 zooms into a small section of the spectra of the two stars,⁷ from the same data set that was used to compute the cross-correlation function in Figure 11. The spectrum of 45 Boötis is plotted twice, with different Doppler shifts applied

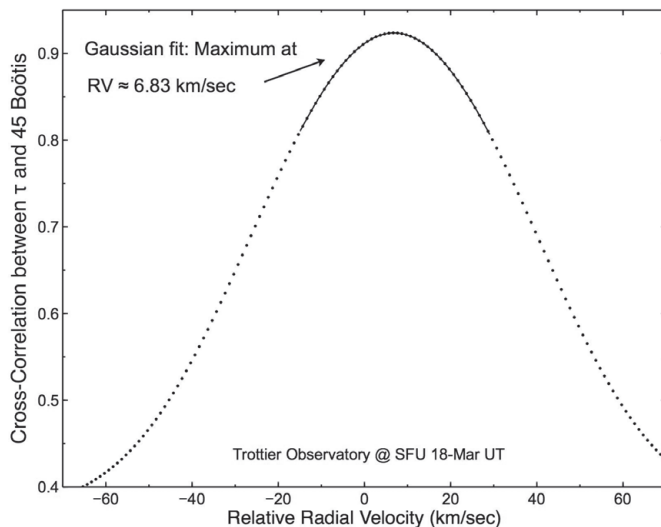


Figure 11 — Cross-correlation between the spectra of τ and 45 Boötis, obtained on the indicated date, as a function of the relative RV. The solid line is a Gaussian fit to the points near the maximum.

arithmetically to the data before making the plot; one plot has been Doppler shifted by 2 km/sec less than the best-fit value for the relative RV between the two stars, and the other by 2 km/sec more than the best fit. This comparison demonstrates that a shift of only a few km/sec can easily be discerned by eye over a small part of the spectrum. This makes it plausible that radial velocities estimated from a cross-correlation analysis that, for appropriate spectral types, simultaneously compares many thousands of absorption lines, can have uncertainties of much less than one km/sec.

Data analysis

As described in the previous section, one of the principal challenges in this study is to control for drift in the spectrometer calibration. In particular, if the data acquisition strategy was successful, then no systematic change in the RV between the two stars, as inferred from the set of sequential measurements from a given night, should exist.

In addition to analyzing the relative RV, it is also instructive to analyze the RV of each star separately. The latter can be done by maximizing an “auto-correlation” function, where the spectrum of a star is compared with itself; specifically, the first spectral function in Eq. (3) is fixed to the star’s spectrum from the first data bin, while the second function is taken from one of the other bins. In this way, the RV inferred from one bin is computed relative to the first.

To extract any RV, one must take account of the observer’s motion relative to the Solar System’s centre of mass, also known as its barycentre (which, to a first approximation, is

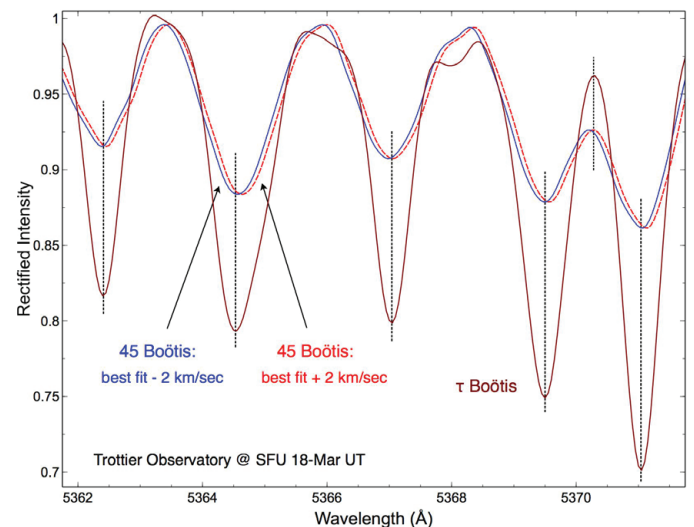


Figure 12 — A small section of the spectra of τ and 45 Boötis, from the same data set that was used to compute the cross-correlation plotted in Figure 11. The spectrum of 45 Boötis is plotted twice, after being Doppler shifted arithmetically by the indicated amounts relative to the best-fit value for the relative RV. The dotted vertical lines are drawn through some min/max points in the spectrum of τ Boötis, to facilitate comparison of the three plots.

Continues on page 166



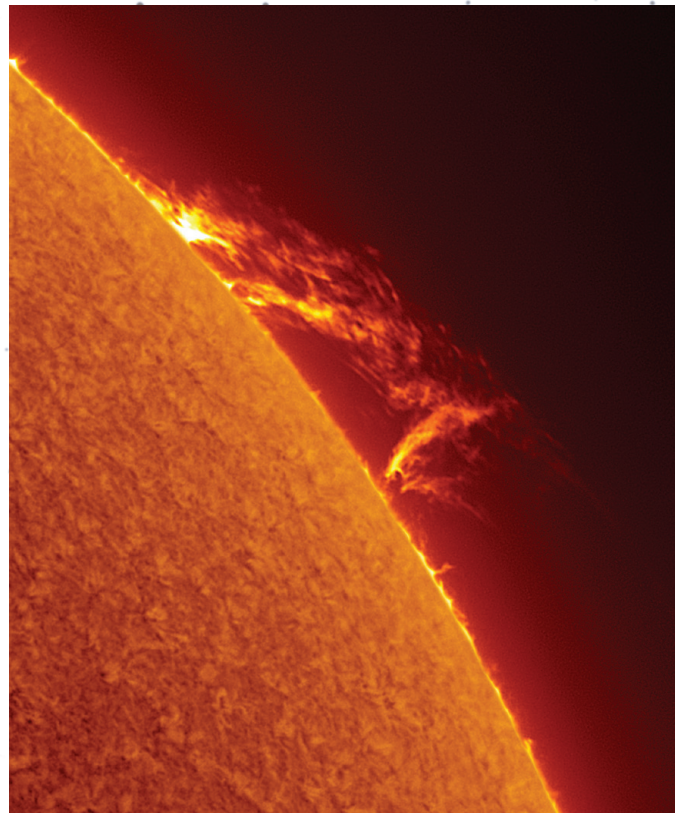
Brian McGaffney imaged M1, The Crab Nebula, from his observatory in Bancroft, Ontario, in November 2014. He decided to reprocess it using updated processing techniques, and add the H α and OIII data acquired more recently. The original image and more-recent narrowband data was acquired with a 17-inch RCOS and an Apogee U16 M using 5- μ m filters. Image acquisition time was about 7 hours.

M71, a loosely packed globular cluster, was imaged by Ron Brecher from his SkyShed in Guelph, Ontario. Ron used an 8" f/8 RC telescope, MI-250 mount, QSI583wsg camera, with Astrodon RGB filters. It was guided with QHY5 and 80-mm f/6 refractor and acquired and guided with Maxim DL. All pre-processing and processing was done in PixInsight. 6x15m and 3x10m R and G; 7x15m and 3x10m B, all unbinned frames (total=6hr 15m).

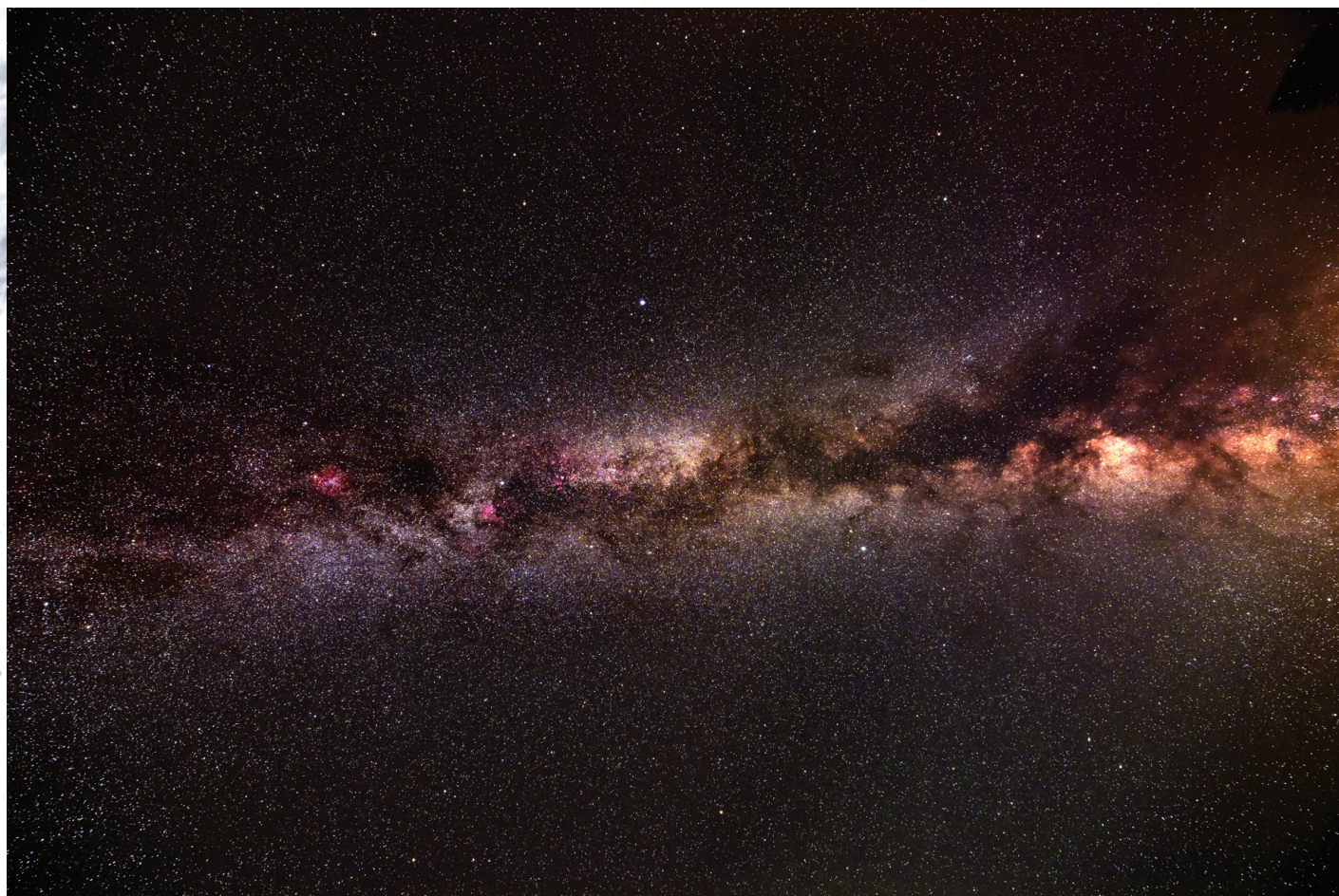


Pen & Pixel

Gary Palmer captured this spectacular prominence on June 1 using his Starwave 115 EDT, Daystar Quark H α , Hypercam 178, iOptron CEM25P, and Sharpcap.



The Milky Way stretches across the sky in this image from Michael Watson. Michael took the photo from Algonquin Park in September 2016 using a Nikkor AF-S 14-24-mm f/2.8G ED lens on a Nikon D810a camera body, mounted on an Astrophysics 1100GTO equatorial mount with a Kirk Enterprises ball head.



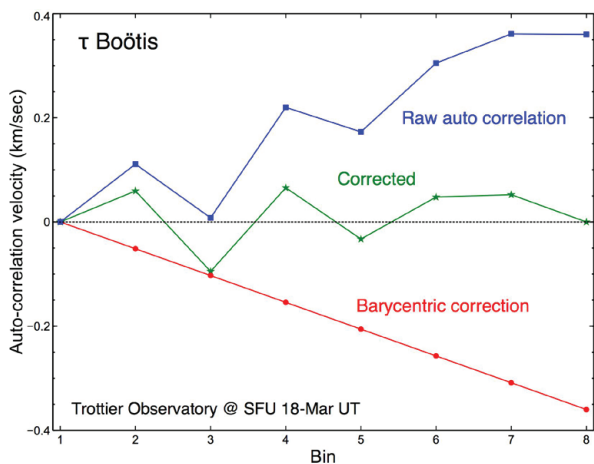


Figure 13 — Change in the radial velocity of τ Boötis, and in the velocity of the observer relative to the Solar System barycentre, over the course of a night.

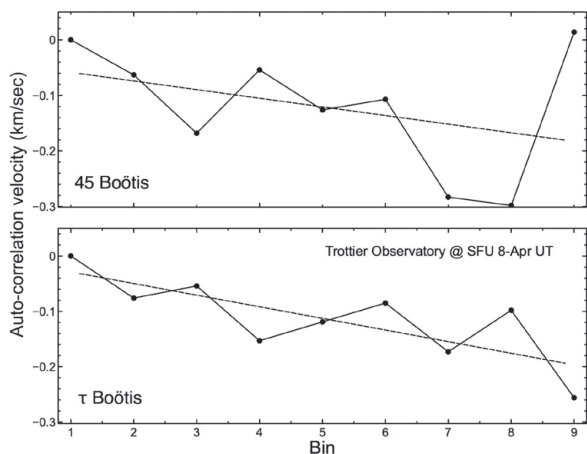


Figure 14 — Change in the apparent radial velocities of the two stars on the indicated date. The dashed lines are linear fits to the data. Barycentric corrections have been taken into account.

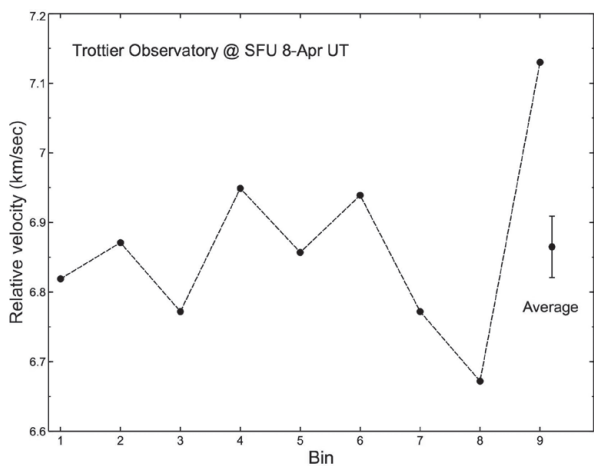


Figure 15 — Relative RV between the two stars, as determined from the cross-correlation between their spectra. The data are from the same set used in Figure 14. The average over the nine bins is also shown; the error bar is the standard error.

the rest frame of the Sun). Earth’s orbital velocity around the Sun is about 30 km/sec, and its component in the direction of a point on the celestial sphere can change significantly, relative to the accuracy of the measurements in this study, over the course of a few days. Perhaps more surprising is that, for exoplanet detection, Earth’s rotational motion must also be taken into account, even over the few hours needed to complete one night of measurement; at our latitude, a point on the surface rotates at about 0.3 km/sec, which is almost as large as the orbital RV of τ Boötis A! The observer’s net velocity around the Solar System barycentre, in the direction of any point on the celestial sphere, can be computed using a number of software packages [6] [14].

The importance of barycentric corrections is illustrated by the plots in Figure 13, which show changes in the apparent radial velocity of τ Boötis over the course of one night of observations. The plot labelled “Raw” shows the change in radial velocity without taking account of barycentric corrections. The barycentric correction, and the corrected radial velocities, are also plotted. The measured data clearly exhibit the overall trend due to motion of the observatory relative to the barycentre, even over this short five-hour period of observations.

From here on, all results will be presented with barycentric corrections taken into account. Returning to consideration of potential drift in the spectrometer, Figure 13 already provides one example of monitoring for drift in the RV of an individual star: no systematic trend is discernable, after the barycentric correction is applied, with the changes from one bin to the next being consistent with random statistical fluctuations.

Noticeable drifts in the spectra occurred on just two or three of the ten nights of observations. The auto-correlations from the night with the most significant drift are shown in Figure 14. Systematic changes in the RVs of both stars are evident; the two trends also appear to be almost identical, as would be expected from spectrometer drift, which should induce roughly the same shift in all measurements taken at roughly the same time.

Fortunately, the drift appears to cancel out when the spectra of the two stars are cross-correlated, as shown in Figure 15. The strategy of measuring the target and reference stars one right after the other, and comparing the two spectra, was apparently successful in controlling for drift.

The final results are obtained by computing an average, denoted by $\overline{v_r}$, of the relative radial velocities extracted from each data bin

$$\overline{v_r} = \frac{1}{N} \sum_{i=1}^N v_{r,i} \quad (6)$$

where N is the number of bins, and $v_{r,i}$ is the estimate from the i -th bin. To estimate the uncertainty in the average, the

so-called standard error was used, denoted here by e_{v_r} , and given by

$$e_{v_r} = \sqrt{\frac{1}{N(N-1)} \sum_{i=1}^N (v_{r,i} - \bar{v}_r)^2} \quad (7)$$

Table 1 lists the results for all ten nights of observations, and Figure 15 shows the average/uncertainty of the data for that particular night.

Equation (7) provides a valid error estimate only if the variations in the individual measurements are due to purely statistical fluctuations. It is possible that there are small residual systematic errors due to spectrometer drift, or other unidentified systematic effects, but the consistency of the error estimates obtained from Eq. (7) will be supported by an overall fit to the data, which will be detailed in the next section.

Date (UT 2016)	No. of Bins	Relative RV (km/sec)
Mar 18, 10:15	8	-6.831(41)
Apr 1, 9:30	9	-6.805(41)
Apr 8, 9:45	9	-6.865(44)
Apr 9, 8:15	7	-7.597(46)
Apr 10, 8:15	8	-7.092(64)
Apr 20, 7:15	7	-7.133(93)
Jun 7, 7:15	7	-7.179(30)
Jun 16, 7:00	7	-6.712(25)
Jun 17, 7:30	6	-7.201(56)
Jun 28, 6:15	6	-7.460(37)

Table 1 – Relative RVs between τ and 45 Boötis on the ten nights of observations. The values in parenthesis are the standard error uncertainties in the last two digits. The date and time is the mid-point of the interval over which the data was acquired, which varied between about three and five hours.

Regarding systematic uncertainties, it turns out that activity in a target star, such as convective spots in its photosphere, can induce shifts in the star’s spectral lines, which can mask the true radial velocity, a phenomenon known as stellar “jitter” [18] [19]. Jitter varies in magnitude with a star’s spectral type, rotation period, and other attributes. For main-sequence F-class stars, like those measured here, jitter can induce shifts as large as 30 m/sec, on time scales comparable to the star’s rotation period (typically a few days for F-class main-sequence stars, see e.g. Ref. [26]).

A related concern in a study such as this one, which relies on relative RV measurements, is the possibility that the RV of

the reference star is not sufficiently stable, perhaps due to the influence of an unknown stellar companion, or unusually large intrinsic jitter. A professional study that monitored 45 Boötis over a period of about 100 days found no significant systematic variation in its RV [27]. The upshot is that the statistical uncertainties obtained here are nearly as small as can be useful for exoplanet detection, unless one controls for the effects of jitter!⁸

Orbital motion of τ Boötis A and the mass of its exoplanet

In order to detect an exoplanet, one looks for a periodic variation in the RV of the host star. With enough measurements, one can find the orbital period, eccentricity, semi-major axis (projected along the line of sight), and the maximum orbital RV of the host star [18] [19].

Given the limited number and precision of the measurements obtained here, a more modest validation will be considered, by taking the period and eccentricity of the orbit as inputs from previous professional studies (see Ref. [8] for a compilation of results). A fit to the data will be used to determine the maximum radial velocity, usually denoted by the symbol K , and the result will be compared with the accepted value of (470 ± 15) m/s. The accepted orbital period is 3.31249(3) days, and the accepted eccentricity is 0.08 ± 0.03 , which is small enough to ignore within the accuracy of this study.

RV data is most usefully plotted against the orbital phase, which is defined by

$$\text{phase} = (t_{\text{obs}} - t_{\text{ref}}) / \text{period} \quad (8)$$

where t_{obs} is the time of an observation and t_{ref} is an arbitrary fixed reference time, and where “decimal” denotes the decimal part of the numerical value of the expression in brackets. In the following, the reference time will be specified by an instant t_{max} at which the RV has its maximum value. The time that it takes for light to travel from a target object to the Earth depends on the Earth’s position in its orbit, and a correction for this effect should be made when computing the phase. For this purpose, time is conventionally specified in terms of the Heliocentric Julian Date (HJD), which is the Julian Date corrected for the difference between the light travel time from the target object to the Sun, and to the Earth. Conversions to HJD can be done with a number of utilities [6] [14]. A published value for an epoch of maximum radial velocity for τ Boötis A is $t_{\text{max}} = (2450235.4 \pm 0.2)$ HJD [9].

For a circular orbit, the radial velocity will follow a simple cosine curve, given by

$$RV = K \cos(\text{phase}) + K_0 \quad (9)$$

where K is the maximum orbital radial velocity, and K_0 is an additive constant related to the overall translational motion of the system. Since the RV of τ Boötis has here been measured relative to that of 45 Boötis, K_0 should be equal to the difference in the translational RVs of the two systems. Previous measurements of systemic RVs can be found from a huge on-line database of astronomical data known as SIMBAD [28], from which an accepted value of $K_0 = -(4.8 \pm 1.2)$ km/sec can be extracted.

The values of the three constants K , K_0 , and t_{ref} in Eq. (9) can be estimated by fitting the cosine curve to the data. A standard least-squares fit to the data in Table 1 produces the following values

$$\begin{aligned} K &= (425 \pm 18) \text{ m/sec} \\ K_0 &= (-7.13 \pm 0.14) \text{ km/sec} \\ t_{\text{ref}} = t_{\text{max}} &= (2450235.55 \pm 0.02) \text{ HJD} \end{aligned} \quad (10)$$

which are all in agreement with the accepted values, within the uncertainties.⁹

The measured radial velocities and the fitted cosine curve are plotted in Figure 16, with the overall additive constant K_0 subtracted from the data points, and removed from the fit curve, for convenience. In order to get a visual impression of the agreement between the data and the accepted value of the maximum orbital RV, the cosine curve of Eq. (9) is also plotted using the accepted central value of 0.47 km/sec for K , and using a value of 0.44 km/sec, which is two standard deviations below the accepted central value. As is already evident from the results in Eq. (10), the agreement between the data and the known RV is very good.

Having determined the orbital RV of the host star, one can set a lower bound on the exoplanet's mass; the actual mass can only be found if the angle of inclination of the orbital plane relative to our line of sight is known, since the radial component of the orbital velocity will always be less than the true velocity, unless it happens that $i=90^\circ$.

For the special case of a circular orbit of an exoplanet with a mass M_p that is much less than the host star's mass M_* , the following formula applies [18] [19]

$$K = 28.4 \text{ m/s} \cdot \left(\frac{P}{1 \text{ yr}}\right)^{-\frac{2}{3}} \left(\frac{M_*}{M_\odot}\right)^3 \left(\frac{M_p \sin i}{M_J}\right) \quad (11)$$

where P is the orbital period, M_\odot is the mass of the Sun, and M_J is the mass of Jupiter. It is instructive to note that in the case of our Solar System, Jupiter induces an orbital speed in

the Sun of only 12.5 m/s, about the same as a car turning a corner, while the Earth generates a tiny speed of 9 cm/s, only a few times faster than a garden snail moving at top speed!

Equation (11) can be solved for the mass of the exoplanet, given the host star's mass and its orbital RV. In the case of τ Boötis b, the host star mass is about $1.3M_\odot$, yielding $M_p \sin i \sim 4M_J$, with an uncertainty of about 10% [8].¹⁰

Conclusions

The exoplanet τ Boötis b was detected from measurements of the radial velocity of its host star, τ Boötis A, at Simon Fraser University's teaching and outreach observatory. The spectrograph used is a commercially manufactured, off-the-shelf unit of echelle design, and is available at a cost that is comparable to high-end imaging camera systems. Although τ Boötis A has one of the largest orbital RVs of any known host, this was a very challenging study, requiring Doppler shifts of the star's absorption spectrum to be measured to 1 part in a few million. Measurements were made on ten nights, which covered most of the orbital cycle, and a fit to the data gave a value for the maximum orbital RV in agreement with the known value, to within about 10%.

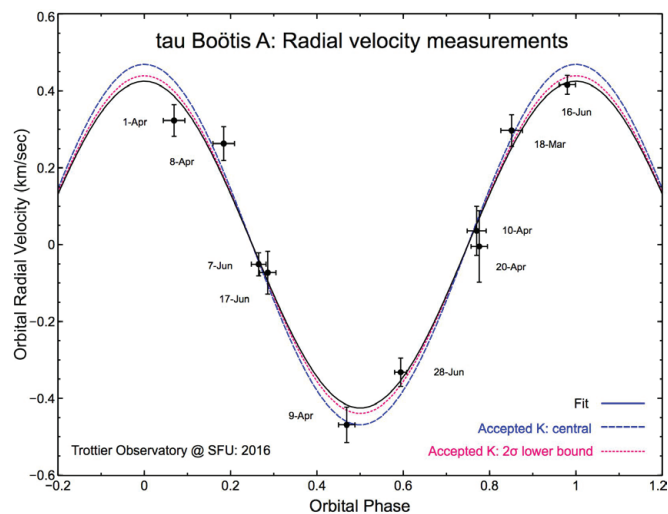


Figure 16 — Orbital radial velocity of τ Boötis A versus its phase. Each data point is labelled by the date of the observation, and the horizontal error bar expresses the amount of time over which data was collected, typically between about three and five hours. The solid line is a best fit to the data for a circular orbit. The dashed and dotted curves illustrate the uncertainty in the accepted value of the orbital RV, as described in the text.

This study was done in connection with a course in observational astronomy under development at SFU, which will be offered as a breadth course for students from the arts and sciences. While exoplanet detection may only be suitable for more-advanced students, there are many interesting astrophysical systems that can be studied by spectroscopy with far

less effort, and in many cases interesting quantitative results can be extracted with simple analysis methods and only a basic understanding of the relevant astrophysics. These kinds of studies can provide educational experiences that closely emulate the practice and excitement of cutting-edge science.

Only a few other exoplanets can be detected using spectrographs that are likely to be accessible at a campus teaching observatory or by amateur astronomers. One particularly interesting case is the star HD 189733 A; it has a transiting hot Jupiter that generates an easily measured light curve, and that produces an orbital RV in the host star that can be detected with the spectrograph used in this study. This would be a particularly exciting project for students, who could measure both the size and mass of the exoplanet, and thereby determine its density, confirming for themselves that it is likely to be a gas giant. An exploratory study of this system is under way at the SFU observatory.

Appendix: Rudimentary principles of an echelle spectrometer

Most spectrometers, from cheap to state-of-the-art, are made using diffraction gratings as the principal dispersive element. Diffraction gratings consist of reflective or transparent surfaces that are etched with many parallel grooves, as illustrated in Figure 17 in the case of a reflection grating. The intensity of the reflected light is reinforced in specific directions, and vanishes in others, resulting in a so-called interference or fringe pattern, as seen when white light is reflected from DVDs and other compact disks, producing a spectrum of colours.

To understand the origin of this behaviour, first consider that the distances travelled to the reflecting surfaces by neighbouring incident light rays will generally differ by some amount d_{inc} , and similarly the distances travelled after reflection will differ by some amount d_{ref} , as shown in Figure 17. If the overall path difference $d_{ref} - d_{inc}$ (which varies with the angles of incidence and reflection) is a whole number of wavelengths λ , then the reflected waves will add construc-

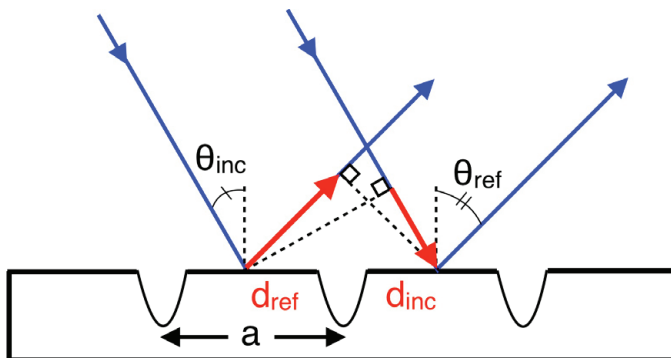


Figure 17 – Reflection of two incident light rays from a diffraction grating. The small rounded dips represent non-reflective etchings in the surface.

tively, to produce a net reflected wave of maximum intensity, as illustrated in Figure 18. If, on the other hand, the path difference equals a “half-integer” number of wavelengths, then the reflected waves will cancel each other out completely, also as illustrated in Figure 18.

The so-called *grating equation* expresses the condition for constructive interference (see e.g. Ref. [1])

$$d_{ref} - d_{inc} = a(\sin \theta_{ref} - \sin \theta_{inc}) \quad (12)$$

$$= n\lambda, \quad n = 0, 1, 2, \dots$$

Maxima and minima in the intensities of different wavelengths occur at different reflection angles θ_{ref} (for a given angle of incidence θ_{inc}), producing the characteristic spread of colours. Successive interference bands are referred to by the order in the sequence, i.e. by the number n in the grating equation.

A key property of diffraction gratings is that the spread, or dispersion, in wavelength increases with the order, as illustrated in Figure 19. This means that to maximize the resolving power of the grating (that is, to split apart neighbouring spectral features to the greatest extent possible), one would like to use the reflected light from the highest possible order.

However, there are two critical drawbacks with using ordinary diffraction gratings. One drawback is that most of the light

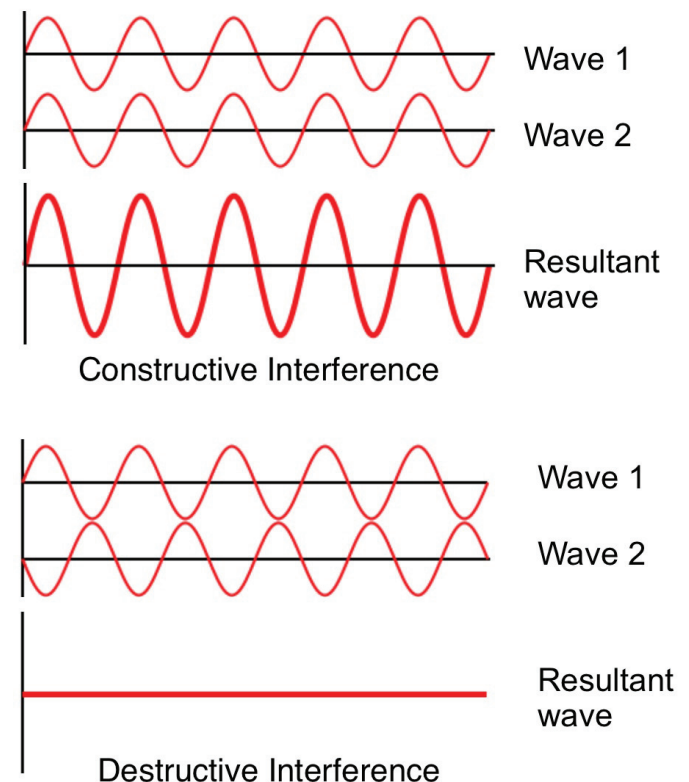


Figure 18 – Examples of constructive and destructive interference (graphic adapted from a Creative Commons source [29]).

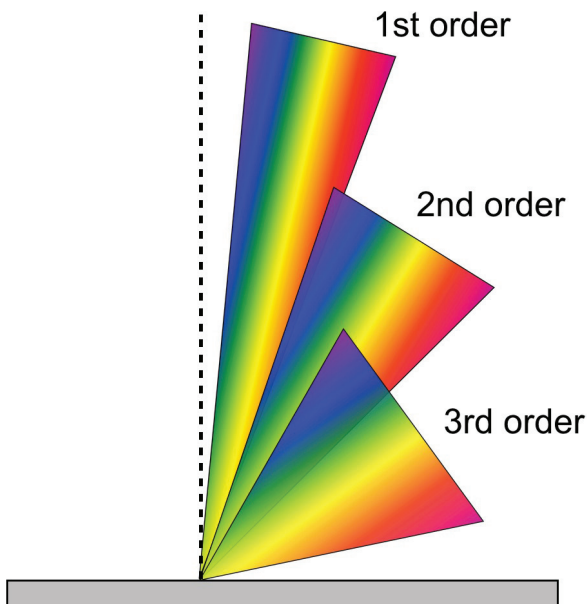


Figure 19 – Dispersion in reflected light from the first three orders of a diffraction grating.

energy is concentrated in the zeroth-order fringe (0^{th}), where all wavelengths emerge at the same angle, and the intensity also drops rapidly at higher orders. It is useful to note that at zeroth order, the angles of incidence and reflection are equal, a situation known as *specular reflection*; this is the familiar situation encountered when light is reflected from a large mirror. The second drawback with ordinary diffraction gratings is illustrated in Figure 19: light of a given wavelength in one order is overlapped by shorter wavelength light from higher orders.¹¹ In practice, there will be a range of wavelengths at a given order that does not suffer from an overlap, which is referred to as the *free spectral range*; this occurs because any detector that records the spectrum will be sensitive only to a limited range of wavelengths. The free spectral range is illustrated in Figure 19 in the case of a sensor that detects mainly optical light, such as a typical CCD chip. Unfortunately, the free spectral range decreases with increasing order, as can also be seen in Figure 19.

Echelle spectrometers use a two-part strategy to alleviate these drawbacks. One part of the strategy is to use a so-called “blazed” reflection grating, where the reflecting facets are inclined at an angle with respect to the mounting surface, as shown in Figure 20. The bias in favour of specular reflection from the inclined facets, combined with interference due to the underlying grating pattern, concentrates the reflected energy at higher orders. It turns out that most of the energy in a particular wavelength emerges in one or two high-order diffraction bands, as suggested in Figure 20 by the reflected red ray (in the case of the *eShel*, for example, the red H α line is near the middle of order 34).

To deal with the overlap of wavelengths from different orders, another dispersive element is introduced, known as a cross-

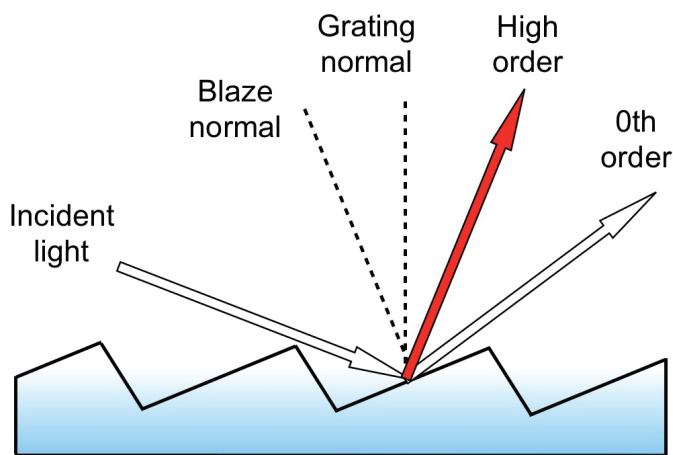


Figure 20 – Illustration of a blazed grating. “Blaze normal” identifies the direction perpendicular to the reflecting facets, while “Grating normal” identifies the direction perpendicular to the grating substrate.

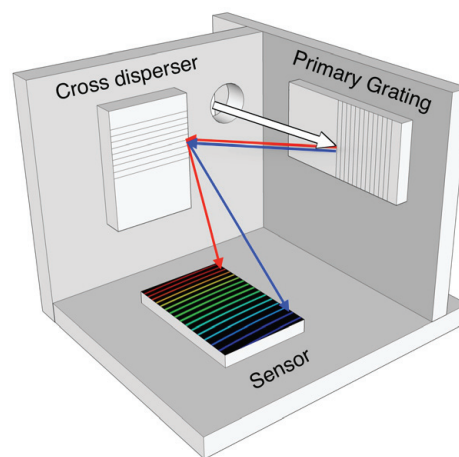


Figure 21 – Schematic of an echelle spectrometer. Only one incident ray of white light is shown, and two overlapped rays (one red, one blue) reflected from the primary blazed grating. Other elements of the spectrometer, including a collimator for the incident light, and a lens to focus the dispersed light on the imaging sensor, are not shown.

dispenser. The cross-disperser is used to spread apart the light that emerges from the primary blazed grating, in a direction perpendicular to the initial dispersion, as illustrated in Figure 21; the cross-disperser can be a low-resolution reflection grating, as in the diagram, or a prism (which is the case with the *eShel*).

As a result of the cross-disperser, the spectrum produced by an echelle consists of rows of dispersed light, as depicted in Figure 21, and in an actual image taken with an *eShel*, shown in Figure 4. Each row in the output corresponds to the spectrum of one order produced by the blazed grating. As seen in Figure 4, the intensity of light is not uniformly distributed across the rungs of an echelle, with the reflected energy at each order concentrated in a specific wavelength of light. In the case of a prism cross-disperser, the bands are curved, since the index of refraction in glass varies with wavelength.

References

- [1] Harrison, K.M. (2011). *Astronomical Spectroscopy for Amateurs*. New York: Springer.
- [2] Robinson, K. (2007). *Spectroscopy: The Key to the Stars*. London: Springer-Verlag.
- [3] Dickinson, T. (2015). Editor's Report: New Canadian Observatory's First Colour Photo. *SkyNews, Vol. XXI, Issue 4* (November/December).
- [4] Trottier, H.D. (2016). Pen & Pixel. *JRASC, Vol. 110, No. 4* (August).
- [5] Simon Fraser University Trottier Observatory, www.sfu.ca/science/trottierobservatory.html.
- [6] Christian Buil, personal website, www.astrosurf.com/buil.
- [7] ARAS Spectroscopy Forum, VV Cephei campaign, www.spectro-aras.com/forum/viewforum.php?f=19&sid=654cc3b0e4bd604475994f0366f6963c.
- [8] The Extrasolar Planets Encyclopedia, www.exoplanet.eu.
- [9] Butler, R.P. et al. (1997). Three new "51 Pegasi-type" planets. *Astrophysical Journal*, 474:L115.
- [10] Kaye, T.G., Vanaverbeke S., and Innis J. (2006). High-precision Radial velocity measurement with a small telescope: Detection of the tau Bootis exoplanet. *J. Br. Astron. Assoc.* 116, 2.
- [11] Lockwood A.C. et al. (2014). Near-IR direct detection of water vapor in tau Boötis b, *Astrophysical Journal Letters*, 783:L29.
- [12] Eversberg, M. and Vollmann, K. (2015). *Spectroscopic Instrumentation: Fundamentals and Guidelines for Astronomers*. Berlin: Springer-Verlag.
- [13] Audela Open Source Astronomy Software, <http://audela.org/dokuwiki/doku.php?id=en:start>.
- [14] Image Reduction and Analysis Facility (IRAF), <http://iraf.noao.edu>.
- [15] ESO-MIDAS, www.eso.org/sci/software/esomidas.
- [16] National Optical Astronomy Observatory Library of Stellar Spectra, www.noao.edu/cflib.
- [17] Kitchin, C. (2012). *Exoplanets: Finding, Exploring, and Understanding Alien Worlds*. New York: Springer.
- [18] Perryman, M. (2011). *The Exoplanet Handbook*. Cambridge: Cambridge University Press.
- [19] Bozza, V., Mancini, L., and Sozzetti, A, Editors (2016). *Methods of Detecting Exoplanets: First Advanced School on Exoplanetary Science*. Springer.
- [20] NASA-Ames graphic (2012). www.nasa.gov/mision_pages/kepler/multimedia/images/transit-light-curve.html.
- [21] ESO Press Photo 22e/07 (2007). www.eso.org/public/images/eso0722e.
- [22] Gary, B.L. (2009). *Exoplanet Observing for Amateurs*. http://brucegary.net/book_EOA/x.htm.
- [23] Exoplanet Transit Database, <http://var2.astro.cz/ETD/>.
- [24] Queloz, D. (1995). Echelle spectroscopy with a CCD at low signal-to-noise ratio. *IAU Symposium No. 167*, 221.
- [25] Bouchy, F., Pepe F., Queloz, D. (2001). Fundamental photon noise limit to radial velocity measurements. *Astronomy & Astrophysics*, 374, 733.
- [26] Nielsen, M.B. et al. (2013). Rotation periods of 12 000 main-sequence Kepler stars. *Astronomy and Astrophysics* 557, L10.
- [27] Galland, F. et al. (2005). Extrasolar planets and brown dwarfs around A-F type stars, Part I. *Astronomy and Astrophysics*, 443, 337.
- [28] SIMBAD Astronomical Database. <http://simbad.u-strasbg.fr/simbad/>.
- [29] Haade (2010). *Interference of Two Waves*, https://commons.wikimedia.org/wiki/File:Interference_of_two_waves.svg

Endnotes

- 1 Interestingly, beginning in fall 2017, the disk of VV Cephei B and the star itself will undergo an eclipse by its giant partner VV Cephei A, and the progress of the eclipse can be monitored with amateur spectrographs. Information on a pro-am campaign to monitor the eclipse can be found in Ref. [7].
- 2 The CDK700 is usually installed at ground level, however at SFU we mounted it on a pedestal to minimize the observatory's footprint. The unusual device seen in Figure 3, hanging from the telescope's visual observing port, effectively acts as a "periscope." It is comprised of two Tele Vue NP101s, connected at their objectives, and is the elegant means by which eyeballs are brought to the eyepiece. The periscope was designed by Nick Seiflow, in consultation with Al Nagler of Tele Vue, and its components were manufactured by PlaneWave Instruments.
- 3 To compute the response function, it is usual to first interpolate over deep absorption lines in the spectra, and to apply a low-pass filter, to eliminate fine features in the spectra that are unrelated to the smooth instrumental response. Early A-class stars are commonly used, since they have relatively few absorption lines. Note that the response function obtained in this way depends on the altitude at which the comparison star is observed, due to differential absorption of light of different wavelengths by the Earth's atmosphere, and is not solely a property of the instrument. Note also that the overall scale of the corrected spectrum is arbitrary, and the result is a plot of *relative* intensity versus wavelength.
- 4 Equation (2) is an approximation that is valid for source speeds much smaller than the speed of light.
- 5 Although routines to evaluate cross-correlation functions are available in the analysis packages used by professionals [14] [15], and also in the more user-friendly package written by Buil [6] (though not in a very convenient form), I wrote my own.
- 6 Rectified spectral functions are used, since the smooth continuum behaviour in a star's spectrum is very insensitive to a Doppler shift. Also, an overall constant is subtracted from the spectral functions, so that the resulting averages are zero, $(I_{1,2})=0$, since overall shifts in the rectified spectra are of no physical consequence.
- 7 The absorption lines in the spectrum of 45 Boötis are wider and shallower than those of τ Boötis, which indicates that 45 Boötis has a much larger rotational speed. This was not anticipated, and in retrospect another choice of reference star might have been preferred.
- 8 A number of techniques for dealing with stellar jitter have been studied by professionals; see e.g. Refs. [18] and [19].
- 9 The chi-squared measure of the goodness-of-fit is about 1.5 per degree-of-freedom, indicating a reasonably reliable fit; this provides a posteriori evidence that that the statistical errors have been reliably estimated.
- 10 The orbital angle of inclination has been inferred from measurements of the RV of the exoplanet itself, from absorption lines in its atmosphere, and is about 45° [11], which implies that the exoplanet mass is approximately 6 times the mass of Jupiter.
- 11 For example, the λ maximum for a given wavelength $\lambda/2$ overlaps with the $n=2$ maximum for wavelength.

Of Observatories and Eclipses

by David Levy, Montreal and Kingston Centres

Brazil is a land that has an incredibly rich legacy in astronomy, and without a doubt the country respects that history. I learned that lesson a couple of hours after my flight landed in Rio de Janeiro to lecture at the Tenth Conference on Astronomy and Astronautics. Before heading off to the meeting venue in Campos dos Goytacazes, a city some 200 kilometres north of Rio, Marcelo Souza insisted that we visit the Observatorio Nacional in Rio. We arrived at what first appeared to be an aging planetarium, but when we entered the front door, we walked into an earlier time.

Brazil has a rich astronomical history, dating back to the middle 17th century, when Portuguese sailors made landfall on what would one day be modern Brazil. They navigated using sextants, but when they arrived, they later followed the developments in Europe and began setting up simple refractor telescopes with small lenses. In its earliest days, without a plethora of telescopes, the naked eye was the primary instrument used to appreciate, learn from, and most of all, enjoy the stars. In fact, while on my tour of this wonderful place, I gave two lectures to classes of young children. Each lecture consisted of a single sentence: “Always enjoy the stars.”



Figure 1 – Sugarloaf Mountain at Rio de Janeiro.

Brazil's national observatory does encourage its visitors to enjoy the stars. I was most impressed with what appeared to be a very long, rounded wood box hanging innocently from the ceiling. But it wasn't a box. It was a gorgeous old tube that, once upon a time, supported a 32-centimetre-diameter lens, which stands displayed in a case nearby. The telescope was intended to be used at this very observatory, but the complex already had a more traditional metal-tubed refractor that the staff was happy with, and which miraculously is still in use today. This metal-tubed telescope is used for public viewing nights every clear Wednesday and Saturday evening.

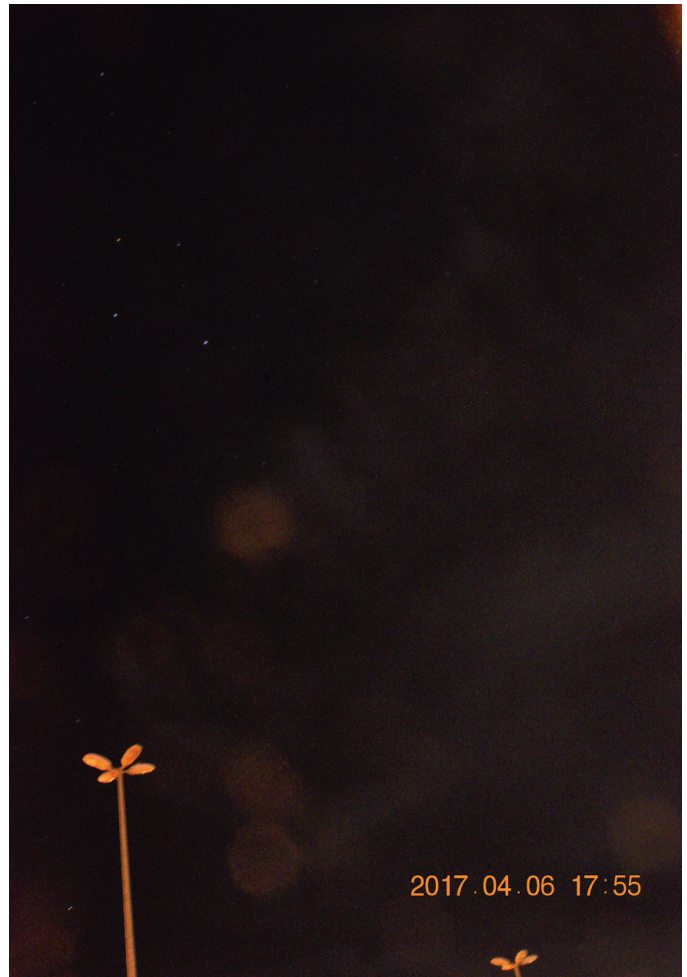


Figure 2 – The Southern Cross photographed from my hotel at Campos.

We can learn much from the National Observatory in Brazil, which takes its history quite seriously. These lovely telescopes were state of the art around the world, from about 1800 through 1930. By the late 20th century, the old refractors had been superseded by the great reflectors, which still do the best scientific observing. Currently, and now the *Hubble Space Telescope*, giant 90-inch reflector built to use in space, enjoys the best pictorial definition of any telescope in the world. These old refractors in Rio de Janeiro, however, still have life left in them. As long as there are young eyes and minds eager to peer through these telescopes, they could live forever.

The partial phases of August's eclipse.

On August 21 this summer, the long shadow of the Moon will race across the United States, offering millions of people a look at the Sun's magnificent atmosphere, its corona. But for the millions more who do not make it to the narrow path of total eclipse, the Sun's light will still be partially cut off by the Moon. Everyone in the United States, and almost all of Canada, will see a partial eclipse that day. How much of the Sun will be covered by the Moon depends on where you live. Tucson, Arizona, to cite an example, will see a maximum eclipse of 58 percent.

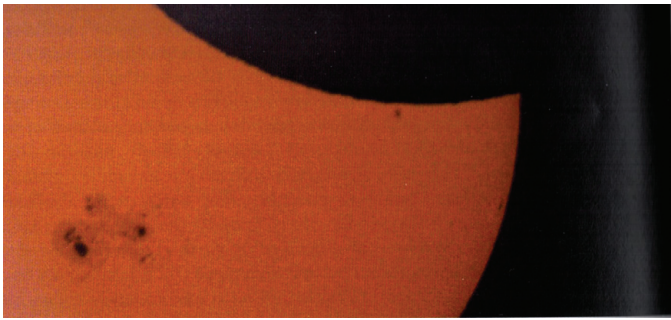


Figure 3 — This is a view of the partial solar eclipse of 2014 October 23. By coincidence, the largest sunspot group of that cycle happened to be on the Sun that day. All images: David Levy

A partial eclipse lacks the drama of a total eclipse, but it is well worth watching nevertheless. The beginning is subtle. The Moon's first bite is barely noticeable, appearing at first as a tiny flat area cutting into the edge of the Sun. Within a few minutes, that "line" becomes curved as the Moon cuts into ever-larger regions of the Sun. As the eclipse progresses, more and more of the Sun gets cut off. Within an hour, half the Sun will be covered and our star will take on the appearance of a crescent.

By this time, you need to pay close attention to the warnings about possible eye damage during a solar eclipse. Never look at the Sun without protection for your eyes. It is dangerous even when there is no eclipse. During an eclipse, the Sun's light is reduced, and you do want to gaze at it, but the dangerous UV and infrared is still there. (During the moment of total eclipse, and only then, is it perfectly safe to gaze at the Sun without protection for your eyes.) Most people have access to eclipse glasses fitted with strips of Mylar plastic that offer excellent protection from the Sun's harmful rays. If you do not have access to a pair, you can project the Sun's image through a pinhole onto a second sheet of paper or cardboard. But do not look through the pinhole. If you have a telescope, you can project the Sun's image onto a piece of cardboard, a wall, or even the ground.

The closer you are to the path of totality, the thinner the crescent will get. If there is a tree nearby, try looking at the spaces between its "leaves' shadows". You should be able to see dozens of crescent Suns, each one projected through a space between the leaves. Their appearance is really quite wonderful. If the eclipse gets deeper than 80 percent, the sky will begin to darken slightly and a general sense of quiet will start to descend across the land.

After maximum eclipse, the story reverses. The sky lightens up, the crescent gets much wider, and after another hour, the Moon leaves the Sun and the eclipse is over.

I know all these things because I have witnessed 90 eclipses since 1959, about 30 of which were either partial or the partial phases of total eclipses. An eclipse offers absolute proof that the Earth is moving through space around the Sun, that the Moon circles the Earth, and that because of a cosmic coincidence, the Moon and the Sun get in each other's way and that occasionally there is an eclipse. We are a part of this graceful movement. Eclipses teach us that we are a part of the Solar System, and on August 21, throughout most of North America, we will get a first-hand demonstration. ★

David H. Levy is arguably one of the most enthusiastic and famous amateur astronomers of our time. Although he has never taken a class in astronomy, he has written over three dozen books, has written for three astronomy magazines, and has appeared on television programs featured on the Discovery and the Science Channels. Among David's accomplishments are 23 comet discoveries, the most famous being Shoemaker-Levy 9 that collided with Jupiter in 1994, a few hundred shared asteroid discoveries, an Emmy for the documentary Three Minutes to Impact, five honorary doctorates in science, and a Ph.D. that combines astronomy and English Literature. Currently, he is the editor of the web magazine Sky's Up!, has a monthly column, Skyward, in the local Vail Voice paper and in other publications. David continues to hunt for comets and asteroids, and he lectures worldwide. David is also President of the National Sharing the Sky Foundation, which tries to inspire people young and old to enjoy the night sky.

RASC Internet Resources



Like us on Facebook



Follow us on Twitter @rasc

www.rasc.ca

Visit the RASC Web site

www.rasc.ca/discussion

Email Discussion Groups

www.rasc.ca/contact

Contact the Society Office

www.rasc.ca/news

RASC eNews

Mask Basics 2



by Blair MacDonald, Halifax Centre
(b.macdonald@ns.sympatico.ca)

In the last edition, we looked at the improvements a simple luminance mask could make when stretching images. It helped to control the background and it brought the nebula out of the background, improving contrast and holding the noise in check.



Figure 1 – Stretched image, with and without a luminance mask applied

Remember the mask was applied to the image on the left, but there are more improvements to be made.

Starless luminance mask

The image on the left was stretched using the simple luminance mask shown below.

The problem with this approach is that the stars are quite bright in the mask. This means that the resulting image will have a great deal of stretch applied to the stars. This tends to



Figure 2 – Simple luminance mask

make for a little star bloat and robs the result of a lot of colour. If only there was a way to remove the stars from the image...

Well, it turns out there is. Astro-specific packages like *Images Plus* have tools that can produce starless masks with a few mouse clicks and a freeware package called *Straton* does a reasonable job as well. There is even an easy way to make the required mask in *Paint Shop Pro* or *Photoshop*. Start by making a duplicate of the luminance mask on another layer. Next, blur the top layer slightly; use a Gaussian blur of about seven pixels. Set the combine mode to difference and the nebula disappears, leaving behind a star-only image.

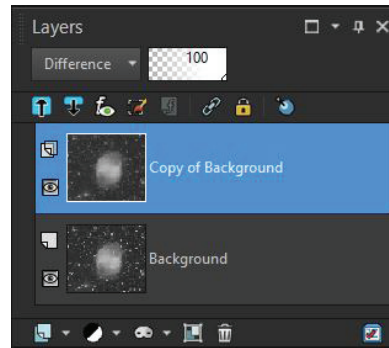


Figure 3 – Star-mask layer stack

Merge the layers and then threshold the result to make a star mask as shown below.

Next, use the Magic Wand tool to select a star in the mask. Set the select mode to brightness and make sure that *contiguous* is not checked. This will select all stars in the mask image. Next,

save the selection to the alpha channel in *Paint Shop Pro* or *Photoshop*. Now return to the original luminance mask and recall the selection. This will produce a selection ring around the stars in the image. Expand the selection by a few pixels so that it is very slightly larger than the stars. With the stars selected, use an erosion or minimum filter to reduce the stars. It will take several iterations to completely remove the stars and some of the large stellar halos may remain. Before cloning out any remaining halos you will have a mask similar to the one shown below.



Figure 4 – Star mask



Figure 5 — Initial starless mask

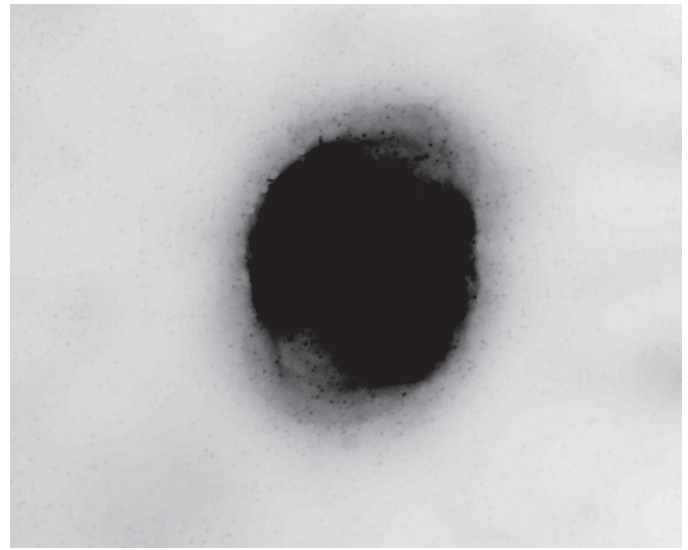


Figure 6 — Blurring mask

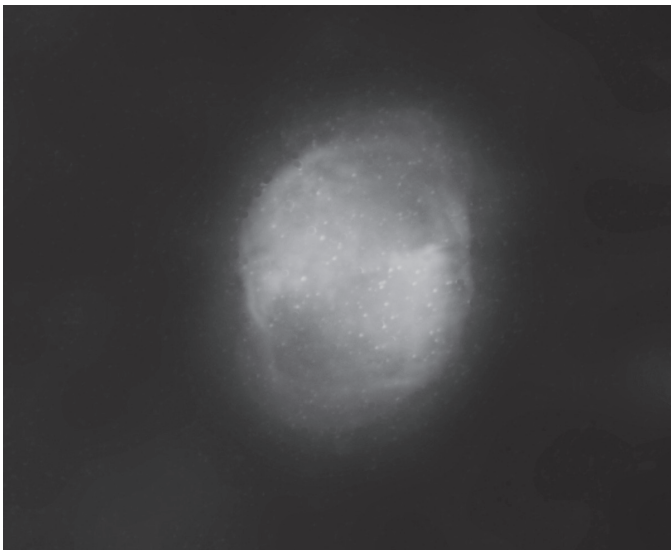


Figure 7 — Final starless mask



Figure 8 — Final stretched image

Clone out the halos and save the mask then duplicate the image and negate it, then use Levels to stretch the result so that you get the nebula in black and close to a white background. This will be used as a mask to blur the starless mask, removing any remaining halos and the remaining small stars. The idea is to keep the detail in the nebula and blur the background, so don't be afraid to paint the white areas of the blurring mask if necessary.

Use the negative mask to control a large-radius Gaussian blur of the starless mask producing the final starless mask shown below.

Now apply the mask to all your stretches of the original image to prevent star bloat and maintain good colour in the stars.

Compare the image in Figure 1 — Stretched image, with and without a luminance mask applied to the image stretched with

a simple luminance mask, and to the image stretched with no mask, and I think you will appreciate the difference.

By using a starless luminance mask, you get the nice dark background of the simple luminance mask with none of the star bloat, and keep much more colour in the stars.

Remember, this column will be based on your questions so keep them coming. You can send them to the list at hfxrasc@lists.rasc.ca or you can send them directly to me at b.macdonald@ns.sympatico.ca. Please put "IC" as the first two letters in the topic so my email filters will sort the questions. ★

Blair MacDonald is an electrical technologist running a research group at an Atlantic Canadian company specializing in digital signal processing and electrical design. He's been an RASC member for 20 years, and has been interested in astrophotography and image processing for about 15 years.

Second Light

An Exoplanet Around a B0-A9.5 Star



by Leslie J. Sage
(l.sage@us.nature.com)

Thousands of planets are now known to orbit around low-mass stars—roughly 1.2 solar masses or less—but only six have been found around A-type stars. This raises the question of whether there is something fundamentally different about the formation process of massive stars, relative to the low-mass ones. Of course, there are observational biases in the searches for planets around massive stars. Scott Gaudi of Ohio State University, and a team of collaborators around the world, has found a planet transiting the star HD 195689, which is a B0-A9.5 star with a visual magnitude of 7.6 (online on *Nature's* website on June 5, in print in the June 22 issue). The planet's atmospheric temperature is about 4600 kelvin on the dayside, or as hot as the surface of a K4 star. The amount of ultraviolet radiation the planet receives might be sufficient to entirely remove the atmosphere before the end of the star's main-sequence lifetime.

WASP-33 was hitherto the hottest star with a transiting planet, with a surface temperature of about 7400 K. Its planet has a dayside temperature estimated to be about 3600 K. The atmosphere is puffed up relative to where theory predicts, and the reason for that is not understood. It has to be related to the amount of stellar radiation, but the specific process by which it is puffed up is not presently known. The atmospheric temperature is comparable to an M dwarf star, but sufficiently cool that

molecules can survive (as indeed they do in the atmospheres of M dwarf stars).

HD 195689, dubbed KELT-9 by Gaudi et al. as it was studied using the Kilodegree Extremely Little Telescope (KELT), is a much hotter star with a surface temperature of about 10,200 K, putting it on the boundary between A and B type stars. Its position in the sky is right ascension = 20h 31m 26.354s, declination = 39° 56' 19.774", in the constellation of Cygnus, and therefore visible from Canada during the summer. It is so bright that it can be seen with binoculars. It is about 200±20 pc from us.

The field surrounding the star was observed about 6000 times from June 2007 to June 2013, to get the light curves shown in the figure. Spectroscopic follow-up observations provided the radial velocities, meaning that both the radius and mass of the planet could be determined. Its mass is about 3 Jupiter masses, and its radius about 2 Jupiter radii. The dayside temperature is about 4600 K. It is puffed up even more than WASP-33b. The planet's temperature is so high that any molecules would be dissociated, and probably the primary source of opacity will be atomic metals such as sodium and magnesium.

KELT-9b orbits its parent star in 1.5 days, at a distance of 0.035 au, or 3.2 stellar radii. That means that it is continually blasted by ultraviolet radiation from the star, which is likely ablating the atmosphere at a sufficiently high rate that it probably could be measured with *Hubble Space Telescope* observations, although the rate is uncertain within a factor of a hundred. At the low end, the atmosphere will survive the star's main-sequence lifetime, but at the high end the atmosphere will be gone before the star moves off the main sequence.

KELT-9, the star, is about 300 million years old, comfortably middle-aged with a main-sequence lifetime of about 500 million years. As it moves off the main sequence it will expand

and cool, eventually engulfing whatever is left of the planet. If the atmosphere survives, it could cause a transient brightening, and lead to unusual abundances in the stellar atmosphere.

So, get out your star charts, find your way to Cygnus and see if you can identify KELT-9 in the sky. It's in the plane of the Milky Way, so the field will be crowded, but it will be quite bright with even a small telescope. When you find it, imagine a planet so close that it is almost touching the star. The transit lasts about four hours,

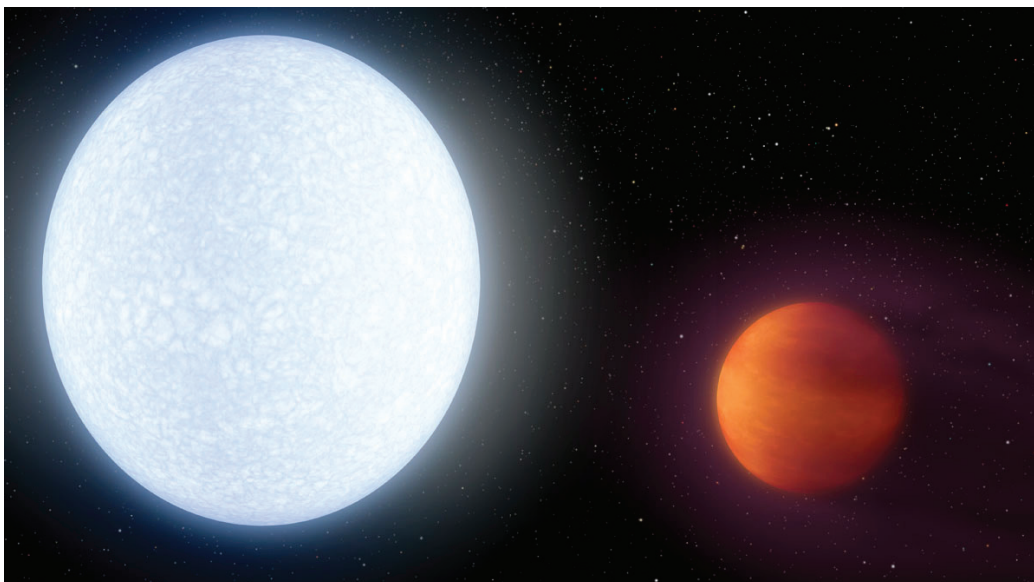


Figure 1 — An artist's impression of the KELT-9 system. Image courtesy of Scott Gaudi and JPL.

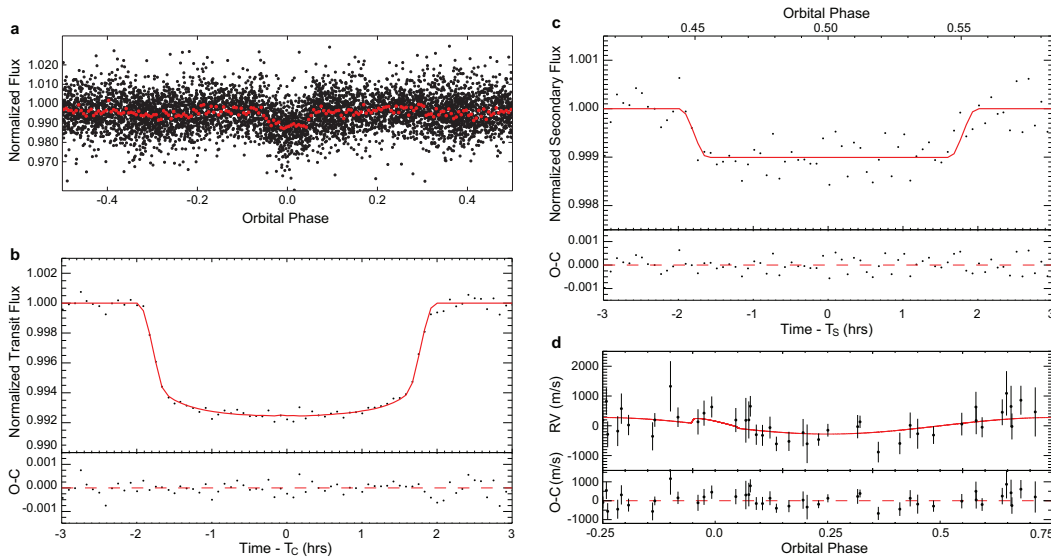


Figure 2 — a) A plot of all the light-curve data, with the binned average shown in red. b) The binned light curve of the primary eclipse from follow-up observations. c) The binned light curve of the secondary eclipse (planet behind the star). d) The Doppler reflex curve of the star. Figure courtesy of Scott Gaudi and Nature.

out of an orbital period of 35.5 hours, and the secondary eclipse the same amount of time, so there is a reasonable chance that when you see the star it will be undergoing either a primary transit or secondary eclipse, though you will not be able to see the loss of light because the dip is only 0.6 percent when the planet passes in front of KELT-9. ★

Leslie J. Sage is Senior Editor, Physical Sciences, for Nature Magazine and a Research Associate in the Astronomy Department at the University of Maryland. He grew up in Burlington, Ontario, where even the bright lights of Toronto did not dim his enthusiasm for astronomy. Currently he studies molecular gas and star formation in galaxies, particularly interacting ones, but is not above looking at a humble planetary object.

SkyShed
POD MAX
www.skyshedpodmax.com
 Ph. 519-345-0036

It's even cooler than we thought it would be

The Shadows of Galaxy Clusters



by Erik Rosolowsky, University of Alberta
(rosolowsky@ualberta.ca)

This column comes in the aftermath of the annual meeting of the Canadian Astronomical Society. My colleagues and I hosted this year's meeting at the University of Alberta in Edmonton. After a year of effort, it was wonderful to have a large part of the Canadian astronomical research community join us for a week-long discussion of new results and upcoming issues facing our community. I spent most of the week running around attending to little details like finding extension cords and cleaning up lecture halls after spills. In the quiet between these little crises, I could sit down and listen to what the astronomers were up to. One of the talks I heard was about the Sunyaev-Zel'Dovich (SZ) effect and how we could use the SZ effect to study the evolution of galaxy clusters. The talk was delivered by Mike McDonald, a Canadian-trained astronomer who is now a professor at the Massachusetts Institute of Technology. At its most basic level, the SZ effect refers to the shadows cast by galaxy clusters on the relic radiation from the Big Bang. Unpacking this blithe description showcases a lot of amazing physics that is studied using observations with radio telescopes.

The first piece of the SZ physics chain is to understand where the radiation comes from. The light under discussion is the given the name of the Cosmic Microwave Background (CMB). The CMB is radiation seen in all directions that appears to be coming from the most distant source possible. Hence, it is thus behind all other sources of electromagnetic radiation and is given the name "background." The radiation is relic of a much younger Universe. The Big Bang theory's central tenet is that the early Universe was much hotter and denser than it is now. It has since expanded and cooled off globally. This simple premise has a huge set of consequences, setting the stage on which the evolution of galaxies and galaxy clusters plays out. The Big Bang theory was conjectured as a natural starting point for the observed expansion of the Universe first seen by Edwin Hubble in the 1920s.

In addition to being hotter and denser, the early Universe would also have been much more uniform than its present state. In the modern Universe, there is a huge range of densities ranging from the near-vacuum of space to high density objects like stars and planets. The fundamental reason for this contrast in density is gravitation: slightly dense regions exert slightly more pull on the surrounding material, increasing their density and thus pulling harder on their surroundings.

This runaway process causes gravitationally driven collapse that is the main actor in creating all the structure we see around us today. In the early Universe, this gravitational collapse was just starting to happen and the density differences were slight: parts in millions (Figure 1). The Universe was just a uniform hot plasma of ionized hydrogen and helium. The ionized nature of the gas comes from the high temperatures: the gas is too hot for the positively charged nuclei of atoms to remain attached to their electrons. The individual particles are moving too fast so that collisions will knock the electrons loose from their bound states. The conditions are quite similar to the outer layers of the Sun where the gas has temperatures of tens or hundreds of thousands of degrees. This is a good description of the Universe between the age of a few minutes up to about 300,000 years.

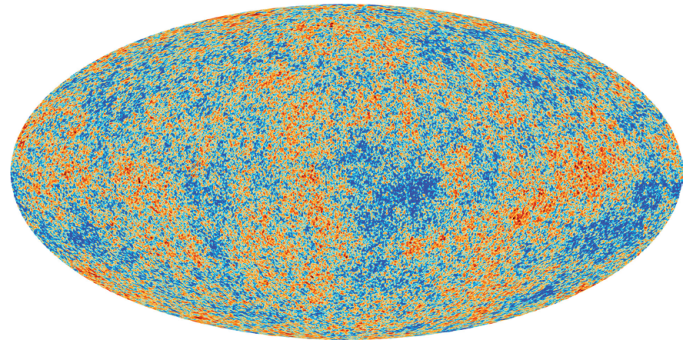


Figure 1 — The Cosmic Microwave Background as observed over the whole sky by the *Planck* satellite. The map shows small bumps and ripples on an overall uniform radiation field. The bumps are only one-millionth the strength of the field, so careful measurements are required to detect these small changes. The small deviations from smoothness highlight the emerging picture of how cosmic structure forms at in the very young Universe. Image Credit: ESA and the Planck Collaboration

Hot, dense plasma is also opaque; we cannot see through the Sun. Individual photons, while travelling at the speed of light, are constantly colliding with the electrons and bouncing off in new directions. Light cannot move quickly through the plasma and it does not travel on a straight line. Key to this opacity is the free nature of the electrons. If the electrons are locked up into atoms, only specific energies of photons can interact with the atoms, corresponding to the energy levels of the atoms. Thus: plasmas are opaque, but neutral gases are mostly transparent, except for very specific colours of light.

The Cosmic Microwave Background arises because the Universe is expanding and cooling off. This expansion reaches a critical point at the age of 300,000 years, where it cools sufficiently that the electrons can be locked up into stable atoms. Relatively quickly, all the photons that were constantly bouncing off electrons and unable to go in a straight line become free to travel. These photons become the Cosmic Microwave Background. They hurtle off across the Universe at the speed of light.

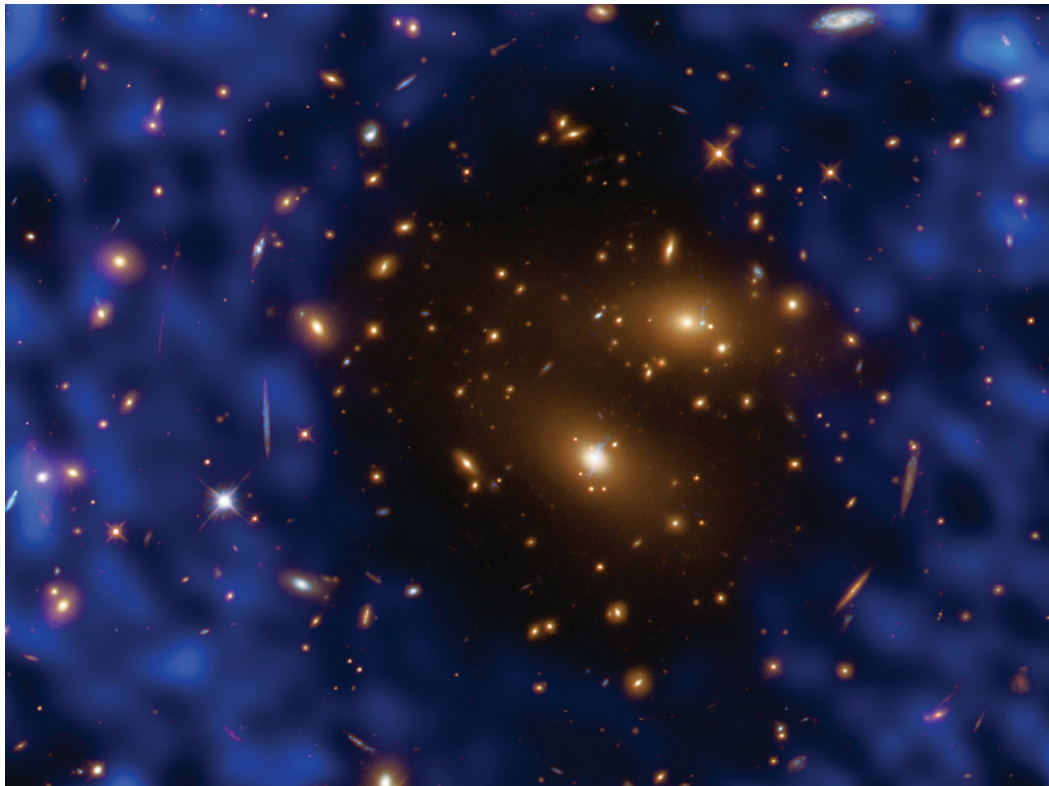


Figure 2 — The Sunyaev-Zel'dovich effect seen around galaxies as observed by the ALMA telescope. The blue image shows the pattern of radiation from the Cosmic Microwave Background and the missing “hole” in the middle is caused by the high temperature gas in the galaxy clusters boosting CMB photon energies. These holes are relatively small and cannot be seen on whole-sky maps like that of Figure 1. Image Credit: ALMA (ESO/NAOJ/NRAO)/T. Kitayama (Toho University, Japan)/ESA/Hubble & NASA

The Universe is constantly expanding in all directions and this expansion also expands the photons, causing them to lose energy. This process is called the cosmological redshift. At the beginning of the journey, these photons are visible light with a similar spectrum to sunlight. By the time these photons travel across the visible Universe, the redshift has pulled the energies down into the long wavelength part of the radio spectrum, which is detectable using radio telescopes. In fact, the original observations of this radiation were made by engineers Arno Penzias and Robert Wilson at Bell Labs. Their persistence in trying to understand this annoying source of noise in their telescope ultimately became one of the fundamental observations of modern astronomy.

This CMB radiation comes from all parts of the sky and remains the single best piece of evidence that the Universe was once hot and dense. The radiation is nearly uniform, but the small deviations from a uniform radiation field give vital information about the evolution of the early Universe. In contrast, the SZ effect is giving information about galaxies and their evolution closer to the current day. This is because large galaxy clusters appear as shadows against the CMB (Figure 2). The reason these clusters cause shadows is because they are filled with extremely hot gas. This gas is heated by the process of galaxy collisions and evolution, where a combination of star formation and jets from the central black holes blow superheated material into the space between galaxies. This hot gas is ionized and the high temperatures mean the free electrons are moving at high speeds. These electrons collide with photons from the CMB and share some of their energy with the photons, boosting the photon energy. The net result

is that photons are pumped up to higher energies, leaving behind a missing piece of the CMB, if you are looking at the “expected” energies in the radio portion of the spectrum.

What is fascinating about this effect is that it appears the same to us at all distances: if there is a cluster, it casts a shadow. This means that we can study clusters over a large set of distances and ask questions about whether the closer targets are different from the more distant ones. Such a study takes advantage of the finite speed of light, so the more-distant targets are seen earlier in their evolution. With all this cleverness in place, we can revisit Mike McDonald’s talk at the meeting. Dr. McDonald looked at 57 galaxy clusters selected by the SZ effect, studying the state of clusters ranging from the present day back to when the Universe was only 1/3 its current age. Using X-ray telescopes, Dr. McDonald could zoom in on these galaxy clusters and probe the high temperature gas. Combining the SZ results and the X-ray observations showed that these galaxies did not show much change in their structure in the past 10 billion years. The clusters did grow, but the overall structure suggests that most of the major cluster formation occurred even earlier on in the Universe. Overall, this clever use of the CMB to find clusters and a careful analysis of the populations is astrophysics at its best. We cannot understand the Universe by watching one system change over time, but we can look at many systems seen at different ages as the next-best-thing.

Erik Rosolowsky is a professor of physics at the University of Alberta where he researches how star formation influences nearby galaxies. He completes this work using radio and millimetre-wave telescopes, computer simulations, and dangerous amounts of coffee.

Solar Eclipse Timings



by Blake Nancarrow, Toronto Centre
(blaken@computer-ease.com)

As a solar eclipse neophyte, I anxiously await the great North American celestial event in August this year. If I'm lucky, I will experience my first total solar eclipse. My packing list grows every day with items I feel I must have. I continue to research and study what will happen and, if I dare, how to photograph the spectacle. I keep testing equipment and batteries and simulating the event. Of course, I hope to employ a good app on my tablet and/or smartphone.

As I discovered the many available applications, I considered helpful and interesting features. I think the app should accurately calculate key times and durations for a given location that is automatically detected. It should have a countdown timer for totality. But perhaps what I thought most useful would be audible responses. I was very interested in an app that would quote timings or do countdowns with spoken words so that I could watch the sky—not the tablet screen—to be aware of and prepare for specific events.

I briefly tried a couple of software tools but was looking for something that worked on both the iOS and Android platforms. At one point, I spotted Solar Eclipse Timer (www.solarecliptimer.com) and it looked very interesting with a pleasing user interface and a number of good features, but I

moved on under the impression it was only available for Apple devices. Perhaps I read it wrong or initially it was only available on iOS, but when I looked at the website again, I happily found the Google Play button. I purchased version 1.3 for Android at \$2.69 and began exploring.

The Solar Eclipse Timer (SET) app opened in portrait mode to the Timer screen (Figure 1). Immediately I noted the wording “Universal Time”

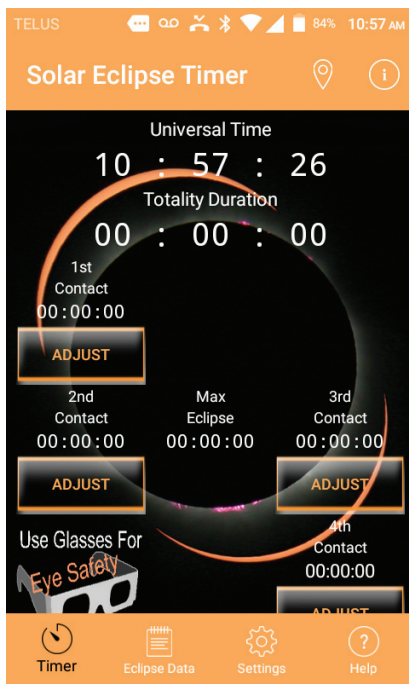


Figure 1 — The main Timer screen from a small Android smartphone.

but via the Settings panel I changed this to read as “Local Time.” I saw where the Timer display would show duration of totality, the calculated values for the first through fourth contact moments, along with the Max Eclipse incident time. With some satisfaction, I noted the safety warning reminding users to wear their eclipse glasses during partial phases. I also enjoyed the background multi-exposure photograph (by the owners) with prominences and hints of the corona bracketed by thin solar crescents.

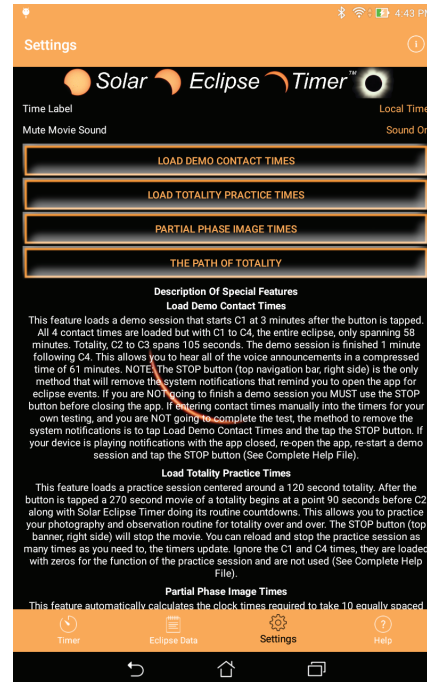


Figure 2 — The Settings screen from 7" Android tablet.

The ADJUST buttons were intriguing. It seems they can be used if the automatically generated times are incorrect or not calculated at all.

I was a little disappointed to not see eclipse magnitude or obscuration values.

In Settings (Figure 2) I guessed at the purpose of the LOAD DEMO CONTACT TIMES button without reading the detailed description. The app prepared

the Timer screen with sample times to help me experience how the tool would function. Effectively, it was as if the eclipse were happening in a few moments. At T minus 3 minutes, I took in the scrolling on-screen prompt telling me to “Prepare For 1st Contact.” I waited for the audio content issued two minutes later. A man’s voice said, “First contact in 60 seconds.” Then, the recorded voice started counting down, “40 seconds... 20 seconds...” I actually felt a little excited! “10 seconds.” I turned up the volume, wondering if I would be able to hear my device during the real event, over the din of anxious humans (I better pack the earbuds). “Five, four, three, two, one,” then an audio tone sounded as a new photograph appeared, one taken just after first contact, with a nibble out of the Sun (like Figure 3).

While I was very pleased with the audio capabilities, I realized the visuals had to be taken with a grain of salt. I caught myself expecting a simulated view like in planetarium software. If I were using Stellarium or SkyTools, for example, I could set the view as if I were examining the horizon. I could configure the view to show a normal presentation like with a camera lens or binoculars, as opposed to a rotated or flipped telescopic view.

I would then see that on August 21 the Moon will encroach from the top-right of the Sun's disk from the west with the ecliptic steeply inclined.

A few minutes later, my ASUS screen brightened and a new message scrolled: "Prepare for Temperature Observation." This was followed up with an audio dispatch, "Forty-five minutes until totality, observe decrease in ambient temperature." The photograph changed, now showing the Moon further into the Sun. At 30 and 15 minutes from second contact, the communiqués repeated. Then the curiously worded message, "Prepare for Lighting Observation," appeared. The verbal prompt at T-10 made it clear I should watch for "changes in ambient lighting." At 8 minutes to go, SET reminded me to listen for changes in fauna and at 3 mins before totality I was encouraged to look for shadow bands. I found all these reminders very helpful and I hope to exploit them on the big day. That said, I wanted hints about planets and bright stars that might be visible—that I intend to look for—unfortunately, the app does not incorporate these.

The long demonstration carried on, periodically updating photos revealing less and less of the Sun's photosphere. At last the main event drew near, SET informed me of second contact in 2 minutes, and showed our star as a thin crescent. Once again, the app started counting down. At 10 seconds, a photo highlighting prominences was shown. After the final 5-second countdown, a tone sounded, the background rendered a coronal image, and an audio message stated, "glasses off." All of a sudden everything seemed to happen very quickly! The Totality Duration timer started counting down (Figure 4), the glasses warning was removed, and before I knew it, the voice

said the maximum eclipse was due in 10 seconds, then 5, and also reminded me to "observe the horizon," when I noticed the photo changed to a diamond ring as the app advised of 3rd contact and prodded, more than once, to put my protective eye-wear back on, and it was rapidly over, just like that! No doubt it will seem faster to me in the plains of Wyoming.

At this stage, the demo did

not continue in real-time, but wound down briskly. It fast-forwarded to fourth contact and concluded. Demo mode can be halted at any time by tapping the Stop button in the top bar.

This initial test was performed with my USB data/power cable plugged into the tablet. With the Android machine running continuously and not shutting off the screen, I didn't miss a

beat. But I knew I needed to try it without external power, which is how I'll be using my mobile device. Sadly, it did not work as I had hoped, but this is likely an issue with my old ASUS. Onboard Help notes discuss device issues that may interfere with notifications. I heard a number of audio tones and prompts to be sure, while my tablet was in sleep mode, like "Eclipse event, open app." Notification messages like "45

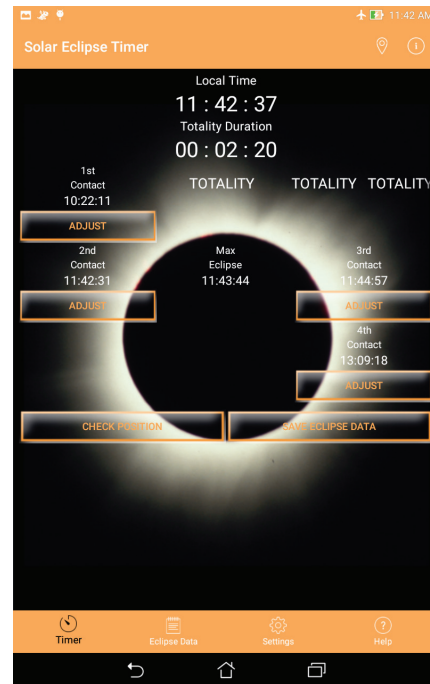


Figure 4 — Timer screen during totality in 2017 August 21 test.

min until Totality/observe ambient temperature" were obvious (like Figure 5). But during testing, 2 minutes from totality, no sound came from my device! Should I not rely too heavily on this app? Or can I keep the tablet from sleeping? I've seen some mobile apps with an option for overriding the automatic power-off; I wished for a convenient switch in this program. Happily, my smartphone, with a newer operating system, worked well!

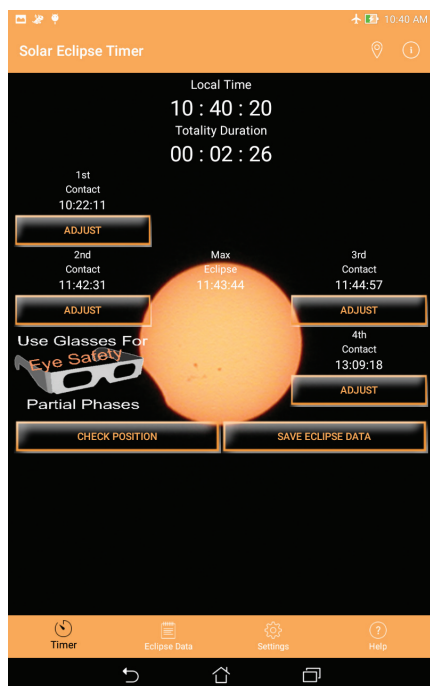


Figure 3 — A full simulation in Casper, Wyoming, after first contact.

**Is your address correct?
Are you moving?**

If you are planning to move, or your address is incorrect on the label of your Journal, please contact the office immediately.

By changing your address in advance, you will continue to receive all issues of SkyNews and the Observer's Handbook.

(416) 924-7973
www.rasc.ca/contact

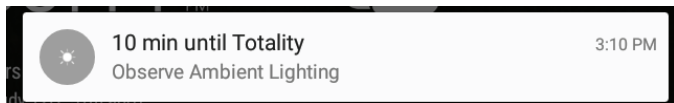


Figure 5 — Android notification shortly before second contact.

I also conducted a test for a future date and time and a location in the shadow path (city of Casper). It was fairly easy to tell the app where I was located after hitting the CHECK POSITION button from the Timer screen. The app only supports latitude and longitude in decimal format. Simulating the date and time of eclipse day in the seat of Natrona County, however, was awkward with no control inside the app proper. It took me a few moments to realize I had to first turn on Airplane mode to block automatic updating from the internet! Then my manually adjusted date/time values in the Android settings were followed.

Practice mode (available from Settings) lets you do real-time trials, perhaps to refine steps on your script or practice a photography or video run. All while the app plays a little movie with audio (from a cruise ship with very excited passengers).

The interesting Partial Phase Images panel shows sample thumbnail photos, but most importantly a timetable with calculated values should you want to shoot multiple images of

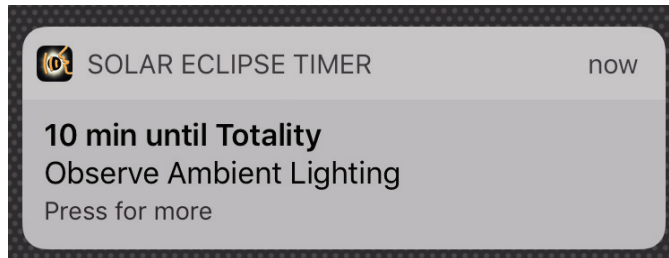


Figure 6 — Apple iOS notification from Solar Eclipse Timer.

the solar eclipse, perhaps for a single-frame multiple-exposure composition.

The SAVE ECLIPSE DATA button from the Timer display can be used to record your local eclipse circumstances, location details, and other notes. It can also act as a log sheet. But the owner explained the primary purpose as being “able to very quickly [save] your coordinates and your times in case [you’re chasing] good weather and you ended up observing at a site you did not expect or plan for.” Once you have saved notes you can access and edit them from the Eclipse Data list.

The indexed Help screens seem very thorough. There is also extensive information on the SET website. Owner Gordon Telepun enthusiastically helped me with various questions and provided screen snapshots from various devices.

There are certainly other apps out there if SET does not grab you. I liked the countdown to the next eclipse and auditory prompts in EclipseDroid. Some apps include interactive location maps and regional weather information. Some simulate a binocular view of the Sun being occulted by the Moon, for a particular location, to help the observer know where to look for first contact. Some get into a bit of the science of eclipses with history, photos, orbital diagrams, upcoming events, etc. One showed detailed technical information like the Moon–Sun size ratios and umbral depth.

Overall, I am pleased with Solar Eclipse Timer. It is straight forward and does what it promises. With its audio prompting, it sounds like it will be a good tool for eclipse day.

Update Bits

A new version (3.1.9) of Backyard EOS was made available back in March.

Do you have a favourite app? Have you written your own app? Let me know! ★

Blake’s interest in astronomy waxed and waned for a number of years, but joining the RASC in 2007 changed all that. He volunteers in education and public outreach, supervises at the Carr Astronomical Observatory, and is a councillor for the Toronto Centre. In daylight, Blake works in the IT industry.

The Royal Astronomical Society of Canada

Vision

To be Canada’s premier organization of amateur and professional astronomers, promoting astronomy to all.

Mission

To enhance understanding of and inspire curiosity about the Universe, through public outreach, education, and support for astronomical research.

Values

- Sharing knowledge and experience
- Collaboration and fellowship
- Enrichment of our community through diversity
- Discovery through the scientific method

Wannabe Stars and CFHT in Canada

by Mary Beth Laychak, Outreach Program Manager, Canada-France-Hawaii Telescope.

The first section of this month's column goes more in depth about a recent CFHT, University of Hawaii, University of Austin, and Keck Observatory news release. I have repurposed the release written by all of those organizations to add more detail and expand a bit on CFHT's role.

* * * * *

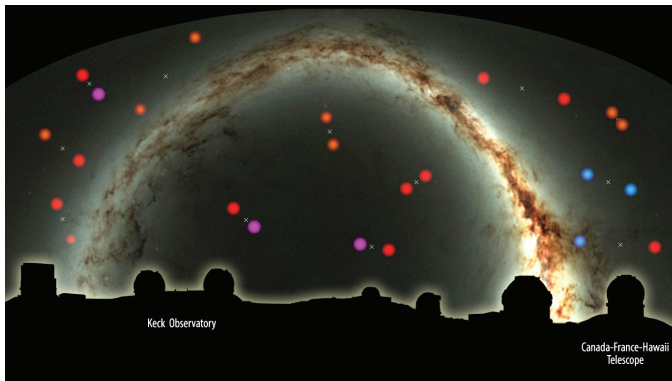


Figure 1 — photo credit Trent Dupuy, Karen Teramura, PS1SC

“When we look up and see the stars shining at night, we are seeing only part of the story,” said Trent Dupuy of the University of Texas at Austin and a graduate of the Institute for Astronomy at the University of Hawaii at Manoa. “Not everything that could be a star ‘makes it,’ and figuring out why this process sometimes fails is just as important as understanding when it succeeds.”

Dupuy is the lead author of the study and presented his research June 5th in a news conference at the semi-annual meeting of the American Astronomical Society in Austin.

Stars form in the heart of nebulae when a cloud of gas and dust collapses due to gravity. As the cloud collapses, the gravitational potential energy of the cloud decreases. The particles in the cloud begin to move faster, increasing their velocities and ultimately the temperature of the cloud. In the centre, the resulting ball of matter becomes hot enough and dense enough to sustain nuclear fusion at its core. Fusion produces huge amounts of energy—it's what makes stars shine. In the Sun's case, it's what makes most life on Earth possible.

But, not all collapsing gas clouds are created equal. Sometimes, the collapsing cloud makes a ball that isn't dense enough to ignite fusion. These “failed stars” are known as brown dwarfs.

This simple division between stars and brown dwarfs has been used for a long time. In fact, astronomers have had theories about how massive the collapsing ball has to be in order to form a star (or not) for over 50 years. However, the dividing line in mass has never been confirmed by experiment.

Now, astronomers Dupuy and Michael Liu of the University of Hawaii, who is a co-author of the study, have done just that. They found that an object must weigh at least 70 Jupiters in order to start hydrogen fusion. If it weighs less, the star does not ignite and becomes a brown dwarf instead.

How did they reach that conclusion? For a decade, the two studied 31 faint brown-dwarf binaries (pairs of these objects that orbit each other) using two powerful telescopes in Hawaii—the W.M. Keck Observatory and Canada-France-Hawaii telescopes—as well as data from the *Hubble Space Telescope*.

Their goal was to measure the masses of the objects in these binaries, since mass defines the boundary between stars and brown dwarfs. Astronomers have been using binaries to measure masses of stars for more than a century. To determine the masses of a binary, one measures the size and speed of the stars' orbits around an invisible point between them where the pull of gravity is equal (known as the “centre of mass”). However, binary brown dwarfs orbit much more slowly than binary stars, due to their lower masses. And because brown dwarfs are dimmer than stars, they can only be well studied with the world's most powerful telescopes.

To measure masses, Dupuy and Liu collected images of the brown-dwarf binaries over several years, tracking their orbital motions using high-precision observations. They used the 10-metre Keck Observatory telescope, along with its laser guide-star adaptive-optics system, and the *Hubble Space Telescope*, to obtain the extremely sharp images needed to distinguish the light from each object in the pair.

However, the price of such zoomed-in, high-resolution images is that there is no reference frame to identify the centre of mass. Wide-field images from the Canada-France-Hawaii Telescope containing hundreds of stars provided the reference grid needed to measure the centre of mass for every binary. The precise positions needed to make these measurements are one of the specialties of WIRCam, the wide-field infrared camera at CFHT.

The team used WIRCam for ten years to carefully map the regions of space around the binary samples to determine parallaxes and proper motion plus constrain the photocentre motion due to the binary orbits of the brown-dwarf pairs. For each target, they obtained data sets on multiple nights in either



Figure 2 — PI Mike Liu with WIRCam at CFHT.
Photo credit: Mary Beth Laychak

J or K filters. The queue observing at CFHT allowed the team to obtain the observations within very specific airmass windows to guard against errors caused by differential chromatic refraction.

The accuracy achieved by the team is remarkable. They can trace the movement of the brown dwarf to the micro-arcsecond as it moves across WIRCam pixels.

For example, they obtained a mean astrometric precision per epoch of 4.0 milliarcseconds on a target not related to this study (but using the same methodology), the rogue planet PSO J318.5-22 announced in 2013. Those observations were obtained over the course of two years, rather than the decade seen in this study.

“Working with Trent Dupuy and Mike Liu over the last decade has not only benefited their work but our understanding of what is possible with WIRCam as well” says Daniel Devost, director of science operations at CFHT. “This is one of the first programs I worked on when I started at CFHT so this makes this discovery even more exciting.”

The result of the decade-long observing program is the first large sample of brown-dwarf masses. The information they have assembled has allowed them to draw a number of conclusions about what distinguishes stars from brown dwarfs.

Objects heavier than 70 Jupiter masses are not cold enough to be brown dwarfs, implying that they are all stars powered by nuclear fusion. Therefore, 70 Jupiters is the critical mass below which objects are fated to be brown dwarfs. This minimum mass is somewhat lower than theories had predicted but still consistent with the latest models of brown-dwarf evolution.

In addition to the mass cutoff, they discovered a surface-temperature cutoff. Any object cooler than 1,600 kelvin (about 1315 °C) is not a star, but a brown dwarf.

This new work will help astronomers understand the conditions under which stars form and evolve—or sometimes fail. In turn, the success or failure of star formation has an impact on how, where, and why planetary systems form.

“As they say, good things come to those who wait. While we’ve had many interesting brown-dwarf results over the past 10 years, this large sample of masses is the big payoff. These measurements will be fundamental to understanding both brown dwarfs and stars for a very long time,” concludes Liu.

Figure 1 is a screen shot from an animation showing several of the binary pairs from the study orbiting around the system’s centre of mass marked by an X. The colours indicate the surface temperature, warmest to coolest: gold, red, magenta, or blue. The background image is a map of the entire sky seen from Hawaii, along with a silhouette of Maunakea, home of CFHT and the Keck Observatory. The binaries are located at roughly their position on the sky, keeping in mind that the actual size of the orbits is about one billionth the area covered by the x.

The full paper can be found at <https://arxiv.org/abs/1703.05775>

The animations can be found at <http://cfht.hawaii.edu/en/news/TrueStarsAndWannabes>

CASCA Teacher Workshop 2017

For the past three years, CFHT and Discover the Universe (www.discovertheuniverse.ca) hosted workshops for local teachers at the annual CASCA meetings. Our inaugural workshop was Hamilton 2015, followed by Winnipeg 2106 and Edmonton 2017. Our Edmonton 2017 workshop was the biggest and, by our estimates, best workshop thus far.

We held the workshop on Tuesday, May 30 for approximately 25 teachers in grades 6–12 in the local Edmonton area. The workshop focused on practical activities that teachers could immediately use in the classroom along with explanations of current hot topics in astronomy. The day began with Julie Boldoc-Duval from Discover the Universe introducing the teachers to the wonders of Canadian astronomy. Julie quoted the Canadian long-term plan, which suggests that Canadian astronomy should be recognized at the same level as Canadian gold medals in hockey. The teachers were suitably impressed with the efforts of Canadian astronomers and the worldwide impact of their astronomical facilities.

Our next activity involved the open-source software *Stellarium*, which brings a planetarium into the classroom and gives students the opportunity to view the night sky from wherever they are in the world. Studies have shown that students who observe and model phenomena such as the phases of the Moon retain a greater understanding than those who simply learn from a book. Julie demonstrated the ins and outs of the software, including how to utilize it in the classroom to model the Moon phases. The teachers loved the program, with many indicating they would be using it in their classroom as soon as possible.



Figure 3 — Julie Boldoc-Duval from *Discover the Universe* speaks with the teachers.

Matt Russo from Canadian Institute for Theoretical Astrophysics (CITA) led the next two sessions about black holes and exoplanets. Matt and others from the University of Toronto and CITA are developing a module about black holes and gravitational waves for *Discover the Universe*. We used a similar gravitational waves activity last year at the Winnipeg workshop, but the addition of the gravitation lensing activity was valuable for the teachers. Matt has custom wine-glass stems that nicely model the curvature of light around black holes. The teachers used the wine glasses along with laser pointers and astronomical images to see how the combination warped light. The gravitational waves activity proved even more topical than we anticipated because of the LIGO announcement of a third detection that occurred two days later.

The exoplanet session contained two components—a breakdown of the Trappist 1 system by Matt and a hands-on activity by myself. Matt was part of a team that modelled the resonance of the Trappist 1 system using musical notes. It was fascinating and engaged the teachers in an unexpected way. See the notes section for a link to an article about Matt’s work in the *New York Times*.

I taught the teachers an activity that I often use with students explaining Solar System formation. We used play dough and cotton balls to model four main steps in planetary formation



Figure 5 — Teachers modelled the four major stages in planet formation. Here is an example of their work modelling planetesimals forming.



Figure 4 — Matt Russo from CITA talks about “cool red stars” (note the sunglasses to show us how cool they are) similar to the host star in Trappist 1.

models—protostar embedded in nebula, accretion disks containing planetesimals, protoplanets, and our full-blown Solar System. Depending on the age of the students, teachers can incorporate conservation laws into the lesson or simply stop at the modelling of the phenomena.

Evaluations of the workshop were very positive. Teachers loved the *Stellarium* session; many commented they would use it in their classroom the next day. The exoplanet session also rated highly. Several teachers indicated they would use the modelling exercise in their class. While we did not talk with the teachers after the LIGO announcement, it would be interesting to see if the session on gravitational waves empowered them to explain the announcement with confidence to their students. One of the most constructive criticisms was the request to incorporate information on how the workshop topics can be aligned with the school curriculum. We plan to follow that recommendation for next year’s workshop, Victoria 2018.

Julie and I started discussing next year’s workshop with the CASCA Victoria planning committee. We have some exciting ideas in mind, so Victoria teachers if you are reading, keep an eye out next spring for the registration and announcement. In the meantime, I strongly encourage teachers and informal educators to check out Julie’s *Discover the Universe* page. It contains a lot of great information, webinars, and teacher workshops. ★

Notes

Matt’s article in the *New York Times* www.nytimes.com/2017/05/10/science/trappist-earth-size-planets-orbits-music.html?_r=0

Matt’s original Trappist 1 video: www.system-sounds.com

Mary Beth Laychak has loved astronomy and space since following the missions of the Star Trek Enterprise. She is the Canada-France-Hawaii Telescope Outreach Coordinator; the CFHT is located on the summit of Maunakea on the Big Island of Hawaii.

John Percy's Universe

Science “Culture” in Canada

by John R. Percy FRASC
(john.percy@utoronto.ca)

I recently had the pleasure of serving on a panel on Science Culture in Canada at the 2017 conference of the Canadian Association of Science Centres (CASC). The panel was organized by Kirsten Vanstone, Executive Director of the Royal Canadian Institute for Science (RCIS). For more than 150 years, the RCIS has played a major role in developing Canada's science culture, especially in the second half of the 19th century. The other panelists were Sandra Corbeil, Director of Strategic Partnerships and Networks at the Canada Science and Technology Museum, and Ivan Semeniuk, science reporter for the *Globe and Mail*. Since Ivan, Kirsten, and I are all astronomers, the panel was slightly unbalanced!

The panel was motivated by a recent report (Council of Canadian Academies, 2014) on *Science Culture: Where Canada Stands*. This report is freely available on-line¹. If you don't have time to read the whole thing, do read the 12-page Executive Summary.

The panel first addressed the question of how we define science culture in Canada. The report suggested that “a society has a strong science culture when it embraces discovery and supports the use of scientific knowledge and methodology. Such a culture encourages the education and training of a highly skilled workforce and the development of an innovative knowledge-based economy. The concept of a science culture is multidimensional, incorporating a number of distinct dimensions pertaining to how individuals and society relate to science and technology. The national context also influences how science culture develops and is expressed.”

As usual, the report stresses the utilitarian and economic value of science. To me, science culture is even broader, and includes:

1. *awareness* of science knowledge and issues, which may come from school, media, community, friends, and family
2. *interest*, which may depend on where the awareness comes from, and from whom, as well as on the intrinsic nature and interest of science itself
3. *understanding*, which may be superficial or deep; this is related to something called science *literacy*
4. *appreciation*, of science's economic, societal, and cultural importance, as well as its interest
5. *engagement*: the extent to which people engage with science through the media, science centres, hobbies, organizations such as the RASC, and even their participation as “citizen scientists”

6. *attitude*: some people have a negative attitude to science, especially if terms like nuclear, genetic, or pharma are involved. Often, this results from not appreciating the difference between science and the applications of science.
7. *skills*: to what extent can people use the methods of science to engage in critical, evidence-based thinking to solve problems in their workplace, or in everyday life? and
8. *training* of highly-skilled personnel; an increasing fraction of jobs in our knowledge-based economy requires science knowledge and skills.

There's also the question of *science in culture*, including the arts. This can include books about science and society (think Margaret Atwood) or books about scientists, such as those written by Dava Sobel. Science figures in art, such as the paintings by the Group of Seven, and in the content and production of many genres of music.

Many indigenous cultures have a much deeper understanding of and respect for the natural world than some of us do, so nature and science—though with a different definition and emphasis than in Western science—play an especially significant role in their culture.

The report presented the results of various surveys of science culture in Canada. These surveys had their limitations, but are better than anecdote and speculation. According to the surveys, Canadians have a positive *attitude* towards science and technology, and fewer reservations than in any of the 17 countries surveyed (though they were less convinced about the “promise” of science). They are highly *interested* in science, ranking first out of 33 countries. They are also highly *engaged*, visiting science centres, and participating in and supporting science activities at a world-leading rate. They rank first out of 35 countries in basic science *literacy*, though the “bar” is not very high. As is widely reported in the media, our school students score relatively highly on international tests of science and math ability, but rank behind countries such as Finland and Singapore. We do, however, produce relatively fewer university graduates in science and engineering (though we rank first in the fraction of our population with post-secondary education). Some of this may be due to economic factors, such as the Canadian private sector's low investment in research and development.

But all is not rosy with science culture in Canada. We rank low in the fraction of engineering degrees awarded to women. There are large gaps in Canadians' exposure to and engagement in science: among low-economic-status and inner-city populations, immigrants, rural and Aboriginal communities, for instance. One of the goals of the report was to investigate how science culture is affected by factors such as age, gender, culture, and economic status. Scientific literacy in Canada may not be deep enough to deal with complex environmental and health topics. Deeply rooted cultural and religious beliefs may conflict with scientific evidence. The Internet and social media are powerful forces for spreading pseudoscience, and “fake

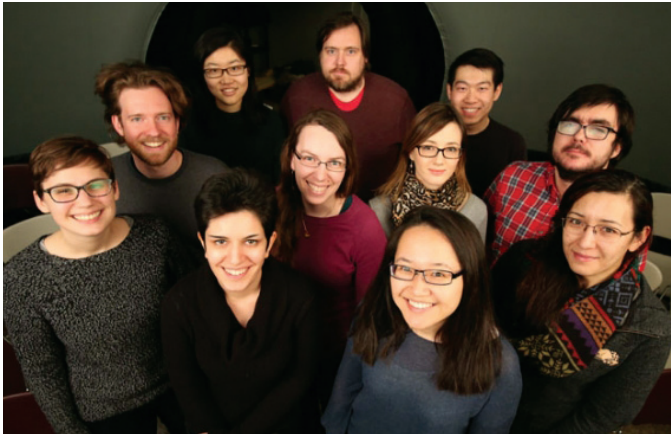


Figure 1 — At the University of Toronto, this group of astronomy graduate students and staff contributed to Canada’s science culture by producing and delivering planetarium shows on the Golden Age of Islamic Astronomy, raising over \$10,000 for the Red Cross refugee fund. They then presented the program in Arabic, for an audience including recently-arrived refugees. Source: Dunlap Institute.

news” about science. I also wonder whether Canadians are as aware of their science *heritage* as are residents of countries like France, Germany, and the UK. A primary expectation of the (Ontario) school science curriculum is for students to be aware of Canada’s achievements in science and technology. But are they?

Another focus of the report was on the components of the informal system that supports science culture, including organizations such as the RASC. The report considers that we are strong in this respect. Over 700 programs and organizations support science culture. On the other hand, we lack funding to support science culture. We have some, and it is especially important to use these funds effectively, using “best practices,” working with knowledgeable partner organizations, and incorporating strategies for evaluation and improvement.

We also do not have a single national organization (comparable to the American Association for the Advancement of Science, in the US) to provide leadership. There are potential leaders, including the Science and Technology Awareness Network². Development of leadership was one of five interventions proposed in the report, along with supporting lifelong science learning, making science inclusive, adapting to new technologies, and enhancing science communication and engagement.

Astronomy has always been an excellent gateway into science engagement, perhaps because it has so many different facets and cultural connections (as compared with theoretical physics, for instance!)

I see this in the Q&A sessions after my public lectures. The questions and comments can range from simple sky phenomena, to history and philosophy and the arts, to the lives of astronomers, to the latest discoveries reported in the media. Because it appeals to people of all ages, a “family approach”

to astronomy outreach can be effective, as the Astronomical Society of the Pacific has found and exploited with its *Family Astro* project³. Children’s enthusiasm for astronomy can rub off on their elders, and vice versa.

What can you and the RASC do to enhance science culture in Canada? First of all: keep up the good work. Remember that the RASC received the prestigious *Michael Smith Award* for excellence in science communication, in 2003. Remember that, during International Year of Astronomy 2009, the RASC, in partnership with CASCA and FAAQ, reached almost two million Canadians face-to-face. This certainly contributed to Canadians’ high level of science engagement! But, as I have said many times before: don’t just “preach to the converted.” Try to take your outreach to the underserved populations mentioned above. Organize events that are hands-on, eyes-on, and minds-on. Enhance your outreach skills. Seek out “best practices.” Read the *Science Culture in Canada* report.

The RASC also enables you and other citizens to *do* science, and science outreach. You can even engage in *science research*, on topics such as asteroids, comets, supernovae, and variable stars. This is the ultimate form of citizen engagement in science.

Partnership helps. An up-and-coming strategy, discussed at a half-day meeting before the CASC meeting, is the formation of “STEM Ecosystems”—local partnerships of organizations that support formal or informal learning opportunities in STEM (STEM is an acronym for science, technology, engineering, and mathematics). In the last 2 years, over 40 such partnerships have formed in the U.S. Vancouver has proposed to be the centre of the first such ecosystem in Canada. Here in the Toronto area, we have been partnering in astronomy outreach for years. I know that many RASC Centres do likewise. I recommend it highly. ★

Acknowledgements

I thank Kirsten Vanstone for organizing the CASC panel, and for reading and commenting on a draft of this article.

Notes

- 1 www.scienceadvice.ca/en/assessments/completed/science-culture.aspx
- 2 www.stanrsst.ca
- 3 www.astrosociety.org/education/k12-educators/family-astro
- 4 <http://STEMEcosystems.org>

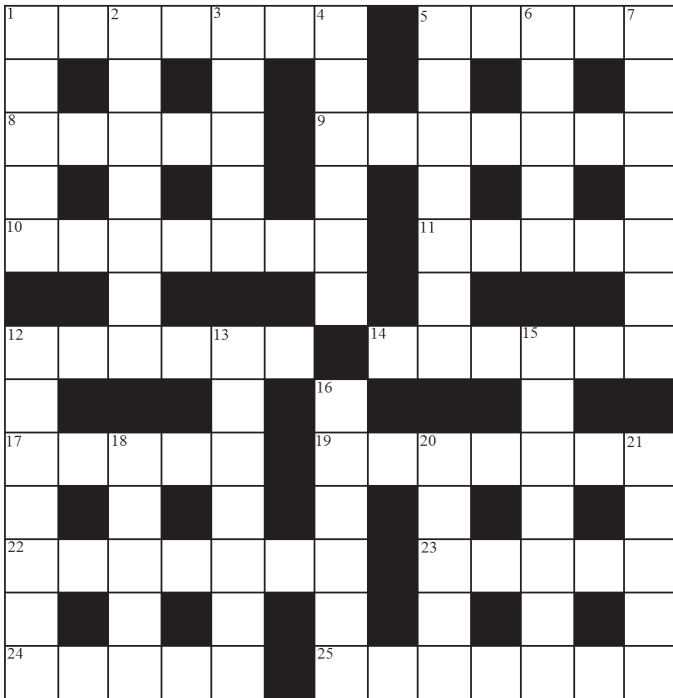
References

Council of Canadian Academies, 2014. *Science Culture: Where Canada Stands*.

John Percy FRASC is Professor Emeritus, Astronomy & Astrophysics and Science Education, University of Toronto.

Astrocryptic

by Curt Nason



ACROSS

1. Lunar cycle in comet cycle (7)
5. Lane observatory in supernova search every 18 years (5)
8. Reorganized, Meade makes an edit (5)
9. Mount placed north of the umbra where the weather sounds poorer (7)
10. Edinburgh Astronomer Royal raised an issue about scattered maps (7)
11. Hugo winner Thomas soundly used at ALMA (5)
12. Hey, everyone inside! He first said where the Sun would disappear! (6)
14. Much of the Universe discovered during totality (6)
17. Unmounted telescope used in test lab for an eclipse (5)
19. He is in will by Monsieur Herschel (7)
22. Oval pills scattered in Alberta football team's room (7)
23. Squint at variable Algol, changing left to right (5)
24. Herb confused myth at Earth's beginning (5)
25. OH contributor missed her eclipse, I hear (7)

DOWN

1. Electrical engineer found in returning total eclipse compiler (5)
2. Black body energy from her malt concoction (7)
3. Newton does dance when they align for an eclipse (5)
4. Crown jewel of totality (6)
5. Edge-on galaxy with spine broken by diffuse light (7)

6. Hyde's creator wrote about artificial intelligence and mounting bars (5)
7. Rough going around in extreme storm to field of maximum totality (7)
12. Live experiment for a claim of Venus (7)
13. Partial to Canada, pieces fall around London (7)
15. Endless economic kerfuffle over exploring Europa or Enceladus (3,4)
16. Type of seeing for binoculars or bi-cultural understanding (3-3)
18. Brent's relation with Fisher extends to the spirals (5)
20. Little hare eats half of guts to gain advantage (3,2)
21. Morgan-Keenan are back in to give us a Pointer (5)

Answers to June's puzzle

ACROSS

1 PISCIMUM (pi+anag); 5 MIMAS (anag-a); 8 ROCHE (Roc+he); 9 MERCURY (mer(Cu)ry); 10 SURFACE (surf ace); 11 NITRE (hidden); 12 LEXELL (hid); 14 URANUS (rev,-B+N); 17 VESTA (anag); 19 CALYPSO (c(anag)o); 22 JOURNAL (Jo+anag+Al); 23 PLUTO (Plato-a+u); 24 YOKED (2 def); 25 SISTERS (2 def)

DOWN

1 PARIS (par/is); 2 SYCORAX (an(Co)ag); 3 IKEYA (I+key+a); 4 MEMBER (anag, beer+mm); 5 MARINER (2 def); 6 MOUNT (2 def); 7 SKY NEWS (hid); 12 LOVEJOY (love+joy); 13 LEARNED (anag) 15 NEPTUNE (anag); 16 SCALES (2 def); 18 SPUNK (Sputnik-ti); 20 LEPUS (anag); 2 OBOLS (an(B)ag)

It's Not All Sirius

by Ted Dunphy



THE ROYAL ASTRONOMICAL SOCIETY OF CANADA

Board of Directors and appointed officers for 2017/2018 | Conseil d'administration et membres attirés pour 2017/2018

Honorary President

John R. Percy, Ph.D., FRASC, Toronto

President

Colin Haig, B.Sc., M.Sc., Hamilton

1st Vice-President

Chris Gainor, B.A., M.Sc., Ph.D., Victoria

2nd Vice-President

Robyn Foret, Calgary

Secretary

Charles Ennis, Sunshine Coast

Treasurer

Anthony Gucciardo, R.N., C.D., Yukon

Director

Heather Laird, Calgary.

Director and Past President

Craig Levine, M.A., London

Director

Rob Thacker, B.Sc., M.Sc., Ph.D, Halifax

Director

Michael Watson, B.A., L.L.B, Unattached

Executive Director

J. Randy Attwood, B.Sc., FRASC

Editors

Journal

Nicole Mortillaro, B.A.A., Toronto

Observer's Handbook

James Edgar, Regina

eBulletin and National Newsletter

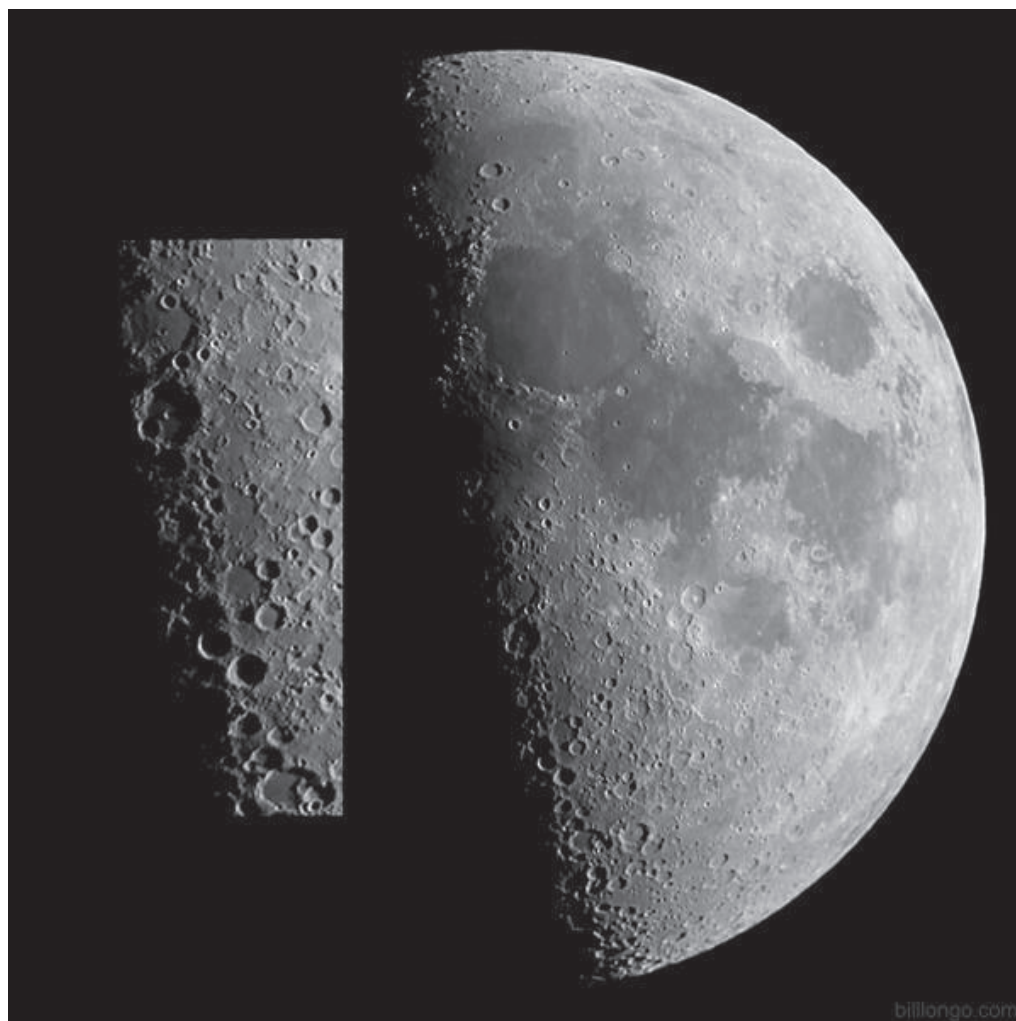
Dave Garner, B.Sc., M.o.A., Kitchener-Waterloo

Observer's Calendar

Paul Gray, Halifax

Great Images

by Bill Longo



This image of the "Lunar X" was taken by Bill Longo in May 2016 using his Celestron 9.25" and a Canon T3.



Journal

Great Images

Malcolm Park photographed this beautiful auroral display on 28-29 May from Bloomfield, Ontario. Malcolm used a Nikon D3s, 24-70 mm f/2.8 lens at 24 mm and f/2.8, taking a 10-sec exposure.